Measuring Material Properties of Tectorial Membranes from Normal and Genetically Modified Mice

by

Kinuko Masaki

Submitted to the Harvard University–Massachusetts Institute of Technology Division of Health Sciences and Technology in partial fulfillment of the requirements for the degree of

Doctor of Philosophy

at the

MASSACHUSETTS INSTITUTE OF TECHNOLOGY

June 2006

Author .....
Harvard University–Massachusetts Institute of Technology Division of Health Sciences and Technology

April 6, 2006

Certified by .....
Dennis M. Freeman
Associate Professor of Electrical Engineering
Thesis Supervisor

Accepted by .....
Martha L. Gray, Ph.D.
Edward Hood Taplin Professor of Medical and Electrical Engineering,
Director, Harvard-MIT Division of Health Sciences and Technology

Measuring Material Properties of Tectorial Membranes from Normal and Genetically Modified Mice

by

Kinuko Masaki

Submitted to the Harvard University–Massachusetts Institute of Technology
Division of Health Sciences and Technology
on April 6, 2006, in partial fulfillment of the requirements for the degree of
Doctor of Philosophy

Abstract

With the discovery of hearing disorders caused by mutations in proteins expressed in the tectorial membrane (TM), the importance of the TM in cochlear mechanics has never been clearer. However, the exact role of the TM in cochlear mechanics remains a mystery. In this thesis, I have investigated material properties of two mouse models of genetic hearing disorders that affect proteins found in the TM, α-tectorin and type XI collagen. The *Tecta* mutants had a missense mutation in α-tectorin, a protein found exclusively in the TM in the organ of Corti. The effect of the mutation was to decrease the fixed charge concentration, which was found to be the primary determinant of the bulk modulus. However, the shear modulus was not affected. *Col*11*a*2 is one of the genes that encodes for type XI collagen. Mutation in this gene causes no significant change in fixed charge concentration and, therefore, bulk modulus. However, the radial shear impedance is lowered. These measurements suggest that TM shear impedance is dominated by radially oriented collagen fibers and plays a key role in driving outer hair cell (OHC) bundle deflection. At the same time, the TM bulk modulus is dominated by the presence of fixed charge and may play a key role in coupling energy from outer to inner hair cells.

Thesis Supervisor: Dennis M. Freeman
Title: Associate Professor of Electrical Engineering

Acknowledgments

I have so many people to thank for helping me get to the point I am now.

First of all, I want to thank my advisor, Denny Freeman. He has taught me the importance of being meticulous and thorough in not only my research but also in my presentation and papers. I have never before cared or noticed that one section was 10 pt Times New Roman and the other section was in Helvetica!! :) I hope that I will continue to put that much attention to details when I leave this lab.

Next, I would like to thank Tom Weiss, who was my secondary advisor. He not only helped me get into the program when I was an undergraduate but he also came out of retirement to help me write and publish a paper which I would not have been able to do without him.

Al Grodzinsky was an invaluable committee member who not only gave me insight about research but also helped me look for post-doctoral positions in the field of tissue engineering.

Chris Shera and Charlie Liberman were wonderful committee members who have helped me at each point in the research process with their insightful comments. They also made sure that each committee meeting was not as painful as it could have been. :)

I cannot thank Nelson Kiang enough for taking interest in a clueless sophmore undergraduate when I took his class and directing me towards the HST SHBT program. Without his guidance, I do not know where I would be now. He not only showed me that there is so much to learn in the field of hearing but that I might even be able to contribute to this field some day.

What would I do without A.J. Aranyosi? :) I cannot even count how many times I ran into his office with a HUGE crisis and he always seemed to make the problems go away!! :) As I once told him, he can make garbage look good!! Its hard to imagine how I would survive in the future without A.J. in the lab to run to to help solve all my problems.

Rooz Ghaffari was the best officemate one can ever wish for. He not only put up

with the craziness at lab (my karoke singing, my talking to myself, and my insane fear of mice) but he was also a great and wonderful friend outside of lab. I will never forget the wonderful times we had!! :)

I also want to thank Wendy Gu for helping Rooz get the mice and killing them for me!! Without both of their help, I would not have been able to do any experiments!! I also want to thank Wendy for helping me with the experiments and also being the only other girl in the lab.

Chris Bergevin and Stan Hong have also been wonderful labmates who were so patient to listen to all my talks and presentations about a zillion times and providing wonderful comments.

I want to thank Rosanne Rouf for being a wonderful wonderful friend!! :) Who would have guessed that when I visited her in Denny's lab when we were seniors, that I would end up doing what she was doing then!! :) Rosanne has helped and encouraged me every step of the way. I cannot thank her enough for always coming over very late at night the day before my presentation to make sure everything made sense.

I want to thank Laila Bartlett for being my best friend and cheering me on every step of the way even when I was depressed beyond belief. She taught me that one can overcome anything with the right outfit and right attitude!! :)

What would I do without Matthew McClain in my life!! :) Without him, I am not sure how I would have survived the insanity of these last two years!! :) He took care of me and made sure I was fed and even put up with me using him as a human punching bag when I was stressed. But most importantly, I want to thank Matt for believing that that I can accomplish anything I put my mind to.

Finally, I would like to thank my parents for always supporting me and encouraging me no matter what and most importantly loving me unconditionally!! :)

Contents

List of Figures

Chapter 1

Introduction

The tectorial membrane (TM) is one of the least understood structures in the ear. The TM is a gelatinous structure which sits on top of the main sensory structure in the ear. Therefore, the TM is thought to play an important role in cochlear mechanics. However, due to its small transparent fragile nature, very few measurements of the TM exist.

However, there are an abundance of models of the TM. The TM has been modeled as a stiff level with a compliant hinge (Davis, 1958; Johnstone and Johnstone, 1966; Rhode and Geisler, 1967; Dallos et al., 1972; Billone and Raynor, 1973a; Neely and Kim, 1983; Geisler, 1986; Kolston, 1988), a resonant mass-spring system (Zwislocki, 1979; Zwislocki and Kletsky, 1979; Allen, 1980; Zwislocki and Kletsky, 1980; Neely and Kim, 1986) or a mass (Mammano and Nobili, 1993a). However, none of these models is based on measurements of the TM and moreover none of them agree with the known molecular properties of the TM. Chapter 2 describes what is know about the molecular composition and architecture of the TM.

Whereas mechanical properties such as point impedance are important in characterizing the specific interactions of the TM to other structures such as the hair bundle, material properties are needed to characterize the molecular mechanisms that underlie mechanical properties. The relation between stress and strain is an important material property and is a key component of many models such as the polyelectrolyte gel model (Freeman et al., 1997). The stress-strain relation of many connective tis-

sues is determined by applying a uniform mechanical stress to a macroscopic uniform section of tissue (Frank et al., 1990). Unfortunately, this method is hard to adapt to the TM, because the TM is small and irregularly shaped. Therefore, osmotic pressure was applied using polyethylene glycol (PEG), and the resulting strain was measured. Chapter 3 describes in detail the method of using PEG to measure the stress-strain relation of the TM from normal mice.

Mouse models of genetic mutations that affect the TM are another powerful tool to probe TM function. By measuring the effect of genetic mutation on material properties, not only will we better understand the nature of some hearing disorders but we will also elucidate the molecular basis of the material properties of the TM.

The TM is made up of many proteins some of which are unique to the extracellular matrix in the ear. For example, α-tectorin is a protein found only in the TM in the adult cochlea. In humans, the Y1870C missense mutation of this protein causes a 50-80 dB hearing loss (Legan et al., 2005). In $Tecta^{Y1870C/+}$ mice, basilar membrane (BM) tuning curves were on average only 8 dB less sensitive than wild-types. However, the compound action potential (CAP) threshold measured at the round window increased on average by 55 dB in $Tecta^{Y1870C/+}$ mice compared to wild-types (Legan et al., 2005). These findings are not consistent with the classic model of TM function described above. Instead, they suggest that the two roles attributed to the TM — shearing OHC hair bundles and coupling OHC forces to IHCs — are mediated by different mechanisms, and only the latter is affected by the *Tecta* mutation. To test these hypotheses, both the bulk and shear properties of the TMs from $TectaY870C/+$ mice were measured and compared to that of wild-types in Chapter 4.

Another mouse model that was investigated had a mutation of the $Col11a2$ gene which encodes type XI collagen. Unlike, α-tectorin, type XI collagen is a quantitatively minor fibrillar component of the TM and is found throughout the body. However, in humans, mutations in $Col11a2$ have been identified as the cause of DFNA13 hearing loss in two large families with hearing loss (McGuirt et al., 1999). These families have mid-frequency hearing loss with no other known phenotypical abnormalities. In mice, there was a 40-50 dB increase in click-evoked auditory brainstem response

(ABR). To understand the molecular mechanism of this hearing loss, both the bulk and shear properties of the TMs from $Col11a2\ -/-$ were measured and compared to that of wild-types in Chapter 5.

In Chapter 6, the stress-strain relation of TMs from normals, $TectaY1870C/+$ and $Col11a2\ -/-$ are compared and a simple molecular based model is developed. This model not only captures the data but also interprets the molecular mechanism underlying the material property changes. Chapter 7 describes additional experiments which were done to clarify the two-layer gel model introduced in Chapter 6. Finally, Chapter 8 not only summarizes the findings of the thesis but also discusses the implications of the experimental results in understanding the role of the TM in cochlear mechanics in both normal and mutant mice.

Chapter 2

TM Composition

2.1 Introduction

The tectorial membrane (TM) is a gelatinous structure overlying the sensory cells in the cochlea. Because of the TM's small size, transparency, and fragility, little was known about the TM. Recently, however, more has been discovered about its composition and structure. However, the exact function of the TM in cochlear mechanics is still unclear. This paper will review what is known about the structure and composition of the TM and its implications in cochlear micromechanics.

This paper will take a bottom up approach on the makeup of the TM. The biochemical composition of the TM will be discussed first. Then, we will see how those biochemical materials organize themselves into different types of fibers. Finally, we will determine how the fibers are organized into different zones in the TM.

2.2 Biochemical Composition

The TM is approximately 97% water. Since the dry weight of mouse TM is 2 μg, the wet weight is about 70 μg (Steel, 1980; Thalmann et al., 1993a). Protein and glycoaminoglycans (GAGs) makes up 58% and 15-20% of the dry weight, respectively (Thalmann et al., 1987; Suzuki et al., 1992). The other 22-27% of the dry weight has not yet been identified. Collagen makes up 40-50% of the protein in TM and the rest

is non-collageous glycoproteins or proteoglycans (Richardson et al., 1987).

2.2.1 Collagen

Collagens are a family of fibrous proteins which are found in all connective tissues. The characteristic feature of typical collagen is its long, stiff, triple-stranded helical structure, in which three collagen polypeptide chains, called α chains, are wound around one another in a ropelike superhelix (Alberts et al., 1994). The three α chains of a given molecule may be identical or the three α chains may be composed of two or three different subtypes. The characteristic amino acid sequence of collagen is G-X-Y where G is glycine, X and Y are usually proline and hydroxyproline. Glycine is regularly spaced at every third residue throughout the central region of the α chain. Due to its small size (having only a hydrogen atom as a side chain), glycine allows the three helical α chains to pack tightly together to form the collagen superhelix. Proline, on the other hand, stabilizes the helical conformation in each α chain because of its ring structure.

Collagen is coded for by more than 25 genes each encoding a distinct collagen α chain. Even though, in principle, more than 10,000 types of collagen can be formed from these α chains, only about 20 types of collagen have been identified, 15 of which are known in mice. These have been grouped into different classes according to their molecular components, their ability to form fibrils, as well as their distribution in the extracellular matrix of connective tissue.

For example, collagen type I, II, III, V and XI make up the fibrillar or the fibril-forming collagen class. Since these collagens have large helical domains which polymerize both side by side and end on end, they form long fibrillar aggregates. Specifically, these collagen molecules assemble into higher-order polymers called fibrils which then assemble into larger, cablelike bundles which are called collagen fibers.

Collagen type IX and XII, on the other hand, are members of the FACIT (fibril-associated collagens with interrupted triple-helices) class of collagen. Because their triple-stranded helical structure is interrupted by one or two short non-helical domains, these collagens cannot form fibrils. However, due to the short non-helical

domains, the FACIT class of collagen are more flexible compared to fibrillar collagen. Fibril-associated collagen associate with fibril-forming collagens, either parallel to the fibrils to form heterotypic fibers, or perpendicular to the fibrils to cross-link adjacent molecules (Slepecky, Savage and Yoo, 1992). These collagens are thought to mediate the interactions of collagen fibrils with one another and with other matrix macromolecules. In this way, they have a role in determining the organization of the fibrils in the matrix (Alberts et al., 1994).

Type II collagen

Type II collagen is the major structural component of the TM, accounting for approximately 40-50% of the protein content. Type II collagen consists of 3 identical polypeptide α chains, α1(II), which are coiled about one another to form a rod-like triple helix. The α1(II) chain is encoded by COL2A1 gene.

Type II collagen forms large cross-banded fibers which are largely responsible for the rigidity of connective tissue matrices. Not only are type II collagen responsible for providing structural stability and tensile strength but they also provide a network for the deposition of proteoglycans. For example, keratan sulfate has been thought to be associated with type II collagen (Khalkhali-Ellis et al., 1987).

Type V collagen

Type V collagen is a fibrillar collagen which makes up less than 10% of the total collagen in any tissue. Type V collagen can be composed of three different α chains [α1(V), α2(V), and α3(V)], encoded by three distinct genes (COL5A1, COL5A2, and COL5A3). Type V collagen can be a homotrimer of three α1 chains, a heterotrimer of two α1 and one α2 chain, or a heterotrimer of α1, α2, and α3 chains. However, in mice, the α3 chain and its encoding gene has not yet been identified.

Type IX collagen

Type IX collagen is a heterotrimer of three distinct α chains [α1(IX), α2(IX), and α3(IX)] encoded by COL9A1, COL9A2, and COL9A3 genes. Type IX collagen

molecules adhere to surface of fibrils containing type II collagen. One of the two arms of the type IX collagen molecule cross-link to type II collagen, while the shorter arm projects into the space around the fibril.

Type IX collagen plays a role in controlling the interaction of type II collagen with its proteoglycans and/or glycoprotein matrix (Thalmann et al., 1987). Also, during fibrillogenesis, type IX collagen limits the diameter of type II collagen fibrils to a characteristic maximum of 10-20 nm. Finally, the type IX collagen molecule serves as a core protein for glycoaminoglycan (GAG) residue which consists of one or two chondroitin or dermatan sulfate chains covalently linked to the $\alpha 2$ chain. This GAG portion of type IX collagen helps maintain proper hydration of the cross-linked fibers thus regulating the spacing, turgor pressure, and biomechanical properties of the fibers (Slepecky, Savage, Cefaratti and Yoo, 1992).

Type XI collagen

Type XI collagen is a quantitatively minor fibrillar component of the extracellular matrix. Type IX collagen is normally a heterotrimer of three different chains. The $\alpha 1$(XI) and $\alpha 2$(XI) are encoded by COL11A1 and COL11A2 while the third chain is a variant of $\alpha 1$(II) collagen, modified post-translationally. Type XI collagen has been associated with type II and IX collagen. Specifically, in cartilage, type XI collagen is thought to be important for maintaining the interfibrillar spacing and fibril diameter of type II collagen (Mendler et al., 1989; Eikenberry et al., 1991; Li et al., 1995).

2.2.2 Non-collagenous glycoproteins

At least three non-collageneous glycoproteins may account for nearly 50% of the total protein content of the TM (Richardson et al., 1987).

α and β-tectorin

α and β-tectorin are the two major non-collageneous proteins in the TM. They are encoded by TECTA and TECTB, respectively. In situ hybridization has shown that

tectorins are unique to the inner ear (Killick et al., 1995). In particular, they found it only in the TM and the otoconial membrane (Goodyear and Richardson, 2002).

α-tectorin encodes a polypeptide of 2150 amino acids with a molecular weight of 239 kDa. α-tectorin is composed of three distinct modules: the amino-terminal region, a large central segment, and the carboxyl-terminal region. The amino-terminal region is similar to part of the first globular domain(G1) of entactin, a basement membrane protein. The central domain is composed of three full and two partial repeats of the D domain found in von Willebrand factor (vWF), zonadhesin, and intestinal muci MUC2. Zonadhesin is a sperm membrane protein that binds to zona pellucida in a species specific manner. Finally, the carboxyl-terminal region contains a single zona pellucida domain similar to that in oocytes. β-tectorin, on the other hand, encodes a smaller polypeptide of only 320 amino acids with a molecular weight of 36 kDa and is composed of only a single zona pellucida domain.

α and β-tectorin have some common properties. First, both α and β-tectorin terminate with a hydrophobic carboxyl (COOH) preceded by a potential endoproteinase cleavage site. This suggests that both tectorins are synthesized as lipid-linked, membrane-bound precursors, targeted to the apical surface of the cochlear epithelium by the lipid and then released into the extracellular compartment by the action of an endoproteinase (Legan et al., 1997). Secondly, both tectorins have a single zona pellucida domain, a 260 amino acid module with eight strictly conserved cysteine residues. This is the only common feature shared by a number of different proteins, all of which either can or do form filament based matrices or gels, and it has been suggested that the single zona pellucida domain may be the element that enables them to form filaments. The presence of this domain in both of the two major components of the filament based non-collagenous matrix of the TM suggests that these two proteins either self-associate via their respective zona pellucida domains to form homomeric filaments or interact with each other via their zona pellucida domains to form heteromeric filaments (Legan et al., 1997).

Mice homozygous for a targeted deletion in α-tectorin have TMs that is detached from both the spiral limbus and the organ of Corti. Moreover, the TMs lack all

non-collagenous matrix. In other words, collagen remains but otogelin and β-tectorin cannot be detected in these TMs (Legan et al., 2000). These observations indicate that α-tectorin is required for and probably forms the major part of the non-collagenous striated-sheet matrix.

The TMs from mice heterzygous for a missense mutation of TECTA, on the other hand, are still attached to the hair bundles (Legan et al., 2005). However, these mice have a 55 dB compound action potential (CAP) threshold increase compared to wild-types. In the TM of these mice, the striated-sheet matrix is missing only in the sulcal region which leads to a disruption in the organization of the collagen fibrils in this area. This finding indicates that the radial fibers in normal mice and humans are critically dependent upon α-tectorin.

Otogelin

Otogelin is a N-glycosylated protein specific to the acellular membranes covering six sensory epithelial patches in inner ear; the TM over the organ of Corti, the otoconial membrane over the maculae of the utricle and saccule, and the cupulae over the cristae of the semicircular canals. Otegelin is encoded by the gene OTOG.

In the TM, otegelin shows up in immunostaining as thick and strongly labeled strands extending radially (Cohen-Salmon et al., 1997). Therefore, otegelin is unlikely to be associated with type B protofibrils (discussed in detail in the following section) which are diffuse and highly concentrated in some superficial regions of the TM. Instead, otogelin is probably associated with type A protofibrils (also discussed in detail in following section) which are radially distributed throughout the TM.

Studies of knockout mice have shown that otogelin is not required for the anchoring of the TM to the spiral limbus; nor is it necessary for the incorporation of α-tectorin and keratan sulfate proteoglycans into the TM (Simmler et al., 2000). However, otogelin seems to play an important role in the interaction or stabilization of type A and type B protofibrils. Therefore, otogelin seems to contribute to the mechanical stability, ductile capacity, and tensile strength of the TM. Deafness observed in mice suggests that resistance of the TM to mechanical stresses generated by compressional

waves is reduced in the absence of otogelin.

2.2.3 Proteoglycans

Proteoglycans are composed of glycosaminoglycans (GAGs) covalently linked to a core protein. Proteoglycans are usually distinguished from other glycoproteins by the nature, quantity and arrangement of their sugar side chains. By definition, at least one of the sugar side chains of proteoglycans must be a GAG. Glycoproteins contain from 1% to 60% carbohydrate by weight in the form of numerous relatively short, branched oligosaccharide chains. The core protein in a proteoglycan is usually a glycoprotein, but it contains as much as 95% carbohydrate by weight, mostly in the form of long unbranched GAG chains, each typically about 80 sugar residues long. Proteoglycans can thus be much larger than glycoproteins (Alberts et al., 1994).

Glycosaminoglycans (GAGs) are unbranched polysaccharide chains composed of repeating disaccharide units. They are called GAGs because one of the two sugar residues in the repeating disaccharide is always an amino sugar, which in most cases is sulfated. The second sugar is usually a uronic acid. Since most of the sugar residues contain sulfate or carboxyl groups, GAGs are highly negatively charged. Four main groups of GAGs have been distinguished by their sugar residues, the type of linkage between these residues, and the number and location of sulfate groups: (1) hyaluronan, (2) chondroitin sulfate and dermatan sulfate, (3) heparan sulfate and heparin, and (4) keratan sulfate (Alberts et al., 1994).

In the TM, chondroitin sulfate and keratan sulfate make up 0.29% and 0.17% of the total wet weight, respectively, or 9.7% and 5.7% of the dry weight. The greatest concentration of keratan sulfate is found in the upper fibrous layer of limbal, middle and marginal regions of the TM. Chondroitin sulfate has a similiar distribution as keratan sulfate, with the highest concentration found in the upper fibrous region. Moreover, both keratan sulfate and chondroitin sulfate increase in concentration from the base to the apex of the cochlea (Munyer and Schulte, 1994). These findings suggest that all these glycoaminoglycans are linked to the same core protein.

Keratan sulfate and chondroitin sulfate are probably involved in determining the

structure of the TM's upper fibrous layer, perhaps by acting as adhesion molecules between collagens or between collagen and some extracellular matrix (ECM) component. The influence of chondroitin sulfate proteoglycans on the cross-linking of collagens and mediation of cell adhesison with fibronectin and certain growth factors has been well documented. Keratan sulfate proteoglycan has also been shown to associate with corneal collagens. The capacity of proteoglycans for entering into multiple interactions with ECM constituents in other systems provides support for a similar role in TM (Munyer and Schulte, 1994).

Proteoglycans appear to be components of the extracellular matrix and not fibrils since they were not associated with any specific fibrils or shown to exhibit regular periodicity, but instead are distributed randomly (Munyer and Schulte, 1994).

2.3 Fibers in TM

Collagens and proteoglycans are organized into fibers. The two main types of fibers in the TM are type A and type B protofibrils.

2.3.1 Type A protofibrils

Type A protofibrils are straight and unbranched. The diameter of these fibers is 10-20 nm and they form distinct bundles which can be seen in light microscopy. Under atomic force microscopy (AFM), these fibers have a morphology characteristic of collagen (Hiyama et al., 1998). Specifically, the fibers have a D-periodicity of 69.1 ± 0.6 nm. Pre-embedding and post-embedding immunocytochemistry showed that type A protofibrils are composed of type II collagen cross-linked with type IX (Slepecky, Savage, Cefaratti and Yoo, 1992). Since type XI collagen has also been proposed to interact with type II collagen, type A protofibrils may also be composed of type XI collagen. Finally, otegelin, a non-collageneous glycoprotein, may also be associated with type A protofibrils (Cohen-Salmon et al., 1997).

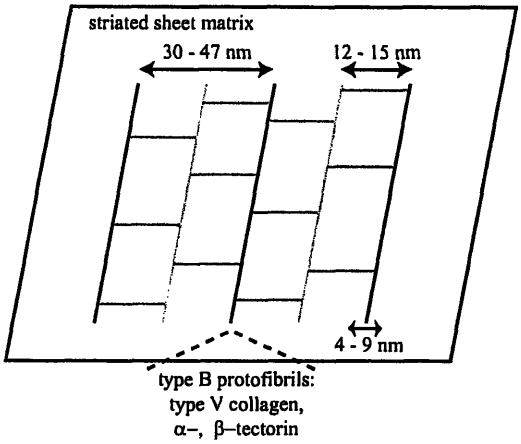

Figure 2-1: The composition and organization of the striated sheet matrix. The black and gray lines illustrates the weakly and strongly hydrated protofibrils, respectively.

2.3.2 Type B protofibrils

Type B protofibrils are coiled and branched. The diameter of these fibers is 4-9 nm. These fibers are organized into a striated sheet and form the matrix in which type A protofibrils are embedded. Type B protofibrils are composed of type V collagen along with non-collagenous glycoproteins, alpha- and beta-tectorin.

Type B protofibrils come in two hydration states: weakly hydrated (loosely packed) and strongly hydrated (tightly packed). Therefore, in tannic acid treatment, the filaments appear as light and dark stained filaments (Hasako and Richardson, 1988a). These two types of filaments are linked together by staggered cross-bridges and arranged in sheets with the filaments lying within the plane of each sheet. The cross-bridges occur at 12-15 nm intervals along the length of the fibrils and the distance between two dark fibrils is between 30-46 nm. The organization of the striated sheet matrix is illustrated in Figure 2-1.

The weakly hydrated protofibrils form the cover net, the marginal band, Hensen's stripe, and the limbal undersurface of the TM. The highly hydrated protofibrils form the matrix within which the type A protofibrils are found. These sheets are either wrapped around or pass in between the type A protofibrils.

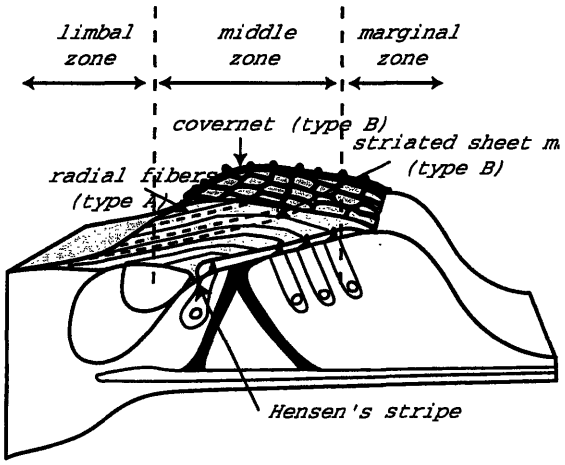

Figure 2-2: The three zones of the TM. This figure also shows the relative position of the striated sheet matrix, radial fibers, Hensen's stripe and the covernet in the TM.

2.4 Radial Zones in the TM

The different types of fibers are organized into three distinct radial zones: the limbal (inner) zone, middle (main body) zone, and marginal (outer) zone as shown in Figure 2-2 (Lim, 1972).

2.4.1 Limbal zone

The limbal zone is the region where the TM attaches to the top of the spiral limbus, in particular, the interdental cells. In this zone, the TM is about 3 μm thick but its thickness increases continuously in the radial direction. The limbal zone is mostly made up of tightly packed strongly-hydrated type B protofibrils. However, near Reissner's membrane and the contact surface with the limbus, weakly-hydrated type B protofibrils exist. Type A protofibrils are also found over parts of the limbal zone.

2.4.2 Middle zone

The middle zone forms the main body of the TM overlying the sensory cells. The upper surface of this zone contains a covernet which is an anastomosing network of thick cables. The underside of this zone contains the Hensen's stripe which is a prominent ridge that runs longitudinally along the TM and is thought to contact

and drive the inner hair cell (IHC) bundles. The outer hair cell (OHC) bundles, on the other hand, are thought to be imbedded in Kimura's membrane/Hardesty's membrane which is also on the underside of the middle zone. Finally, the rest of the middle zone is the fibrous layer which contains fibers embedded in an amorphous substance.

Both the covernet and the Hensen's stripe have the ultrastructural appearance of dense weakly-hydrated type B protofibrils. The homogeneous basal layer, on the other hand, has a 1 um thick layer of parallel, closely packed type A protofibrils which are not rigidly oriented radially but run in the direction of caecum cupulare.

The fibrous layer contains fibers with two distinct orientations. The major fibers run radially while the minor fibers run more or less longitudinally. The radial fibers are made up mostly of type A protofibrils. Type A protofibrils climb obliquely from the homogeneous basal layer to the surface of the TM with an inter-bundle distance of 2.5 μm in association with type B protofibrils. This slanted fibrillar arrangement coincides well with the slanted arrangement of the *W* formation of the OHC stereocilia (Lim, 1986). In the upper half of the membrane, the fibers run horizontally again, parallel to the basilar membrane (BM), and end in the limbal zone. The minor fibers are made up mostly of Type B protofibrils and run more or less longitudinally. They form the "amorphous matrix" in which the type A protofibrils are embedded.

2.4.3 Marginal zone

The marginal zone contains the marginal band and marginal net which make up the marginal complex. This complex is continuous with the covernet and the Hardesty's membrane in the middle zone. It is made up mostly of coiled, irregular knots of weakly-hydrated type B protofibrils. The marginal net is thought to attach the TM to the last row of Dieter's cells. The last row of OHCs also attaches to the TM at the level of the marginal band or, in some instances, on the marginal net.

2.5 Implications of TM composition

Composition plays a key role in determining mechanical properties of any structure. In the TM, the major components are collagen, glycoaminoglycans (GAGs), and glycoproteins. Each plays an important role in determining the mechanical properties of the TM.

2.5.1 Effect of collagen

Collagen is a main component of many connective tissues. Collagen fibrils are known to form structures that resist tensile forces. For example, cartilage which is subject to weight-bearing load and constant movement, is composed of type II, IX, and XI collagen. As in cartilage, the TM seems to be a structure specialized for absorbing stress. For example, type A protofibrils are composed mainly of type II collagen which provides structural stabilization and mechanical strength to the TM in deflecting hair cell stereocilia. Moreover, type II collagen is co-localized with type IX collagen, a cross-linking collagen, which further helps in imparting the TM with biomechanical properties similar to those needed in regions of known stress. In contrast, in other parts of the inner ear, where the structures are not known to be subjected to any mechanical stress, type II collagen is present in absence of type IX collagen.

A general property of collagen bundles is that they tend to be aligned in the direction of maximum stress thus forming trajectories indicating the direction of stress (Hasako and Richardson, 1988a). The direction of the stress maintained by the TM can be inferred by the ultrastructural details of the TM. In particular, the slanted fibrillar arrangement of the collagens on the underside of the TM coincides well with the slanted arrangement of the "W" formation of the stereocilia of the OHCs. This alignment of the collagen fibers implies that the OHC stereocilia push against the TM in the radial direction in vivo.

2.5.2 Effect of glycoproteins and proteoglycans

Glycoproteins and proteoglycans are responsible for the net negative charge of the TM since the saccharide residues of their carbohydrate chains contain carboxyl and sulfate groups which are ionized at physiological pH. The presence of fixed charge on the matrix of TM fibrils affects the property of membrane in a number of ways. First, since like charges repel, the greater the fixed charge concentration, the greater the resulting electrostatic repulsion force. Therefore, fixed charge helps resist compressive forces. Secondly, the presence of charges in the membrane will affect the rate of diffusion through the TM. In other words, fixed charge may serve as a sieve which regulates molecular flow according to size and charge. Finally, in cartilage, proteoglycans normally form large aggregates with highly negative charge densities and fill the interstices between collagen fibers, thereby attracting water and creating turgor pressure which provides stiffness and shape to the tissue. Therefore, the proteoglycans in the TM may also influence the overall degree of hydration of the tissue.

2.5.3 Determining fixed charge concentration

The complete compositional breakdown of the TM is not yet known. However, from what is known, a lower bound on the fixed charge concentration in the TM can be estimated. For example, 0.5% of the wet weight is GAGs. The two main GAGs in the TM are chondroitin sulfate (CS) and keratan sulfate (KS) whose concentration ratio is 1.7 (i.e. if KS and CS were the only GAGs, KS and CS would be 0.185% and 0.315% of total wet weight, respectively). If we take into account that 97% of TM is water, the concentration of both CS and KS can be determined. Specifically, the concentration of CS is 6.9 mmol/L [= (3.15 gm CS/liter TM) * (mol CS/457 gm)] and that of KS is 4.2 mmol/L [= (1.85 gm KS/liter TM) * (mol KS/444 gm)]. CS has both a carboxyl and sulfate side group which are both ionized at physiological pH. Therefore, the concentration of negative charge contributed by CS is 13.8 mmol/L [= 2 * 6.9]. KS, on the other hand, has only a sulfate side group which is ionized at

physiological pH. Therefore, KS contributes 4.2 mmol/L of negative charge.

Proteins also contribute to the fixed charge concentration in TM. 58% of the dry weight of TM is protein of which 55% is non-collagenous. The majority of non-collagenous protein is tectorin (α- and β-tectorin), and the rest is otogelin. Therefore, as a first order estimate, both α- and β-tectorin are predicted to be about 25%, and otogelin is estimated to be 5% of total protein concentration. From these values, the concentration of these proteins can be estimated. Specifically, the concentration of α-tectorin is 1.1 mmol/L [= (4.4 gm/L of TM) * (mol TECTA/239534.87 gm)], concentration of β-tectorin is 0.35 mmol/L [= (4.4 gm/L of TM) * (mol TECTB/36985.47 gm)], and concentration of otogelin is 0.0028 mmol/L [= (0.87 gm/L of TM) * (mol OTOG/313410.98 gm)].

To determine the charge of each of these proteins, the amino acid seqeuence of each protein was determined. Amino acids contain side-chain groups which are either basic (e.g. lysine, arginine, and histidine), acidic (e.g. aspartic acid and glutamic acid) or uncharged (e.g. glycine, alanine, valine, leucine, isoleucine, proline, phenylalanine, methionine, trytophan, and cysteine). The charge of a protein is determined by the number of basic or acidic side groups. For example, OTOG has a charge of -93, TECTA has a charge of -58, and TECTB has a charge of $+3$.

By knowing both the concentration of protein and their respective charges, the concentration of charge contributed from each protein can be determined. Specifically, α-tectorin contributes 1.1 mmol/L of negative charge, β-tectorin contributes 0.35 mmol/L of positive charge, and otogelin contributes 0.26 mmol/L of negative charge.

From these simple calculations, the net charge contributed by the non-collageneous proteins and the GAGs is about 19 mmol/L of negative charge. This calculations helps to establish an approximate lower bound for the concentration of charge in the TM.

Chapter 3

Poroelastic Bulk Properties of the TM Measured with Osmotic Stress

This chapter has been accepted as a paper in Biophysical Journal. The other co-authors are Thomas F. Weiss and Dennis M. Freeman.

3.1 Introduction

The tectorial membrane (TM) is a gelatinous structure that overlies the mechanically sensitive hair bundles of sensory cells in the cochlea. Mouse models with specific mutations of TM components have been shown to exhibit hearing loss suggesting that the TM plays an important role in hearing (McGuirt et al., 1999; Legan et al., 2000; Legan et al., 2005; Simmler et al., 2000). However, these studies do not elucidate the mechanistic role of the TM.

In the absence of detailed information on the mechanical properties of the TM, theoreticians had to make assumptions about its mechanical properties. In some cochlear models, the TM has been thought to be mechanically stiff and therefore act as a lever (Davis, 1958). Other models have treated the TM primarily as a mechanical load (Mammano and Nobili, 1993a). Finally, some have treated the TM as a spring and mass which together act as a resonant system (Allen, 1980; Neely and Kim, 1983). Unfortunately, recent measurements of mechanical properties of the

TM do not agree with any of these cochlear models (Freeman, Abnet, Hemmert, Tsai and Weiss, 2003). Instead, dynamic point stiffness measurements have shown that the TM impedance lies between that of a pure viscous and a pure elastic element. However, no simple cascade of lumped-parameter viscous and elastic elements fits the measurements. New models of the TM are clearly needed, and new measurements are required to define these models.

The fact that the TM is 97% water and contains macromolecular polyelectrolytes suggests that the TM is a gel (Weiss and Freeman, 1997b; Freeman, Masaki, McAllister, Wei and Weiss, 2003). In other biological gels composed of a fluid and solid phase, such as cartilage and corneal stroma, the theory of poroelasticity has been successfully applied to describe deformational behavior (McCutchen, 1982; Grodzinksy, 1983). Poroelastic models explicitly account for the viscous flow of fluid through pores when the specimen undergoes stress. One important constitutive relation of a poroelastic material is the equilibrium stress-strain relation. A constant stress applied to any material results in a time-varying strain which eventually comes to equilibrium. The relation between the applied stress and the equilibrium strain is called the *equilibrium stress-strain relation.* Another important bulk property of poroelastic materials is the effective pore radius. Knowing the pore radius allows for the calculation of intermolecular interactions at the molecular level and the hydraulic permeability of the TM. Both of these properties can be measured in many larger specimens such as cartilage by placing the tissue in a dynastat and applying mechanical pressure and measuring the resulting strain.

However, due to the small size (1/5 the thickness of a human hair) and fragility of the TM, the dynastat method is difficult to use. One approach to determining the bulk modulus of the TM is to measure the point indentation with atomic force microscopy and to use a model to compute the bulk modulus (Shoelson et al., 2004). Here we introduce a method that utilizes osmotic pressure to exert stress, and we calculate the bulk modulus directly from the measured strain. Previously, it has been shown on other specimens that using osmotic pressure to apply stress is similar to using mechanical pressure (Maroudas and Bannon, 1981; Schneiderman et al., 1986;

Basser et al., 1998). In preliminary studies, polyethylene glycol (PEG) solutions were used to apply osmotic pressure to the TM (Freeman, Masaki, McAllister, Wei and Weiss, 2003; Masaki et al., 2002; Richter and Dallos, 2003). However, there are two important caveats to using this method.

First, the osmotic pressure of PEG solutions must be determined. Measurements of the osmotic pressure of high molecular weight (MW) PEG solutions are not routine. Furthermore, the osmotic pressure of PEG solutions does not obey van't Hoff's law but is a nonlinear function of concentration and depends upon MW. Second, if PEG can penetrate the TM, then its osmotic pressure is not fully expressed. In this paper, we have addressed and resolved these two issues and have used PEG-induced osmotic stress to measure strain and to estimate both the equilibrium stress-strain relation and the effective pore radius of the mouse TM.

3.2 Methods

3.2.1 Methods common to experiments on TM and PMAA specimens

Many of the methods used to measure the stress-strain relation of specimens, both the TM and PMAA (polymethacrylic acid) gels, are similar to those used in previous studies of the TM (Freeman et al., 1994; Freeman et al., 1997; Shah et al., 1995). Briefly, the specimen was placed on a glass slide, decorated with TransFluoSpheres carboxylate modified fluorescent microspheres (i.e. beads), and immersed in a bathing solution. Images of sections of the specimen were recorded after the specimen was immersed in a given solution for at least one hour. One hour was found to be sufficient time for the TM position to stabilize (Freeman, Masaki, McAllister, Wei and Weiss, 2003). Since bright-field images show that beads end up resting on the surface of the specimen, bead position was used as a marker for the specimen surface. Bead positions were tracked to estimate changes in specimen height in solutions of different composition.

Solutions

All the solutions were variations of an artificial endolymph (AE) solution which contained in mM: 2 NaCl, 3 dextrose, 0.02 $CaCl_2$, 5 HEPES, and 174 KCl. This composition closely matches the measured ionic composition of endolymph in the mammalian cochlea (Bosher and Warren, 1978; Sterkers et al., 1984; Sterkers et al., 1988; Ikeda et al., 1987). The pH of the solution was adjusted to 7.3. PEG solutions were made by adding PEG to the same stock solution of AE to insure that the only difference in solutions was due to PEG. PEGs of molecular weights of 20, 40, 108, 205, 438, and 511 kDa were used to vary the osmotic pressures over the range 0-10 kPa.

Measurement methods

The measurement system consisted of a compound microscope (Zeiss Axioplan2) with a 25× water immersion objective with numerical aperture of 0.8, fluorescence filter block (Nikon blue excitation filter block B-2A) with an excitation filter wavelength of 450-490 nm, a dichromatic mirror with cut-on wavelength of 500 nm, and emission filter with cut-on wavelength of 515 nm, CCD camera (Pulnix TM1010), a video digitizer (Imaging Technology PC-DIG), and personal computer (Dell Precision 410). Images were taken at 1 μm spacing, 1 hour after each solution change. In addition to bright field images, fluorescent images were also collected to facilitate the measurement of bead position. The images from the CCD camera were digitized and saved for later analysis.

The z-locations of the beads as defined in Figure 3-1 were determined with subpixel accuracy. First, the user selected beads to be tracked on both the specimen and the glass slide. The location of each bead was detected by first isolating a $30 \times 30 \times 100$ pixel volume ($= 10.8 \times 10.8 \times 100$ μm^3 volume) surrounding the initial location of the bead. Power, P, in the z-plane is defined as

$$P(k) = \sum_i \sum_j B^2(i,j,k), \tag{3.1}$$

where i, j, and k are the digitized positions in the x, y, and z planes, respectively,

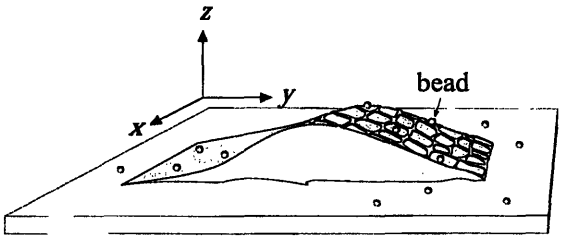

Figure 3-1: Schematic diagram of an isolated TM decorated with fluorescent beads. The x, y, z coordinates of bead locations are defined as shown.

and B is the digitized brightness. The k-plane for which the power was maximum is k_{max}. Sub-pixel resolution was obtained by interpolating the power function as a function of k and determining the value of z at peak power. This value of z has sub-pixel accuracy. The interpolation was done by determining a least-squared fit of a quadratic function to the power values at k_{max} and 3 planes on either side of k_{max}.

The x and y locations of beads could change from image to image for two reasons. The beads could change locations with respect to the glass slide on which the TM was mounted and the glass slide position could change. To determine the latter motion, we tracked marker beads attached to the glass slide. The transformation (both translation and rotation) from the first image to all later images was determined for these marker beads. The same transformation was applied to all beads in that image. This process corrected the bead positions for changes in position of the slide between images. Once every image was corrected for motion of the slide, corresponding beads were found by finding the bead with the smallest squared distance from the original position of the bead. Video images were reviewed to visually confirm the matches between corresponding beads.

Solution exchange protocol

The viscosity of solutions that contain PEG increases with both the MW and concentration of PEG. When either PEG MW or concentration was large, the resulting fluid was too viscous to be perfused by peristaltic pumps. Therefore, all solution changes were done manually by transferring the old solution out and perfusing the new solution into the chamber with a micropipette. For each solution change, this procedure

was repeated at least four times to minimize contamination of the current test solution with the previous one. Moreover, for all experiments using PEG of different MW, care was taken to perfuse the specimen with higher MW PEG first to minimize the chance that smaller MW PEGs diffused into the specimen. Finally, between every change of solution osmotic pressure or PEG MW, the bathing solution was changed to AE to determine whether the specimen returned to its isotonic volume.

Data analysis

To characterize TM thickness, we measured the z-positions of beads relative to that of the underlying glass as follows. First, the positions (x_n, y_n, z_n) of each of the n beads attached to the glass surface were determined. A plane of the form

$$z_{\text{glass}}(x, y) = ax + by + c \tag{3.2}$$

was then fit to these positions by finding the values of a, b, and c that minimize the sum of squared differences

$$\sum_n (z_n - z_{\text{glass}}(x_n, y_n))^2. \tag{3.3}$$

The measured positions (x_m, y_m, z_m) of each bead on the TM then provided an estimate of TM thickness at the point (x_m, y_m):

$$\Delta z(x_m, y_m) = z_m - z_{\text{glass}}(x_m, y_m). \tag{3.4}$$

To determine the relation between strain and stress for the TM, we measured TM thicknesses in baths with different concentrations of PEG with different indices of refraction. Therefore, we had to insure that measurements of bead position in different solutions were not affected by differences in solution index of refraction. Since our measurements were obtained with a water immersion microscope objective, the primary affect of the change in index of refraction is a change in the plane of best focus of the objective. Each of our measurements of TM thickness is based on the

difference in the z-positions of pairs of beads that were both measured in the same solution of PEG. Thus the difference should be insensitive to PEG concentration. To test this idea, we measured the thickness of a microfabricated test structure whose thickness was independently determined to be 14 μm. The measured thickness of the structure differed by less than 0.19 μm when measured with water and when measured with the highest concentration of PEG (511,000 Da) used in this study.

The ratio of bead height in the presence of PEG to that in its absence is the fractional bead height, v_z, caused by the osmotic pressure of PEG. The z-component of the strain, ϵ_z, is calculated from v_z by the relation

$$\epsilon_z = 1 - v_z. \tag{3.5}$$

3.2.2 Osmotic pressure of PEG solutions

The osmotic pressure of PEG solutions for high MW PEG cannot be measured reliably with a conventional vapor-pressure osmometer; more sophisticated methods are required (Hasse et al., 1995). In addition, the osmotic pressure of PEG solutions does not obey van't Hoff's law so that it cannot be computed as proportional to the PEG concentration. Fortunately, a model has been developed for the dependence of the osmotic pressure of PEG solutions on both the concentration of PEG and its MW which fits the measurements well for $200 \leq \text{MW} \leq 40,000$ Da. We have used PEGs with MW above this range and hence we have checked the validity of the model for the higher MW used in our experiments.

Model for osmotic pressure of PEG

The osmotic pressure of an ideal solution is defined by van't Hoff's law

$$\pi_s = RTC_s, \tag{3.6}$$

where R is the molar gas constant, T is the absolute temperature, and C_s is the total concentration of solute.

However, experimental measurements have shown that the relation between PEG concentration and osmotic pressure deviates significantly from van't Hoff's law in two ways (Parsegian et al., 1988; Schiller et al., 1988; Hasse et al., 1995). The osmotic pressure is a non-linear function of concentration and depends upon MW. Therefore, osmotic pressure is not a colligative property for PEG solutions.

For a non-ideal solution, the osmotic pressure, π_s, can be expressed as

$$\pi_s = RTC_sM_s\left(\frac{1}{M_s} + \alpha C_s + \beta {C_s}^2 + ...\right), \tag{3.7}$$

where M_s is the molecular weight of the solute, and α and β are the virial coefficients. The first term in this expression describes van't Hoff's law. The virial coefficients of PEG in aqueous solution were determined using both laser-light scattering data and isopiestic data (Hasse et al., 1995) and are given by the following equations,

$$\alpha = 2.49\left(\frac{1}{T} - \frac{1}{T_\theta}\right), \tag{3.8}$$

$$\beta = 29.3\left(\frac{1}{T} - \frac{1}{T_\theta}\right), \tag{3.9}$$

where the reference temperature $T_\theta = 375.5$ K. α has units of mol·cm^3/g^2 and β has units of mol·cm^6/g^3. The virial coefficients, α and β, are independent of MW within the range 200-40,000 Da.

Figure 3-2 shows the dependence of osmotic pressure on PEG concentration and MW predicted by this theory. The deviation of osmotic pressure from van't Hoff's law increases as both the PEG concentration and the MW increase.

Tests with PMAA gels

In order to determine whether the theory described by Equations 3.7-3.9 could be extrapolated to the range of PEG MWs we used in experiments on the TM, we tested the theory by measuring the stress-strain relation of a PMAA gels whose stress-strain relations had been measured using hydraulic pressure.

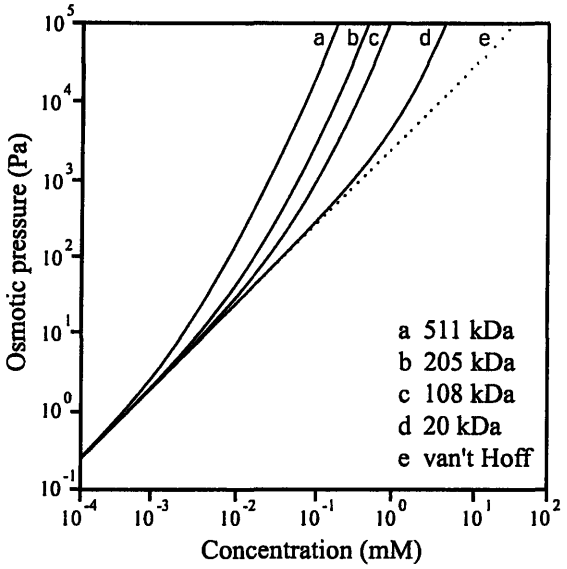

Figure 3-2: Osmotic pressure for PEG of different MW as a function of concentration. The dotted line represents the relation between osmotic pressure and concentration given by van't Hoff's law which is independent of MW. The solid curves show the relation between pressure and concentration according to Equations 3.7-3.9 with T = 298 K.

Method of making polymethacrylic acid (PMAA) gels The composition of the PMAA gel was as described previously (Quinn and Grodzinsky, 1993). However, to mimic the TM experiment as closely as possible, the PMAA gels were stuck on a glass slide and had a maximum thickness of about 100 μm. The gel was polymerized on a pre-treated glass slide. The glass slide was treated by spin-coating a solution containing 3 mL of distilled water, 1.8 mL of acetic acid, and 1.2 mL of 3-(Trimethoxysilyl)propyl methacrylate 98% solution (Ngola et al., 2001). Once the glass slide was treated, less than 1 μL of gel solution was pipetted on the glass slide and a coverslip was placed on top of the gel solution. Another glass slide was placed on top of the coverslip so that the coverslip could be clamped into position. The whole ensemble was placed in a 60 degree water bath for 4 hours to allow the gel further time to polymerize. After polymerization, the glass slide and cover slip that covered the PMAA gel were removed and the gel was washed overnight in deionized water. The gel was then placed in an unbuffered 50 mM KCl solution at pH 11 for 2 days.

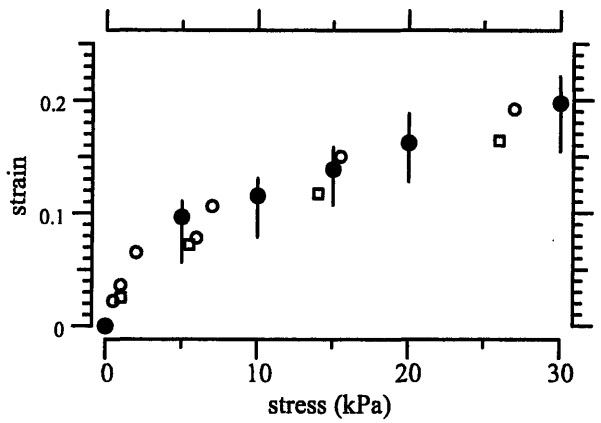

Figure 3-3: Equilibrium stress-strain relation of a PMAA gel. The filled circles represent the median value of the strain for a given stress applied using PEG solutions to exert osmotic pressure. The vertical lines shows the interquartile range. The solutions contained 174 mM KCl. The open symbols represent the stress-strain relation measured using hydraulic pressure with a dynastat in different KCl concentrations; open circles and open squares represent KCl concentration of 100 mM and 200 mM, respectively (Quinn and Grodzinsky, 1993).

Stress-strain relations of PMAA gels obtained with both osmotic pressure using PEG solutions and with hydraulic pressure Using methods identical to those used to measure the stress-strain relation of the TM, we measured the stress-strain relation of PMAA gels using PEG with a MW of 511 kDa. The PEG concentrations were calculated according to Equations 3.7-3.9 to achieve a desired osmotic pressure in the range 0-30 kPa. Higher osmotic pressures could not be applied since the PEG solutions became too viscous. However, the maximum osmotic pressure used (30 kPa) on the PMAA gels exceeded the maximum used on the TM (10 kPa).

The stress-strain relation of the PMAA gel is shown in Figure 3-3 both for our measurements using PEG to generate osmotic stress and for measurements on similar gels using hydraulic pressure applied in a dynastat (Quinn and Grodzinsky, 1993). The fact that the stress-strain relation obtained osmotically is similar to that obtained hydraulically suggests that the osmotic pressure obtained using Equations 3.7-3.9 is valid for MW as high as 511 kDa and osmotic pressure as high as 30 kDa. Therefore, we have used these equations to compute the osmotic pressure of PEG solutions in experiments on the TM.

3.2.3 Preparation of the TM

Adult male mice (strain ICR, 25-32 grams, Taconic) were asphyxiated with CO_2 and then decapitated. The pinnae and surrounding tissues were removed and the temporal bone was isolated. Both the oval and round windows were opened and AE solution was perfused into the round window to flush out the perilymph. This was done to reduce TM exposure to perilymph to which the TM is not normally exposed in situ. Under a dissecting microscope, the temporal bone was chipped away to isolate the cochlea. The cochlea was then placed in AE and the rest of the surgery was done in a petri dish filled with AE. The microscope illumination was adjusted between bright field and dark field illumination so that the TM could be identified. The TM was isolated from the rest of the cochlea using an eyelash. Tissue adhesive (Cell Tak, Collaborative Research, Bedford, MA) was placed at the bottom of the experimental chamber and washed with both ethanol and deionized water. Using a micropipette with a glass tip, the TM was transferred from the petri dish to the experimental chamber filled with AE. The TM was positioned on the Cell Tak with an eyelash to prevent the TM from drifting around in the chamber once the experiment started. The TM could land with the covernet up or down because we saw no significant difference in the stress-strain relation for the two conditions. Therefore, covernet orientation is not reported here. To improve visualization of the TM surface, beads with diameters of approximately 1 μm and maximum excitation wavelength of 488 nm and maximum emission wavelength of 560 nm were pipetted onto both the TM and the glass slide.

The care and use of animals reported in this study were approved by the Massachusetts Institute of Technology Committee on Animal Care.

3.3 Results

3.3.1 Effect of PEG on TM structure

Effect on TM fibrillar structure

To determine the effect of PEG on TM fibrillar structure, bright field images of the TM were taken throughout the experiment as shown in Figure 3-4. Figure 3-4a shows an image taken at the beginning of the experiment in AE. Radial and longitudinal fibers as well as Hensen's stripe and the limbal attachment are prominent. Figure 3-4b shows the TM when immersed in AE solution containing PEG of MW 511 kDa exerting an osmotic pressure of 10 kPa. In this focal plane, both the radial and longitudinal fibers are still discernible although less prominent than in Figure 3-4a, but Hensen's stripe and the limbal attachment are barely discernible. When returned to AE solution (Figure 3-4c), the TM appearance is similar to that seen at the beginning of the experiment (Figure 3-4a). Thus, the fibrillar structure of the TM seen in light microscopy showed reversible changes in response to changes in osmotic pressure. Furthermore, in measurements with PEGs of different MWs and different osmotic pressures, it was our impression that it was the osmotic pressure, rather than either the PEG MW or concentration, that resulted in these reversible changes in the fibrillar structure.

Effect of PEG on TM thickness

The effect of PEG on TM thickness is illustrated in Figure 3-5 which shows fluorescent images of the beads on both the TM and the glass slide taken at different focal planes and in different bathing solutions. Initially, when the TM was immersed in AE solution, the fluorescent beads were in focus 40 μm from the glass slide indicating that the TM at this location was 40 μm thick. In the presence of an AE solution containing PEG with a MW of 511 kDa with an osmotic pressure of 250 Pa, the beads were in focus 30 μm from the glass slide indicating that the TM shrank by 10 μm. Finally, when the TM was returned to AE solution, the beads on the top of

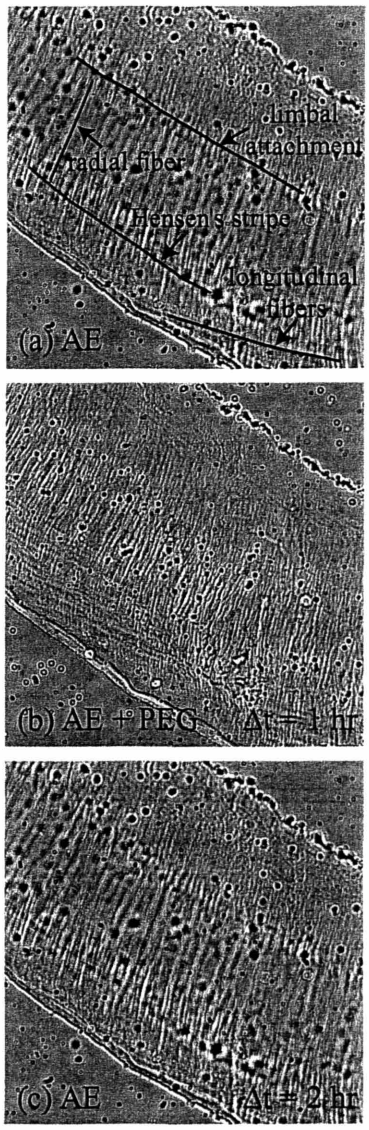

Figure 3-4: Bright field images of the TM when exposed to (a) AE, (b) AE + PEG with MW 511 kDa at a concentration required to apply an osmotic pressure of 10 kPa, (c) AE. Images were normalized by dividing each pixel by the average value of its neighbors in a 51 x 51 pixel region. One longitudinal and radial fiber, Hensen's stripe and limbal attachment have been traced in (a). Δt, shown in the lower right of panel (b) and (c), represents the time elapsed since image (a) was obtained.

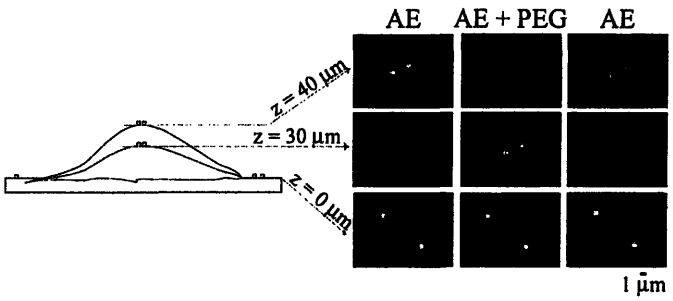

Figure 3-5: The right side shows fluorescent images of two beads on the TM and two on the glass slide. The columns correspond to different bathing solutions. Each row shows images in a different focal plane. The left side shows a schematic diagram of the profile of the TM and glass slide. In AE, the beads are in focus at a height of 40 μm. When PEG is added to the AE solution, the TM shrinks and hence the two beads on the surface of the TM are in focus at 30 μm. The beads on the surface of the glass slide remain in focus at the same height in both solutions.

the TM were in focus 40 μm from the glass slide indicating that the TM returned to approximately its original thickness. These results indicate that the thickness of the TM shows reversible shrinkage in response to increases in osmotic pressure.

3.3.2 Dependence of TM strain on PEG MW for isosmotic solutions

A previous study showed that increasing the osmotic pressure of the bathing solution produced quite different changes in TM thickness when different solutes were used. Addition of 10 mmol/L of glucose produced no discernible change in thickness, whereas addition of 10 mmol/L of PEG with MW of 20 kDa produced a sustained shrinkage of the TM (Freeman, Masaki, McAllister, Wei and Weiss, 2003, see figure 17). This was interpreted to indicate that glucose freely penetrated the TM and hence did not produce an osmotic effect. In contrast, PEG with MW of 20 kDa did not penetrate the TM as freely as did glucose.

To determine the extent to which PEG penetrates the TM, we measured the TM thickness for PEG of different MWs at the same osmotic pressure of 250 Pa. The concentration of PEG required to obtain an osmotic pressure of 250 Pa was determined by Equations 3.7-3.9. Figure 3-6 shows the change in TM thickness for 3 experiments

when the TM was exposed to solutions containing PEG with different MWs. Almost all the points lie below a line of unity slope indicating that for all MWs the TM shrank in response to an increase in osmotic pressure. To a first order, changes in thickness at each osmotic pressure are proportional to the original thickness over most of the TM. These results are consistent with those seen in a previous study (Shah et al., 1995). However, with closer analysis, dependence on radial position was seen as shown in section 3.3.4. Note also that the slope of the regression line is appreciably higher for MW of 20 and 40 kDa than for the other MWs indicating that the shrinkage of the TM is smaller at the lower MWs. This point is made more clearly in Figure 3-7 which summarizes the data of Figure 3-6 by plotting the strain as a function of PEG MW. The strain was computed from the fractional change in TM thickness by Equation 3.5. For PEG MW $\geq$ 200 kDa, the average TM strain is independent of MW. However, for MW $\leq$ 100 kDa, the TM strain is appreciably smaller. To determine whether the difference in strain between lower and higher MWs is statistically significant, the mean and standard error of the mean are plotted in Figure 3-8 for both lower and higher MW. A t-test of these data showed that the difference in mean strains between these two populations was highly significant (p-value of 1.6×10^{-22}).

3.3.3 Average stress-strain relation of the TM

The stress-strain relation was measured in 16 segments of the TM; 11 from the apical-middle regions of the TM and 5 from the basal region. Their larger size makes apical-middle segments easier to manipulate than basal segments. The stress-strain relation was measured in the two regions of the TM in order to determine whether this relation varied with longitudinal position in the cochlea.

Nonlinear stress-strain function

To determine the stress-strain relation of the TM, stress was applied by subjecting the TM to osmotic pressure in the range 0.025-10 kPa with solutions that contained PEG with a MW of 511 kDa. At this MW, PEG does not appear to permeate the

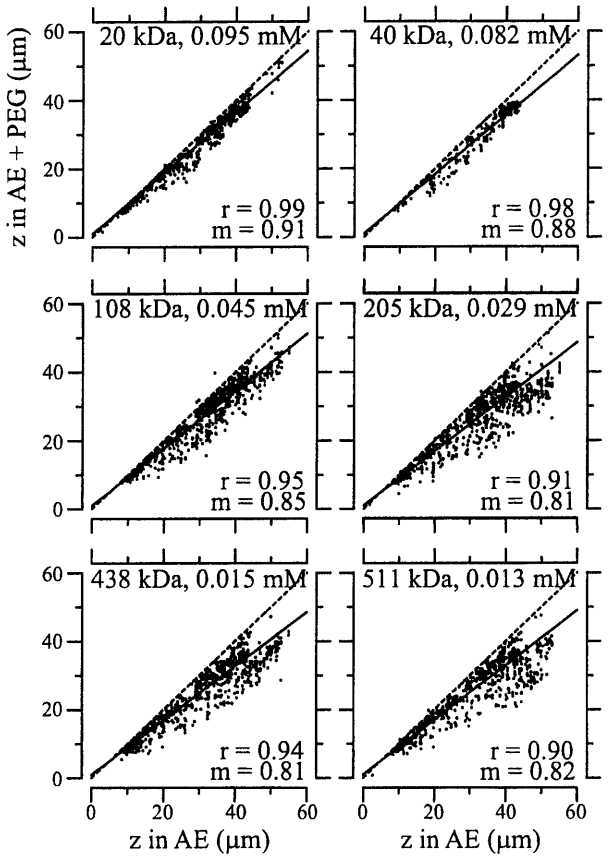

Figure 3-6: Effect of isosmotic solutions with different PEG MW on TM thickness. Thickness (z) of TMs from the apical-middle regions in PEG solutions versus that in the absence of PEG. Each solution contained AE. Different concentrations of PEG were added to each solution so that the osmotic pressure exerted by that particular MW PEG was equal to 250 Pa according to Equations 3.7-3.9. Each dot represents one bead on one of 3 TMs. The solid and dashed lines represent a regression line fit to the data and a line of unity slope, respectively. The values of the slope and correlation coefficient of the regression lines are given by m and r, respectively.

TM appreciably. Thus, PEG should exert its full osmotic pressure. We measured the change in thickness of the TM relative to its thickness in AE solutions that contained no PEG and used Equation 3.5 to compute the strain.

Figure 3-9 shows the change in TM thickness relative to its original thickness for all the beads in 11 experiments from the apical-middle region of the cochlea when the TM was exposed to solutions of different osmotic pressures. The vast preponderance of the data points fell below a line of equality showing that the TM shrank in response to an increase in osmotic pressure. The slope of the solid line represents the median fractional change in TM thickness for a given osmotic pressure. As the osmotic

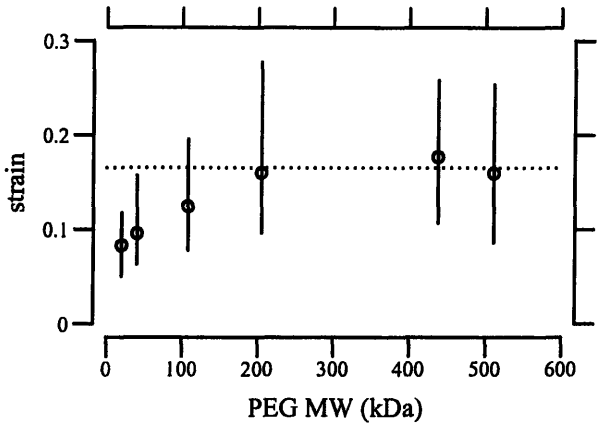

Figure 3-7: TM strain as a function of PEG MW for an applied osmotic pressure of 250 Pa. This plot summarizes data from the same experiments as in Figure 3-6. The circles represents the median strain. The lengths of the solid vertical lines indicate the interquartile range of the measurements. The horizontal line is at a strain of 0.16, which is the average value for MW $\geq$ 200 kDa.

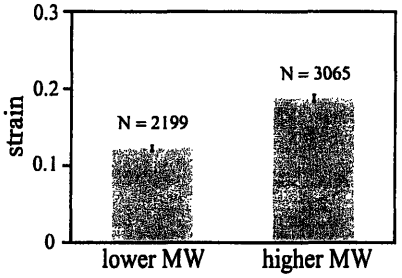

Figure 3-8: Histogram of strain for two ranges of MW; same data as in Figure 3-7. The lower MW includes all the data for MW $\leq$ 100 kDa and the higher MW includes all the data for MW $\geq$ 200 kDa. The height of each bar equals the mean strain and the vertical line segments have lengths that equal twice the standard error of the mean. N is the number of data points.

pressure increased, the TM shrank more as indicated by the decrease in the slope of the regression line. The correlation coefficient of the fit also decreased from 0.99 at low osmotic pressures when there was little shrinkage of the TM to 0.68 at the highest osmotic pressure when the shrinkage of the TM was appreciable.

Figure 3-10 shows the measured strain as a function of applied stress for one TM from the apical-middle region. Previous researchers (Quinn and Grodzinsky, 1993), who measured stress-strain relations of polyelectrolyte gels, found it useful to fit their measurements with power functions. Therefore, we tried to fit the stress-strain relation of the TM with the following power function

$$\epsilon_z = a\sigma^b, \tag{3.10}$$

where σ is the stress and ϵ_z is the $z-$component of the strain. We fit this power function to the measured stress-strain relation of each TM so as to minimize the mean squared error between the measurements and the power function in log-log coordinates. Each fit yielded estimates of the parameters of the power function. The fit of a power function to the measurements of one TM is shown in Figure 3-10.

For the j^{th} TM we obtained the estimates of the power function parameters $\{a_j, b_j\}$. The median and interquartile range of these estimates were $\{\tilde{a},\tilde{b}\}$ and $\{\text{IQR}_a,\text{IQR}_b\}$, respectively. Figure 3-11 summarizes the fit of the power law to all our data from apical-middle and basal segments of the TM plotted in logarithmic coordinates, which plot a power function as a straight line. The apical-middle data are from the same 11 experiments as in Figure 3-9. The composite data are fit closely by a power function over most of the range of stress. The parameters of the fit of power functions to the stress-strain functions are shown in Table 3.1. Since the data from all apical-middle sections of the TM were pooled, irrespective of radial or longitudinal position within the segments, the results reflect the strain averaged over location in the TM segment for this region.

The power function fit to our data is least satisfactory at the lowest range of stress, which is the most important range for the stress generated in response to acoustic stimulation of the ear. Hence, we estimated the chord longitudinal modulus at the lowest stresses with linear regression. This analysis yielded median longitudinal modulus of 0.45 kPa with an interquartile range of 0.3 kPa. This estimate of longitudinal modulus is not very different from that shown in Table 3.1 at the lowest stress.

Modulus-stress function

Because the stress-strain function of the TM is nonlinear, the bulk modulus is not uniquely defined. Moreover, the strains in the radial and longitudinal directions were small (Shah et al., 1995), hence the moduli that was measured is the longitudinal

	Apical-middle	Basal
N	11	5
Stress-strain function fits		
$\tilde{a}$, IQR_a	0.31, 0.11	0.10, 0.10
$\tilde{b}$, IQR_b	0.31, 0.08	0.21, 0.19
Modulus-stress function fits		
$\tilde{M}_c$, IQR_M (@ 25 Pa)	0.47, 0.11 kPa	0.53, 0.34 kPa
$\tilde{M}_c$, IQR_M (@ 5 kPa)	11.52, 4.02 kPa	24.92, 69.66 kPa
$\tilde{c}$, IQR_c	3.26, 1.41 kPa	10.12, 11.72 kPa
$\tilde{d}$, IQR_d	0.69, 0.06	0.78, 0.19
TM thickness		
$\tilde{h}$, IQR_h	43.75, 6.00 μm	31.60, 4.50 μm

Table 3.1: Results obtained for apical-middle and basal segments of the TM. N is the number of TMs. Estimates are given of the parameters of power functions fit to measured stress-strain functions and modulus-stress functions. The value of the chord modulus (kPa) is shown at a low stress (25 Pa) and high stress (5 kPa). The thickness of each TM was measured at Hensen's stripe when the TM was immersed in AE. The median and interquartile range, IQR, are given for each variable.

modulus (Quinn and Grodzinsky, 1993). The *chord* and *slope* longitudinal modulus, M_c and M_s, respectively, can be defined in terms of the z-component of the strain as follows,

$$M_c = \frac{\sigma}{\epsilon_z} \quad \text{and} \quad M_s = \frac{d\sigma}{d\epsilon_z}, \tag{3.11}$$

where both moduli depend upon the stress. If the stress-strain function is a power function as in Equation 3.10, then the two moduli become

$$M_c = \frac{\sigma^{1-b}}{a} \quad \text{and} \quad M_s = \frac{\sigma^{1-b}}{ab}, \tag{3.12}$$

which shows that the two moduli differ only by a factor of b. The modulus-stress function is also a power function but the exponent differs from that of the stress-strain function.

Since calculation of the slope modulus is inherently more variable because first differences of strain values are taken, and since the slope modulus gives no additional information over the chord modulus, we computed the chord modulus directly from the measured data and plotted this modulus against the applied stress (Figure 3-12). Once again the data are plotted in logarithmic coordinates so that power functions plot as straight lines. The results show that the chord modulus increases with stress approximately as a power function for both the apical-middle and basal TM segments. The largest deviations are at low stress, when the modulus increases for apical-middle segments. We do not expect the power function to fit the measurements at asymptotically low stresses since the power function predicts that the modulus goes to zero at low stress, which is not reasonable. However, the results show directly that the TM becomes stiffer with increasing stress. To estimate the parameters of the power function we fit the data with power functions of the form

$$M_c = c\sigma^d, \tag{3.13}$$

and the results are summarized in Table 3.1.

3.3.4 Spatial dependence of the stress-strain relation of TM

Dependence on the radial direction

Figure 3-13 shows the distribution of beads on the TM as a function of radial position along the TM both in AE and in AE with a concentration of PEG to increase the osmotic pressure by 10 kPa. Radial position was measured from the outer edge of the TM because this edge was better defined than was the inner edge. These results are plotted irrespective of longitudinal distance along the TM. In AE, the thickness of the radial profile has a broad maximum in the region near the limbal attachment of the TM; the TM is much thinner at its edges. With an increase in osmotic pressure, the TM thickness decreases at virtually all radial positions. This general pattern in the radial dependence of TM thickness and its dependence on osmotic pressure was seen in all our results. The change in thickness was largest for the largest osmotic

pressures.

To determine whether there is a radial dependence to *strain*, we examined strain as a function of radial position for all the data. We selected data obtained at an osmotic pressure of 10 kPa for detailed comparison because the osmotically induced displacements were largest at this high osmotic pressure so that strain could be computed over a large radial extent. The strain computed from the measurements shown in Figure 3-13 is plotted on the top panel of Figure 3-14. This is an example of a TM that showed a small but systematic decrease in strain in the radial direction. In particular, in 6 of the 7 TMs the strain was somewhat larger in the outer region of the TM between the outer edge and the limbal zone attachment than in the inner region between the limbal zone attachment and the inner edge. These two regions have been called the *middle and marginal zone* and the *limbal zone*, respectively (Lim, 1972). Results from one TM (bottom panel in Figure 3-14) showed a different pattern of radial dependence of strain.

To summarize our results we pooled the data from all 7 TMs. For each TM, we combined all the data from the outer portion of the TM and computed the mean of those results. Because the strain at 10 kPa varied from one TM to another, we normalized all the strains to the mean strain in the outer region. The pooled results are shown in Figure 3-15. The histogram shows that there is a small difference in strain between the outer and inner regions of the TM, which a t-test shows is a highly significant difference (p-value of 2.0×10^{-11}). The strain in the inner region is about 20% smaller than in the outer region suggesting that the inner region is about 20% stiffer than the outer region.

Dependence on the longitudinal direction

The most direct way to examine the longitudinal dependence of strain is to compare the results from the apical-middle region with those from the basal region. Figure 3-11 compares the stress-strain relation for the 11 apical-middle segments with the 5 basal segments of the TM. The strain is systematically larger in apical-middle segments than in basal segments. Comparison of the parameters of the fit of the power law to stress-

strain functions (Table 3.1) show that there is only a small difference in exponent b but that the strain scale factor a is appreciably larger in apical-middle segments than in basal segments. Consistent with these results, the chord modulus computed from the stress-strain function (Figure 3-12 and Table 3.1) also shows that the exponent of the power function does not differ greatly between apical-middle and basal segments, but the scale factor is larger for basal segments indicating that the basal segments are stiffer than apical-middle segments. Furthermore, if both the stress-strain and modulus-stress functions are consistent power functions, the exponent d should equal $1 - b$ which it does approximately. Finally, the chord bulk modulus at the lowest stresses was estimated with linear regression to be 0.88 kPa with an interquartile range of 0.64 kPa. This value is within the range of longitudinal modulus values for a basal segment shown in Table 1 at the lowest strain.

3.3.5 Thickness of the TM

To see if the geometry of the TM might be related to the difference in stress-strain functions, we measured the thickness of each TM. The results (Table 3.1) show that the apical-middle segments were significantly thicker than basal segments.

3.4 Discussion

3.4.1 Use of osmotic pressure to apply stress

Use of osmotic pressure to apply mechanical stress to the TM has some desirable features. No mechanical contact with the TM is required; stress is applied by changing the chemical composition of the bathing solution. In contrast, the use of mechanical probes to apply stress to the TM yields mechanical characteristics that depend upon the dimensions of the probe. Thus, the osmotic pressure method is suitable for measuring bulk mechanical properties of small, fragile tissue of non-uniform geometry that are easily damaged by mechanical probes. The principal disadvantage of the method is that only static, equilibrium properties of these tissues can be measured;

other methods are required to measure dynamic mechanical characteristics.

Non-osmotic effects of PEG on the TM

Our intention was to use PEG to change the osmotic pressure of the bathing solution. We now consider whether or not it is likely that PEG produced other, unintended effects on the TM. Figure 3-4 indicates that the effects of PEG on the appearance of the TM in light microscopy are reversible. Furthermore, we observed that the effect of PEG on the TM architecture varied with applied stress rather than with PEG MW or concentration.

Since the TM is very sensitive to Ca^{+2} concentration (Shah et al., 1995), perhaps PEG interacts with the Ca^{+2} in the bath solution. If PEG were to bind Ca^{+2}, the Ca^{+2} concentration in the bath would decrease causing the TM to swell (Shah et al., 1995). However, Figure 3-11 shows that increasing the PEG concentration results in shrinkage of the TM. Alternatively, PEG might release bound Ca^{+2} from the TM, thereby, increasing the Ca^{+2} concentration in the bath. However, previous studies have shown that even if the concentration increased 100 fold (i.e. from 20 μM to 2 mM), the TM would only shrink 0.7 μm or approximately 1.75% (Shah et al., 1995). Therefore, the primary effect of PEG could not be the binding of Ca^{+2}. In general, the effects of changes in electrolyte concentration produce much smaller changes in TM volume than do changes in osmotic pressure. It seems most likely that the changes in the TM in response to changes in PEG concentration are due to changes in osmotic pressure.

Equivalence of osmotic and hydraulic pressure

Theories assume (Van't Hoff, 1886) and measurements confirm (Mauro, 1957) that osmotic and hydraulic pressures are equivalent. This equivalence has been noted in measurements on connective tissues (Maroudas and Bannon, 1981; Schneiderman et al., 1986; Basser et al., 1998). Because the osmotic pressure of a PEG solution depends nonlinearly on both the concentration and MW of PEG (Figure 3-2), establishing this equivalence is not trivial. Using a theory for dependence of osmotic

pressure on PEG concentration and MW (Hasse et al., 1995) allowed us to compute the osmotic pressure of our solutions. We tested the equivalence of hydraulic and osmotic pressure on PMAA gels (Figure 3-3). The results showed the strain on the gel were the same for hydraulic pressures that were equivalent to osmotic pressures predicted by the theory even at relatively high stress. This was strong evidence that osmotic pressure could be used to apply a known mechanical stress to the TM.

3.4.2 TM filtration

Reflection coefficient

If PEG were excluded from the TM for all MW of PEG, we would expect the strain produced by a fixed stress to be independent of MW. The results (Figure 3-7) show that this is indeed the case for MW $\geq$ 200 kDa, but not below that value. Thus, below 200 kDa the osmotic pressure of PEG is not fully expressed. The extent to which osmotic pressure is fully expressed or not can be quantified by the reflection coefficient, ρ, which is the ratio of the effective osmotic pressure to the osmotic pressure (Weiss, 1996),

$$\rho = \frac{\sigma_{\text{eff}}}{\sigma}. \tag{3.14}$$

If we use the power function fit of the data, then we get

$$\rho = \frac{(\epsilon_{z,\text{eff}}/a)^{1/b}}{(\epsilon_z/a)^{1/b}} = \left(\frac{\epsilon_{z,\text{eff}}}{\epsilon_z}\right)^{1/b}, \tag{3.15}$$

where $\epsilon_{z,\text{eff}}$ is the measured strain and ϵ_z is the strain expected if the osmotic pressure were fully expressed. Thus, Figure 3-7 can be recast as a plot of the reflection coefficient as a function of MW (Figure 3-16). The reflection coefficient approaches unity for MW $\geq$ 200 kDa indicating that the osmotic pressure is fully expressed, i.e., PEG is fully reflected from the TM. Below that value, the effective osmotic pressure is lower than the osmotic pressure calculated from the PEG concentration and MW, i.e., PEG permeates the TM to some extent. If PEG permeated the TM freely, the

reflection coefficient would be zero.

Estimation of the maximum pore radius of the TM

One simple mechanism that accounts for an effective osmotic pressure that is less than the osmotic pressure of the solution is for PEG to enter the TM. With this interpretation, Figure 3-16 indicates that PEG with MW $\geq$ 200 kDa is excluded from the TM, but below that value PEG permeates the TM. Thus, the results from Figure 3-7 can be used to estimate the *pore radius* of the TM. First, we need to compute the radius of PEG for different MWs. The radius of gyration of PEG, which defines the thickness of the shell surrounding PEG, has been determined experimentally (Bhat and Timasheff, 1992). The radius of gyration is

$$R_g = \left(\frac{3\eta W}{10\pi N \zeta^3} \right)^{\frac{1}{3}}, \tag{3.16}$$

where W is the MW of PEG, N is the Avogadro number and ζ is the Flory-Fox parameter which is taken as 0.8. η is the intrinsic viscosity of PEG solution, which is

$$\eta = 0.0646 W^{0.645}. \tag{3.17}$$

Figure 3-17 shows the radius of gyration calculated using Equations 3.16 and 3.17 as a function of PEG MW. PEG with MW $\geq$ 200 kDa is excluded from the TM. The radius of gyration of PEG with a MW of 200 kDa is about 22 nm. Thus, we infer that the maximum pore radius of the TM is approximately 22 nm. This is a conservative figure since the probe PEG molecules we used have a distribution of MWs. For example, PEG with a nominal MW of 100 kDa contains a small fraction of PEG molecules with lower and higher MWs. Thus, the fact that the reflection coefficient is less than 1 at a MW of 100 kDa (Figure 3-16) may have resulted from a small amount of lower MW PEG in solution. Thus, the maximum pore radius is likely to be somewhat smaller than 22 nm. In any case, these results imply that ions and small solutes can freely diffuse into the TM but larger organic molecules such as proteins are excluded. The molecular architecture of the TM reveals the presence of weakly hydrated and

strongly hydrated type B protofibrils, which are linked together by staggering cross-bridges which occur at 12-15 nm intervals (Hasako and Richardson, 1988b). Thus, this fibrillar structure has dimensions of the right order of magnitude to form the pores that exclude high-MW PEG from the TM.

Pore dimensions play an important role in the dynamic mechanical properties of cartilage (Grodzinksy, 1983). Since the TM is made up of similar proteins we expect the pore dimensions to be important for TM dynamics as well. For example, we would expect the diffusion coefficient of ions in the TM and the osmotic permeability to decrease as the pore radius decreases. This would lead to an increase in the time constant of diffusion and osmosis and, thereby, decrease the rate of TM response to stimuli.

Caveat on the use of osmotic pressure to measure tissue mechanical properties

PEGs are available for a large range of MWs. We found that PEGs of different MWs produced different strains of the TM even when the stress applied was the same. We have interpreted this finding to indicate that low MW PEGs can permeate the TM and hence produce a smaller effective osmotic pressure than higher MW PEGs. Hence, use of PEG to apply a known mechanical stress to a tissue requires not only that the osmotic pressure be calculated correctly, but also that the PEG not permeate the tissue appreciably.

3.4.3 Comparison with previous measurements on the TM obtained with mechanical probes

The point stiffness of the TM has previously been measured by calibrated hairs (von Bekesy, 1960) and a glass micropette (Zwislocki and Cefaratti, 1989). These measurement techniques estimated the transverse point stiffness to be $0.1-10$ N/m and 0.125 N/m, respectively. Recently, the TM's dynamic point stiffness has also been measured using a magnetic bead (Abnet and Freeman, 2000; Freeman, Abnet, Hemmert,

Tsai and Weiss, 2003). From these measurements, the point stiffness at 10 Hz was found to be 0.14, 0.40, and 0.04–0.22 N/m in the longitudinal, radial, and transverse directions, respectively.

The relationship between point stiffness and longitudinal modulus depends on the mechanical properties of the TM. If we assume the material to be semi-infinite, homogeneous, and elastic, the relation between point stiffness, S, and longitudinal modulus, M, is given by

$$S = \frac{2Mr(1-2\nu)}{(1-\nu)^2}, \tag{3.18}$$

where r is the radius of the circular contact region, and ν is Poisson's ratio (Timoshenko and Goodier, 1970).

To test whether our point stiffness estimates agree with previously published results, we estimated r to be 10 μm for results obtained previously (Freeman, Abnet, Hemmert, Tsai and Weiss, 2003), ν to be close to 0 for the equilibrium condition at which M was measured and M to be 0.45 kPa. For the physiologically relevant M value, the linear regression fit to the chord modulus value measured at the lowest stress was used. However, it is important to keep in mind that this value is an upper bound on the actual physiologically relevant value. Using these numbers, the point stiffness was found to be around 0.009 N/m which is close to the lower end of the previously published results for transverse point stiffness. Moreover, *in vitro* we estimate r to be the radius of a hair bundle which is approximately 5 μm and take ν to be close to 0, the point stiffness is estimated to be around 0.014 N/m which is about an order of magnitude stiffer than hair bundles (0.001-0.006 N/m) (Langer et al., 2001). However, this conclusion needs to be checked with measurements of the dynamic bulk modulus of the TM at physiological stress levels.

3.4.4 Comparison to equilibrium longitudinal modulus of other connective tissues

The longitudinal modulus of the TM is compared to those of other connective tissues in Figure 3-18. As in the previous section, for the longitudinal modulus of the TM, the linear regression fit to the chord modulus value measured at the lowest stress was used. The longitudinal modulus of a number of connective tissues spans a range of 10^2 to 10^{10} Pa. The comparisons of bulk moduli among connective tissues must be viewed with caution. The stress-strain relations of most connective tissues are nonlinear, making estimation of a single value for the modulus somewhat arbitrary. Sources of variability for these measurements also result from differences in type of tissue specimens, species, methods, etc. Estimates are based on measurements of tension as well as compression. Nevertheless, the range of values for different connective tissues spans 8 orders of magnitude, so while one might argue about the exact rank order of tissues by their bulk moduli, the difference between the stiffest tissues and the least stiff tissues is not in doubt. The modulus of the TM is the smallest of those shown and is about 7 orders of magnitude lower than for mollusc shell, tooth enamel, cortical bone, and tooth dentin. It is also 4 orders of magnitude smaller than articular cartilage even though the solid compositions of the TM and articular cartilage are very similar. However, the TM (97% water) is more hydrated than is articular cartilage (65 % water). The longitudinal modulus of the TM is more compliant than either the sea anemone mesogloea and intraocular lens, two of the most flexile tissues tested.

3.4.5 Implications for a gel model of the TM

Previous measurements of the TM have been interpreted in terms of a model of the TM as a polyelectrolyte gel (Weiss and Freeman, 1997b; Weiss and Freeman, 1997a; Freeman, Masaki, McAllister, Wei and Weiss, 2003). In this model, the mechanical constitutive relation of the TM, which relates its change in volume to stress, obeys Hooke's law. That is, the *microscopic longitudinal modulus* of the model is constant.

The number of fixed charge in the model is also constant. Thus, it was of interest to see whether or not this model could fit the nonlinear stress-strain relation measured with PEG induced osmotic pressure changes.

With constant microscopic longitudinal modulus and fixed charge concentration, the gel model does produce a nonlinear stress-strain relation. However, we have not been able to fit the measurements with this model (Figure 3-19). When we chose either the microscopic bulk modulus or the fixed charge concentration to be functions of stress, it was possible to obtain adequate fits of our measurements (Figure 3-19). Another way of fitting the measurements is to assume that the TM is not homogeneous but instead consists of 2 different gels with different material properties; this model also fit the data as shown in Figure 3-19. These results show that the measurements can be fit either by a one-layer gel model with non-linear constitutive relations or by a two-layer gel model with linear constitutive relations. Our data are not sufficient to allow us to distinguish among these alternatives.

Even though the molecular orgin of the nonlinearity of the bulk modulus is unclear, the longitudinal modulus in conjunction with the pore radius provides a quantitative basis for developing a poroelastic model of the TM. The poroelastic model might describe the measured frequency dependence of TM properties such as shear impedance which has been shown to be inconsistent with simple viscoelastic models [40].

3.4.6 Spatial dependence of TM properties

The TM properties vary in both the radial and longitudinal directions. In the radial direction, Figure 3-14 shows that the strain is 20% smaller in the inner region than in the outer region for the same stress. These results are qualitatively similar to the shear modulus measurements made with atomic force microscope (AFM) (Shoelson et al., 2004), which also found that the TM is more rigid toward the inner zones. Both of these results imply that the hair bundles contact a more compliant region of the TM. Perhaps this pattern allows the compliance of the hair bundles to more closely match that of the TM.

However, unlike the AFM measurements, which found no trend in longitudinal

elasticity (Shoelson et al., 2004), Figure 3-11 shows that the basal region of the TM has a larger equilibrium longitudinal modulus than the apical region. In addition, results obtained by others (Edge et al., 1998; Keiler and Richter, 2001) as well as by us (Table 3.1) show that the TM thickness decreases from apex to base. The fact that TM dimensions and material properties vary from apex to base suggests that the TM may have a role in tonotopic organization of cochlear macromechanics as well as micromechanics.

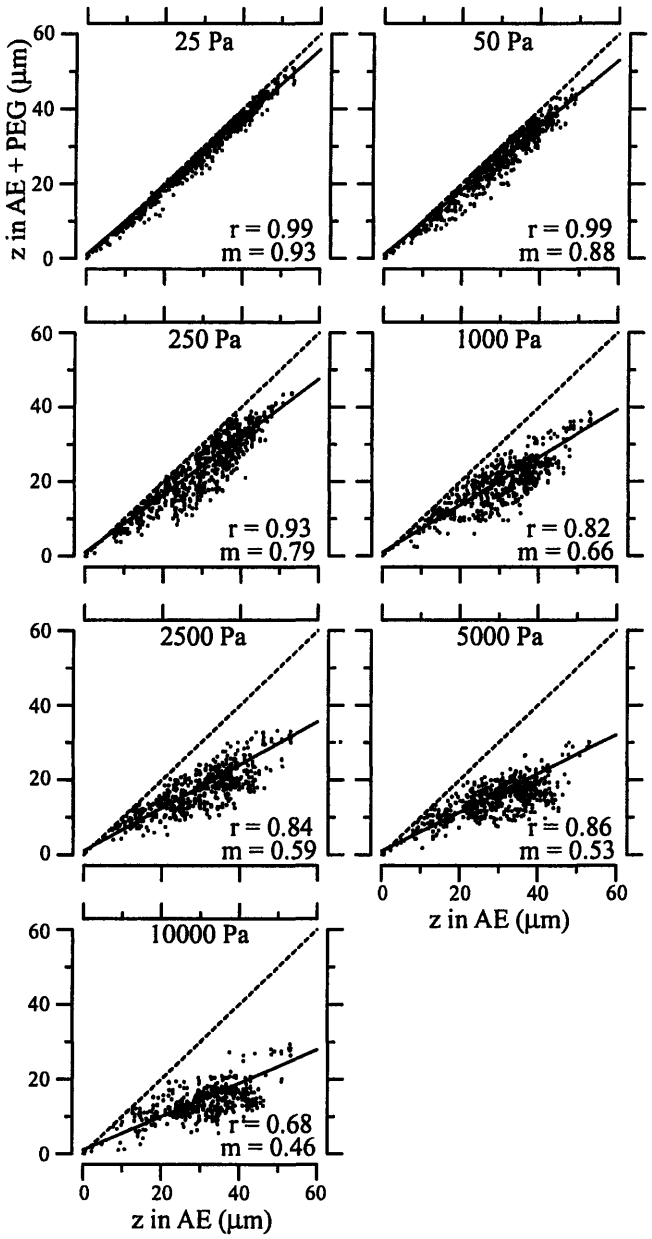

Figure 3-9: Effect of osmotic pressure on TM thickness. Thickness (z) of the TM in PEG solutions versus that in the absence of PEG. Only apical-middle segments of the TM were used. The PEG solutions were made with PEG with a MW of 511 kDa. Each dot represents one bead on one of the 11 TMs. The solid and dashed lines represent a regression line fit to the data and a line of unity slope, respectively. The values of the slope and correlation coefficient of the regression lines are given by m and r, respectively.

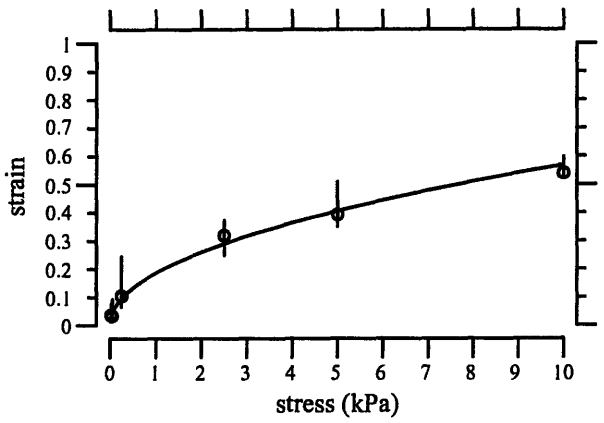

Figure 3-10: Strain as a function of applied stress for a TM segment from the apical-middle region. The strain was computed from the fractional change in TM thickness by Equation 3.5. The plot symbols are the median strains and the lengths of the vertical lines show the interquartile ranges of the measurements. The solid line is a power function fit to the data according to Equation 3.10 with $a = 0.24$ and $b = 0.36$.

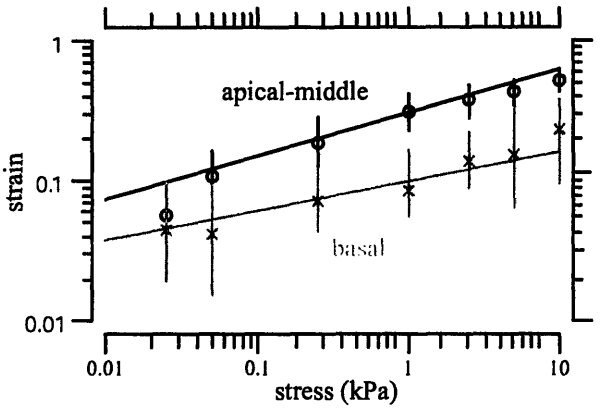

Figure 3-11: TM stress-strain functions for all of the basal and apical-middle segments of the TM. Plot symbols represent the median strains and the lengths of vertical lines show the interquartile ranges. The solid line is a power law fit to the data according to Equation 3.10 with $a = 0.31$ and $b = 0.31$ for the apical-middle segments and $a = 0.10$ and $b = 0.21$ for the basal segments. The basal data are grey to help distinguish them from the apical-middle data.

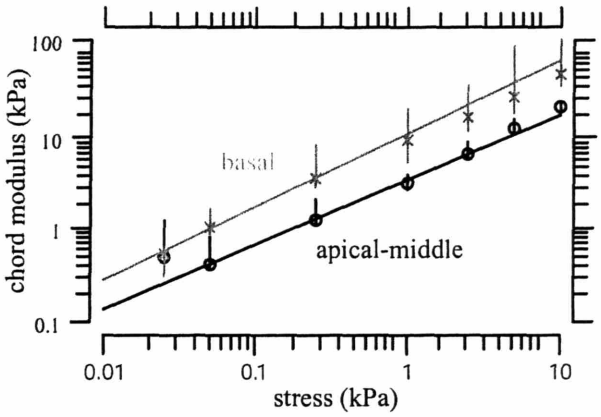

Figure 3-12: The chord modulus defined by Equation 3.11 was computed for all 11 apical-middle and all 5 basal segments. Plot symbols represent the median strain and the lengths of vertical lines shows the interquartile range. The lines through the data are regression line fit to the basal and apical-middle data whose parameters are given in Table 3.1. The basal data are grey to help distinguish them from the apical-middle data.

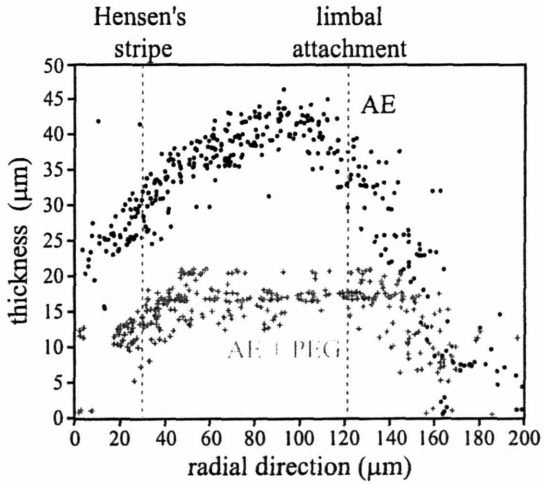

Figure 3-13: Example of the effect of osmotic pressure on TM thickness in the radial direction for one TM from the apical-middle region of the TM. Each dot represents the height of one bead on the TM when the TM is bathed in AE. The (+) symbols show the height of the same beads when the TM is immersed in AE plus PEG. A concentration of PEG, with a MW of 511 kDa, was used to produce an osmotic pressure of 10 kPa. Radial distance was measured from the outer edge toward the modiolus. The locations of anatomical landmarks are indicated by dotted vertical lines.

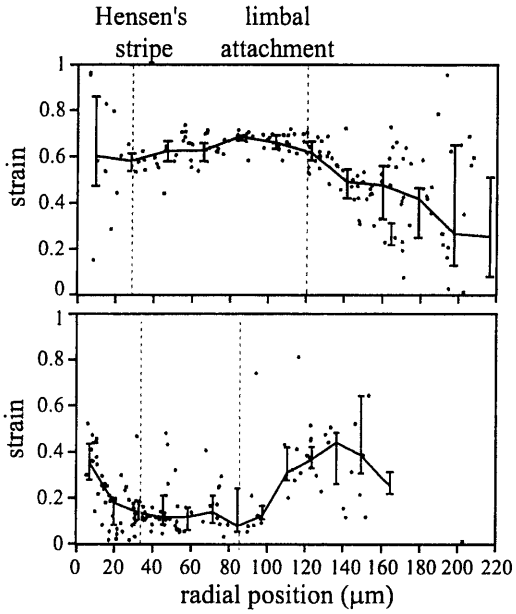

Figure 3-14: Strain as a function of radial position. These are examples of strain as a function of radial position measured from the outer to the inner edge of the TM at a stress of 10 kPa for two TMs. The thin lines connect the median strains computed in 20 μm bins; the vertical line segments represent the interquartile ranges of the measurements in the bins. The top panel is from the same data as shown in Figure 3-13. The bottom panel shows the radial dependence of strain for a different TM. The locations of anatomical landmarks are indicated by dotted vertical lines.

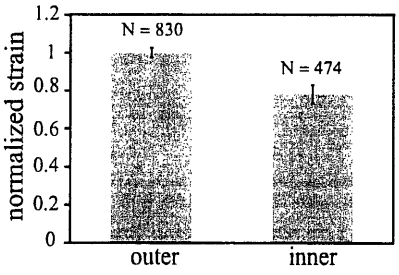

Figure 3-15: Strain as a function of radial position from 7 TMs at an osmotic pressure of 10 kPa. For each TM segment, we computed the strain of all points located on the outer segment of the TM from the limbal attachment. We computed the mean of these values and normalized the strains to this mean value. The height of each bar equals the mean strain and the vertical line segments have lengths that equal twice the standard error of the mean. N is the number of data points.

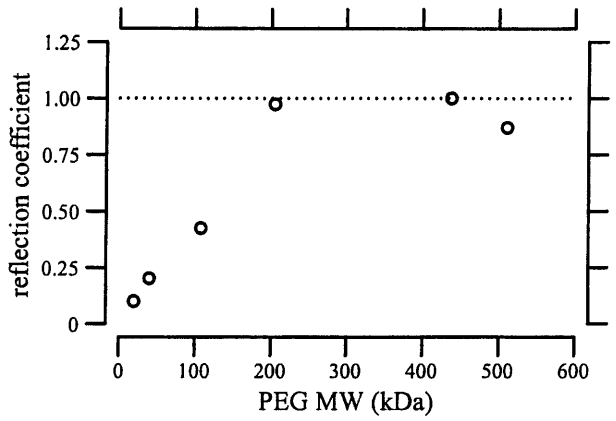

Figure 3-16: Reflection coefficient versus MW of PEG solution. The reflection coefficient was computed from the median strain in Figure 3-7 using Equation 3.14 under the assumption that the maximum reflection coefficient was one.

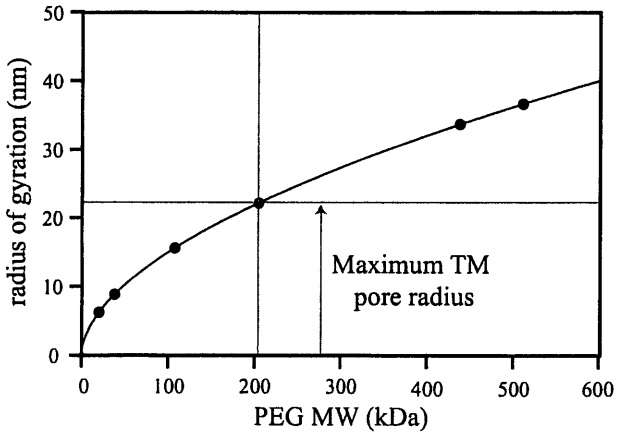

Figure 3-17: Radius of gyration versus MW of PEG as calculated from Equations 3.16 and 3.17 (solid line). The data points are the values of the radius of gyration for each MW of PEG used in our experiments.

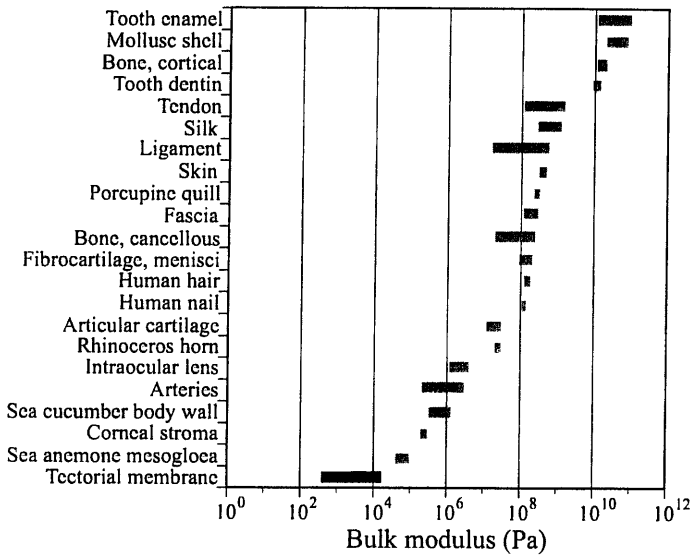

Figure 3-18: Comparison of bulk moduli of several connective tissues (Grodzinksy, 1983; Koehl, 1977; Denny and Gosline, 1980; Parry and Craig, 1988; Thalmann et al., 1993b; Katz, 1995; Chirila, 1998; Chirila and Hong, 1998; Currey, 1998; Deng and Guidoin, 1998; Gharpuray, 1998; Healy, 1998; Keaveny, 1998; Parsons, 1998; Woo and Levine, 1998; Mak and Zhang, 1998; Gosline, 1971; Özkaya and Nordin, 1999; Currey, 1980; Motokawa, 1984; Hoeltzel et al., 1992).

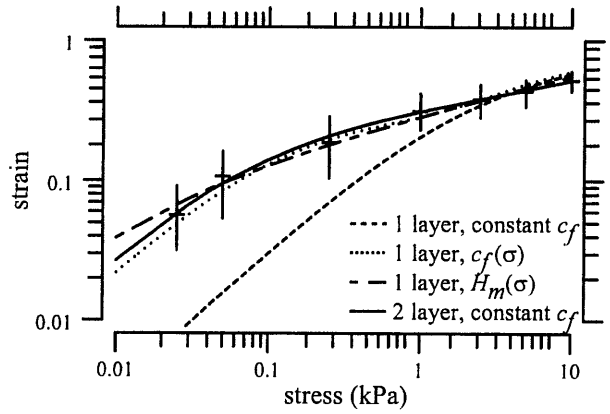

Figure 3-19: Least-squares fit of data for: one-layer gel model with constant fixed charge concentration (c_f) (dashed line), one-layer gel model with a c_f that depends on stress (dotted line), one-layer gel model with microscopic bulk modulus (M_m) that depends on stress (short-long dashed line), and two-layer gel model with constant c_f (solid line). All of these models except for the one-layer model with varying M_m have a M_m of 0 kPa. The best fit to the one-layer gel model had a c_f of -30 mmol/L. The one-layer gel with variable c_f, had a c_f that varied from -11.75 mmol/L at low stress levels to -27.75 mmol/L at high stress levels according to the function, $c_f = 28 - 17e^{-1.2\sigma}$. The one-layer gel with varying M_m had a M_m that depended on stress as follows, $M_m = 3.39e^{\sigma}$. In this fit, c_f was -27.5 mmol/L. For the fit to the two-layer gel model, layer 1 is 40% of total volume of the gel and has c_f of -6 mmol/L, layer 2 is 60% of the gel and has c_f of -78 mmol/L.

Chapter 4

A mutation in α-tectorin decreases the bulk modulus and fixed charge density of the tectorial membrane

This chapter is paper I am writing with the following co-authors: Roozbeh Ghaffari, Wendy Gu, Guy Richardson and Dennis Freeman.

4.1 Introduction

The tectorial membrane (TM) is an acellular gelatinous structure which is on top of hair cells in the organ of Corti. Sound-induced vibrations of the organ are believed to drive radial shearing displacement of the TM relative to the reticular lamina (RL) (Davis, 1958). The shearing forces generated by this relative motion are believed to deflect outer hair cell (OHC) bundles directly and to deflect inner hair cell (IHC) bundles through fluid interactions. The deflection of OHC bundles drives electromechanical processes in both the cell body (Brownell et al., 1985) and hair bundles (Kennedy et al., 2005), one or both of which are believed to underlie cochlear amplification. The amplified signal from either the cell body or the hair bundles or both are then used to drive IHC bundle deflection, which provides the majority of auditory input to the central nervous system. Consequently, the TM plays at least two me-

chanical roles in hearing: driving the cochlear amplifier, and coupling the amplified signal to the sensory cells.

A recent study (Legan et al., 2005) provides evidence that these two roles of the TM are separable. A mouse model of a non-syndromic hereditary hearing loss has been developed which has a missense mutation in $\alpha-tectorin$, a protein that is specific to the TM in the adult cochlea (Legan et al., 2000). In humans, the Y1870C missense mutation has been shown to cause 50-80 dB hearing loss. In $Tecta^{Y1870C/+}$ mice, basilar membrane (BM) tuning curves were on average only 8 dB less sensitive than wild-types (Legan et al., 2005). This small difference suggests that the amplification process powered by OHCs is at most only slightly affected in these mice. However, the compound action potential (CAP) threshold measured at the round window increased on average by 55 dB in $Tecta^{Y1870C/+}$ mice compared to wild-types (Legan et al., 2005), indicating that the amplified signal is not properly coupled to the deflection of IHC bundles. These findings suggest that two roles attributed to the TM — shearing OHC hair bundles and coupling OHC forces to IHCs — are mediated by different mechanisms, and only the latter is affected by the *Tecta* mutation.

One plausible explanation for these findings is that OHC bundle deflections are driven by TM shearing forces, but the coupling of motion from outer to inner hair cells occurs through a different mechanism. This explanation suggests that shear impedance of the TM is mediated by a process independent of α-tectorin while other material properties such as bulk modulus are strongly dependent on α-tectorin. In this paper we test this hypothesis by measuring both shear and bulk material properties of TMs from wild-type and $Tecta^{Y1870C/+}$ mice (hereafter referred to as wild-type and $Tecta^{Y1870C/+}$ TMs).

4.2 Methods

4.2.1 Preparation of the isolated TM

Tecta$^{1870C/+}$ transgenic and wild-type mice 6-10 weeks old were asphyxiated with CO_2 and then decapitated. The pinnae and surrounding tissues were removed and the temporal bone was isolated. While observing through a dissecting microscope the temporal bone was chipped away with a scalpel to isolate the cochlea. The cochlea was placed in an artificial endolymph (AE) solution containing (in mmol/L): 174 KCl, 2 NaCl, 0.02 $CaCl_2$, and 5 HEPES, with pH adjusted to 7.3. The cochlea was widely opened to allow access to the organ of Corti. The TM was isolated from the rest of the organ by probing the organ with an eyelash. Individual pieces of TM were located and transferred via pipette to a glass slide. This slide was coated with 0.3 μL of Cell-Tak bio-adhesive (BD Biosciences, Bedford, MA) to immobilize the TM on the slide surface. This immobilization served three purposes: (1) it kept the TM from being carried out with the effluent as various fluids were perfused; (2) it reduced bulk motion of the TM to allow microfabricated probes to exert shearing forces on the TM; (3) it allowed TM volume changes to be calculated by tracking the positions of beads on the TM and the surrounding glass slide.

4.2.2 Measuring stress-strain relation

The methods used to measure the stress-strain relation of the TM are as published previously (Masaki, Weiss and Freeman, 2006). Briefly, the TMs from *Tecta*$^{1870C/+}$ mice were placed on a glass slide. The surface of the TM was decorated with Trans-FluoSphere carboxylate modified fluorescent microspheres (i.e., beads) to improve visualization of the TM surface. The TM was immersed in AE containing various concentrations of polyethylene glycol (PEG) with a molecular weight (MW) of 511 kDa. The applied osmotic pressure for each solution ranged from 0–10 kPa, and was computed from the concentration and molecular weight of PEG as described previously (Masaki, Weiss and Freeman, 2006). Images of sections of the specimen were

recorded after the specimen was immersed in a given solution for at least one hour. One hour was found to be sufficient time for the TM position to stabilize (Freeman, Masaki, McAllister, Wei and Weiss, 2003). Position of the beads on the surface were tracked to estimate changes in TM height in solutions of different compositions. The positional accuracy of this measurement technique is approximately 0.1 μm. The $z-$component of the strain, ϵ_z, is given by

$$\epsilon_z = 1 - v_z, \tag{4.1}$$

where v_z is the ratio of bead height in the presence of PEG to that in its absence.

4.2.3 Measuring fixed charge concentration

The fixed charge within the TM attracts mobile counterions, and thus establishes an electrical potential between the TM and the bath according to the Donnan relation (Weiss and Freeman, 1997b). This potential is given by

$$V = \frac{RT}{F} \ln\left(\sqrt{\left(\frac{c_f}{C_\Sigma}\right)^2 + 1} - \frac{c_f}{C_\Sigma}\right), \tag{4.2}$$

where V is the potential of the TM relative to the bath, R is the molar gas constant, T is the absolute temperature, F is Faraday's costant, c_f is the fixed charge concentration in the TM, $C_\Sigma = \Sigma_i c_i$ is the sum of the concentrations c_i of each ion in the bath. Since the TM lacks an insulating membrane, the electrical impedance between the inside and outside of the TM is small. Consequently, stable measurements of the Donnan potential is hard to obtain using microelectrodes, which have a relatively high impedance. If the TM is placed between two baths, however, a Donnan potential will be established between the TM and each bath. When the two baths contain different ionic strength solutions, these two Donnan potentials will not cancel, and a potential difference will be established between the baths. This potential difference can be measured with low-impedance electrodes, and the fixed charge concentration c_f of the TM can be determined from the difference of two equations of the form of

equation 4.2.

To measure this inter-bath potential, we have used a planar clamp technique (Ghaffari et al., 2005). Briefly, the TM was placed directly over a 15 μm radius microaperture which separated two bath solutions of differing ionic strengths. The small size of the aperture guaranteed that the TM was part of the electrical pathway connecting the baths. One bath contained AE, while the other contained variants of AE with a range of KCl concentrations: 21, 32, 43, 87, and 174 mM. The electrical potential between the baths was measured with Ag/AgCl microelectrodes (A-M Systems, WA) immersed in micropipets containing 3 M KCl and agarose. These electrodes were coupled to an amplifier (DAM60-G Differential Amplifier, World Precision Instruments, FL) that drove a multimeter (TX3 True RMS Multimeter, Tektronix). The AC and DC potentials measured by the multimeter were digitally recorded during 2–3 second intervals. Each test bath was perfused for 10–30 minutes at a time, and each bath was perfused at least twice over the course of an experiment.

In addition to the Donnan potential, a liquid junction potential (LJP) can be established due to the differing ionic strength of the two baths. This LJP occurs because the ions diffusing across the boundary may have differing mobilities; the ion that diffuses more easily establishes a potential that creates an electrodiffusive equilibrium. In the current set of experiments this LJP is expected to be small, since K^+ and Cl^- have similar mobilities. To determine the contribution of the LJP to the measured potential between baths, the TM was periodically lifted from the hole separating the two baths and the resulting LJP was measured directly.

4.2.4 Measuring shear impedance

Shearing forces were applied in both the radial and longitudinal direction by means of a microfabricated probe gu-05?. The probe consisted of a base which was driven by a piezoactuator, a 30 $\times$ 30 μm shearing plate which contacted the TM, and a flexible arm which connected the base to the plate. A micromanipulator was used to position the microfabricated probe on the TM surface. To ensure contact, the probe was lowered until the TM fibrillar structures were visibly deformed by the plate. The

radial fibers of the TM were used as a landmark to orient the radial and longitudinal axes of the probe.

Physiological displacements of approximately 0.5−1 μm were applied by means of the piezoactuator at audio frequencies of 10-9000 Hz. Stroboscopic illumination was used so that images of the TM and the probe could be collected at eight evenly spaced phases of the stimulus. Optical flow algorithms were used to measure displacements of both the probe and the TM relative to the base from the images (Horn, 1986; Horn and Weldon Jr., 1988). The noise due to ambient vibrations was estimated by measuring the motion of the probe when the drive to the piezoactuator was disconnected. The resulting noise floor was about 3 nm.

The shear impedance of the TM was calculated from the displacement data by assuming a no-slip condition between the plate and the TM underneath it. The balance of forces was determined by

$$F_p(\omega) = k_p(A_b - A_p e^{j\theta}) = j\omega Z_{TM} A_p e^{j\theta} \tag{4.3}$$

where $F_p(\omega)$ is the force exerted by the probe on the TM, k_p is the stiffness of the probe, A_b and A_p are the magnitudes of motion of the base and plate of the probe, respectively, θ is the phase of motion of the plate relative to the base, j is $\sqrt{-1}$, ω is angular frequency, $Z_{TM} = b_{TM} - j\frac{k_{TM}}{\omega}$ is the impedance of the TM, b_{TM} is the damping constant of the TM, and k_{TM} is the point stiffness of the TM. Solving for Z_{TM} gives

$$Z_{TM} = -\frac{k_p}{\omega}\frac{A_b}{A_p}\sin\theta + j\frac{k_p}{\omega}(1 - \frac{A_b}{A_p}\cos\theta). \tag{4.4}$$

The imaginary part of the Z_{TM} is the elastic component of TM impedance, while the real part is the viscous component. This formulation assumes that the mass of the TM does not contribute significantly to the shear impedance, since the base of the TM was attached to the slide. The measurements show that over the frequency range measured, TM mass did not contribute significantly to the impedance (section 4.3.3).

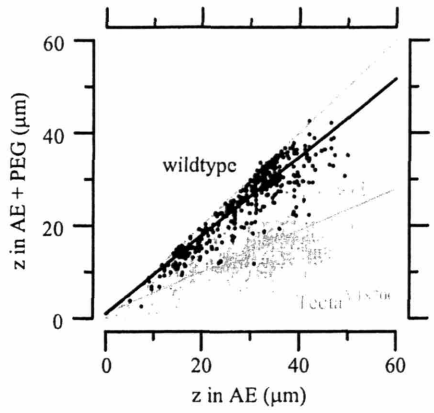

Figure 4-1: Effect of osmotic pressure on TM thickness in $Tecta^{Y1870C/+}$ and wild-type mice. Thickness (z) of the TM in 10 kPa PEG solutions versus that in the absence of PEG. Each dot represents one bead on one of 11 TMs for wild-types and 9 TMs in $Tecta^{Y1870C/+}$ mice. The solid lines represent a regression line fit to the data. The slope of the regression line was 0.46 and 0.86 for wild-type and $Tecta^{Y1870C/+}$ mice, respectively.

4.3 Results

4.3.1 Stress-strain relation

To determine the stress-strain relation, stress was applied by subjecting the TM to osmotic pressure in the range of 0–10 kPa using solutions containing 511 kDa PEG. We measured the change in thickness of the TM relative to its thickness in AE solutions that contained no PEG and used Equation 4.1 to compute strain. Figure 4-1 shows the change in TM thickness relative to its original thickness for all the beads in 9 $Tecta^{Y1870C/+}$ and 11 wild-type TM segments when the TM was exposed to 10 kPa PEG solution. The slope of the solid line represents the median fractional change in TM thickness for both $Tecta^{Y1870C/+}$ and wild-type TMs. The TM segments from $Tecta^{Y1870C/+}$ mice exhibited less strain than wild-types for a given osmotic pressure. This can be clearly seen in Figure 4-2 which summarizes the stress-strain relation for $Tecta^{Y1870C/+}$ and wild-type TM segments at all osmotic pressures measured. At small stresses, the strain is nearly identical for TMs from $Tecta^{Y1870C/+}$ and wild-type mice. At larger stresses, the strain is up to six times larger for TMs from wild-type mice. Moreover, at all stresses the *incremental* strain for an incremental stress (i.e., the slope of the stress-strain relation) is lower for TMs from $Tecta^{Y1870C/+}$ mice.

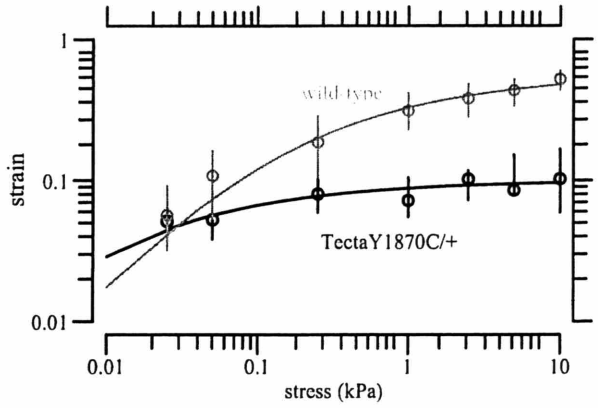

Figure 4-2: TM stress-strain relation for $Tecta^{Y1870C/+}$ ($n = 9$) and wild-type ($n = 11$) TM segments. The circles are the median strains and the lengths of the vertical lines show the interquartile ranges of the measurements. The curves are least squares fits of a gel model of the TM with one compressible and one incompressible region. For TM segments from wild-types, the compressible region had a fixed charge of -9.9 mmol/L and made up 58% of the TM volume. For TM segments from $Tecta^{Y1870C/+}$ mice, the compressible region had a fixed charge of -2.2 mmol/L and made up 10% of the TM volume.

These measurements were fit with a polyelectrolyte gel model of the TM (Masaki, Richardson, Smith and Freeman, 2006). In this model, the TM is effectively split into two functionally distinct material phases. The first phase has an infinite mechanical compliance, so that osmotic pressures are resisted entirely by the presence of fixed charges in the TM matrix. The second phase is functionally incompressible in response to osmotic pressure applied by PEG, i.e., this phase imposes an upper bound on the strain. The curves in figure 4-2 show the best fit of this model to both sets of measurements. For TMs from wild-type mice, the first region contains a fixed charge concentration of -9.9 mmol/L and makes up 58% of the total volume of the TM. For TMs from $Tecta^{Y1870C/+}$ mice, the first region contains a fixed charge concentration of -2.2 mmol/L and makes up 10% of the total volume.

4.3.2 Dependence of electrical potential on KCl concentration

A variety of measurements support the idea that the TM contains significant fixed charge, and that this charge plays a mechanical role (reviewed in Freeman et al, 2003a). Model fits to the measurements in section 4.3.1 also support this interpre-

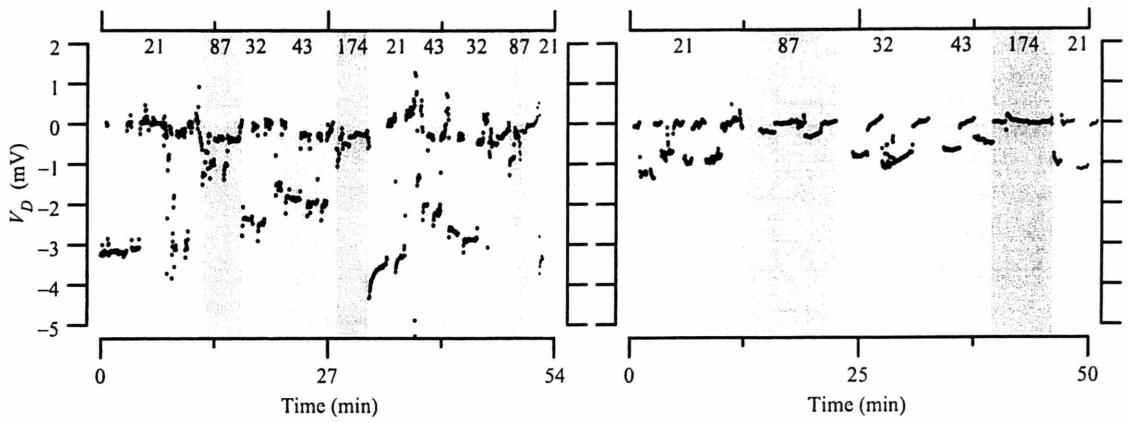

Figure 4-3: Potential difference V_D between two baths as a function of time for TMs from a wild-type (left) and $Tecta^{Y1870C/+}$ (right) mouse. The shaded regions indicate times over which various test baths were perfused. The numbers at the top of each shaded region indicate the KCl concentration of the test bath during that period of time. During each test bath perfusion, the TM was periodically removed from the hole to separate the TM-dependent from the TM-independent contribution to the net potential difference. The rapid transitions between V_D values within one perfusion period indicate times for which the TM was removed or replaced.

tation. To determine the concentration of fixed charge in TMs from $Tecta^{Y1870C/+}$ mutants, the electrical potential across the TM was measured as the TM was exposed to various baths. This potential is established according to the Donnan relation (see methods), and is a direct function of fixed charge concentration. Figure 4-3 compares the electrical potentials measured for a TM taken from a wild-type mouse (left panel) to those measured for a TM from a $Tecta^{Y1870C/+}$ mouse (right panel). For a given bath KCl concentration, the potential across the TM was significantly larger for the wild-type than the $Tecta^{Y1870C/+}$ TM. For both cases, removing the TM from the aperture separating the baths shorted the potential to zero, indicating that these potentials resulted from the presence of the TM. When test baths were perfused multiple times for a single TM, the potentials were similar for the different perfusion periods.

Figure 4-4 summarizes voltage measurements from 5 TM segments from wild-types and 3 TM segments from $Tecta^{Y1870C/+}$ mice. For both wild-type and $Tecta^{Y1870C/+}$ TM segments, the measured potential difference became more negative for smaller KCl concentrations. The measured potential differences were smaller at each bath concentration for TMs from $Tecta^{Y1870C/+}$ mice than for wild-types. These differences

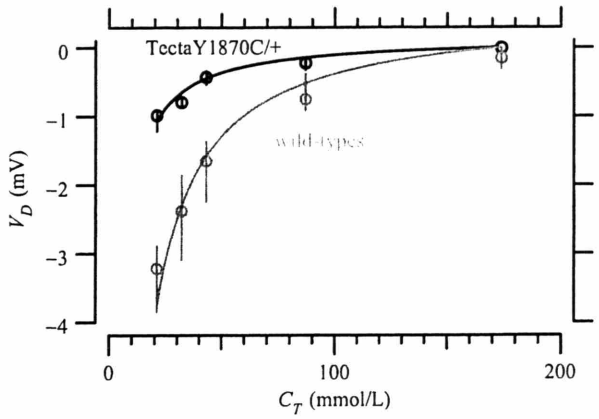

Figure 4-4: Potential difference V_D between two baths as a function of KCl bath concentration C_T for 5 TM segments from wild-type and 3 TM segments from $Tecta^{Y1870C/+}$ mice. Circles are the median V_D and vertical lines show the interquartile ranges of the measurements. The solid line is the least squares fit of the medians to equation 4.2. The median and interquartile ranges for the least squares fits of c_f were 7.1 ± 2.0 mM and 2.2 ± 0.11 mM for TM segments from wild-types and $Tecta^{Y1870C/+}$ mice, respectively.

were significantly larger than the variability across TMs for a given type.

The fixed charge concentrations, c_f, of TMs from $Tecta^{1870C/+}$ and wild-type mice were determined by fitting the measured voltages with the difference of two equations of the form of equation 4.2. The C_Σ values were taken to be those of the two baths, and a value of c_f was found that best fit the data in a least-squares sense. These fits fell within the interquartile range of the measurements for nearly all bath concentrations. The best fit c_f values for wild-type and $Tecta^{Y1870C/+}$ TMs were 7.1 and 2.2 mmol/L, respectively. These values are comparable to those estimated from measurements of bulk modulus (section 4.3.1).

4.3.3 Shear impedance in the radial and longitudinal direction

To determine the shear impedance, shearing forces were exerted in both the radial and longitudinal direction at different stimulation frequencies using a microfabricated probe. Figure 4-5 summarizes the magnitude and phase of shear impedance of 6 and 4 TM segments from wild-type and $Tecta^{Y1870C/+}$ mice, respectively. The magnitudes of the shear impedance for the TMs from $Tecta^{Y1870C/+}$ mice were on average

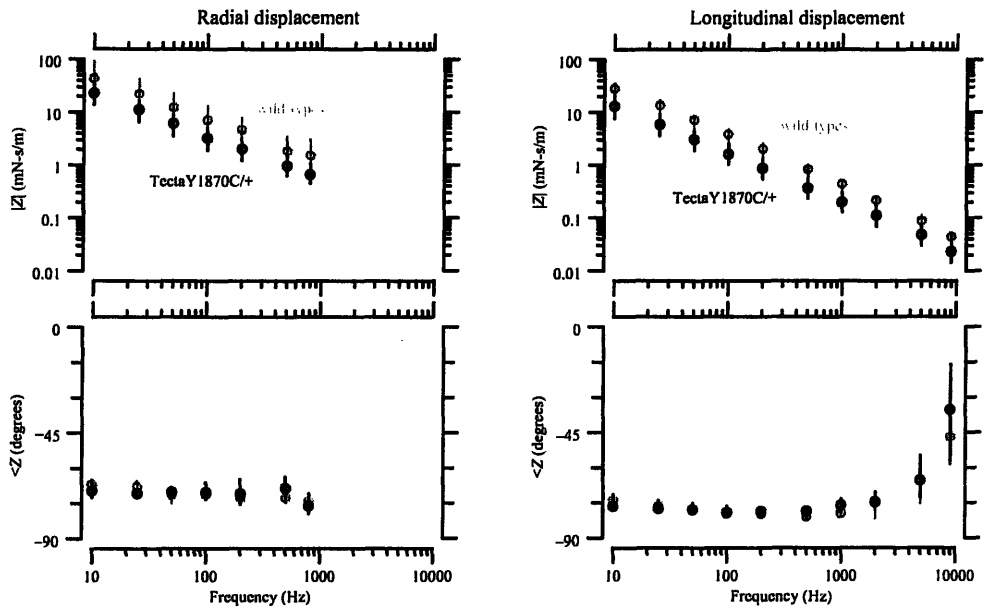

Figure 4-5: Magnitude (top) and phase (bottom) of shear impedance as a function of frequency for both radial (left) and longitudinal (right) excitation. The plot symbols are the median values and the lengths of the vertical lines show the interquartile ranges of the measurements.

7 dB lower in the radial direction and 5 dB lower in the longitudinal direction compared to those of wild-types. However, the slopes of the magnitude versus frequency curves were similar for wild-types and $Tecta^{Y1870C/+}$ TMs in both radial (-15.9 ± 0.4 dB/decade for wild-types and -15.8 ± 0.5 dB/decade for mutant) and longitudinal (-18.9 ± 0.6 dB/decade for wild-types and -18.3 ± 0.3 for mutant) directions. Therefore, the missense mutation altered the viscous and elastic components of the shear impedance in the same proportion.

The shear impedance of TMs from both $Tecta^{Y1870C/+}$ mice and wild-types were between that of a purely viscous material and a purely elastic material. For a purely viscous material, the magnitude of the impedance would be independent of frequency and the phase would be equal to zero. On the other hand, a purely elastic material would have a magnitude which would fall 20 dB per decade and a phase equal to -90^o. $Tecta^{Y1870C/+}$ and wild-type TMs both had a phase between -60^o and -75^o in both the radial and longitudinal directions except at very high frequencies. The frequency dependence of the shear impedance magnitude was also slightly less than 20 dB per decade in both the radial and longitudinal direction. Therefore, the TMs

from both $Tecta^{Y1870C/+}$ and wild-type mice have properties that fall between those of a viscous and an elastic material, and are more elastic than viscous.

4.3.4 Shearing displacement vs. distance from probe

The shearing displacement of the TM decreases with distance from the point of force application. Figure 4-6 shows measurements of normalized shearing displacement as a function of distance from the force probe for 5 wild-type and 5 $Tecta^{Y1870C/+}$ TM segments in response to radial forces. The shearing displacements were normalized to the motion of the plate. There is a general trend for the displacement at a given distance from the probe to be smaller for $Tecta^{Y1870C/+}$ TMs than for wild-type TMs. However, with the exception of the response vs. longitudinal distance for longitudinal displacement, this trend was not statistically significant. The response generally fell more rapidly with distance over the first 20 μm followed by a more gradual decrease for larger distances. These two components are characterized by the relative displacement amplitudes d_r and d_l at a distance of 15-50 μm in the radial and longitudinal directions, and by exponential space constants λ_r and λ_l for larger distances. The values of these parameters for all TMs measured are summarized in Table 4.1. No statistically significant differences were seen in any of these parameters.

4.4 Discussion

4.4.1 The nature of the incompressible region in both wild-types and mutants

The model fits of the TM response to applied osmotic pressure suggest that the TM contains two functionally distinct material phases: one in which osmotic pressures are resisted entirely by charge, and one which is functionally incompressible. One plausible interpretation of this incompressibility is that part of the TM has an extremely large bulk modulus so that the forces exerted by PEG induce negligible volume change. Another is that the TM is highly porous, so that the PEG molecules

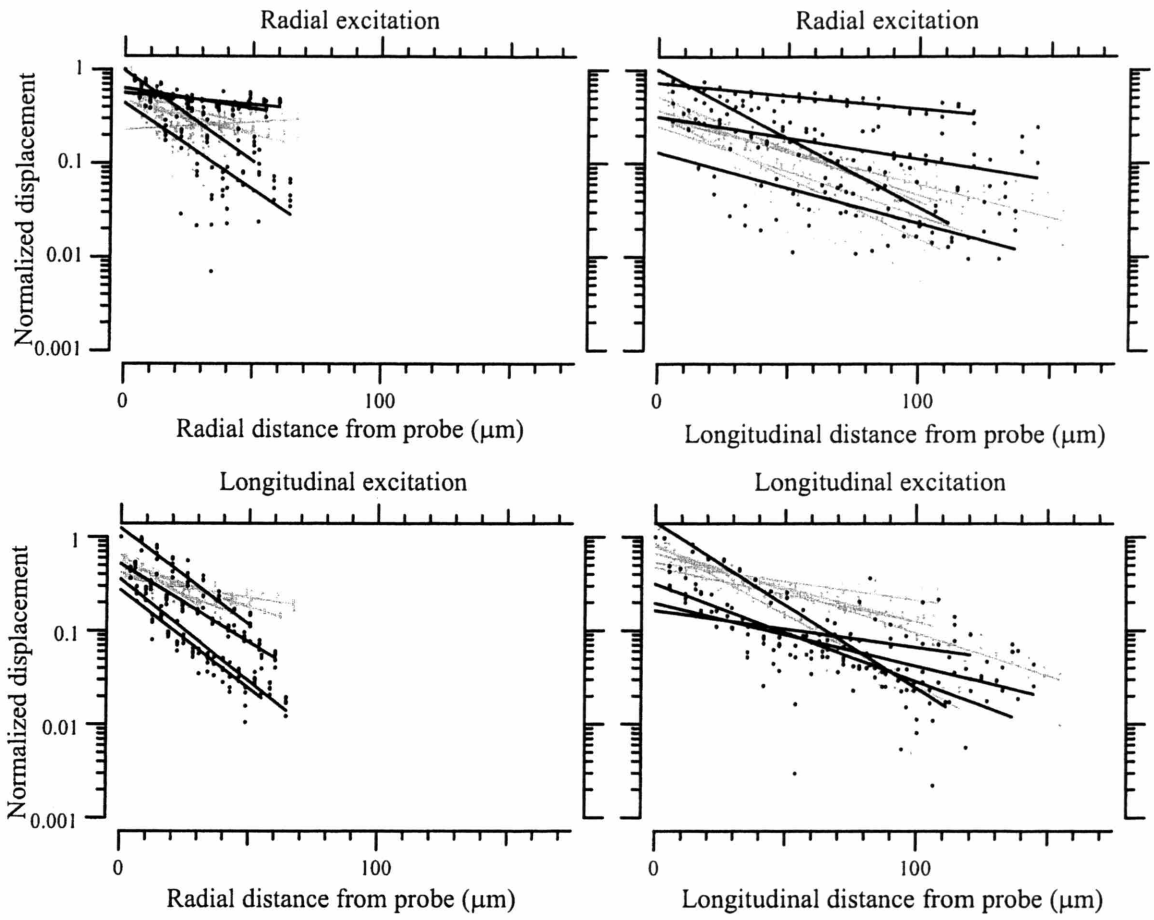

Figure 4-6: Shearing displacement as a function of radial (left) and longitudinal (right) distance from probe for radial (top) and longitudinal (bottom) displacements at 500 Hz. Displacements are normalized to the displacement of the shearing probe. Grey circles indicate displacements of five wild-type TMs and black circles indicate displacements of five $Tecta^{Y1870C/+}$ TMs. The solid lines are fits of exponential functions to data points measured at distances farther than 20 μm from the probe for each TM, and are not constrained to pass through (0,1).

penetrate the TM and exert no osmotic pressure. Measurements of the charge and shear properties of the TM support this latter explanation. The fixed charge concentration of the entire TM as measured in section 4.3.2 is comparable to that of the compressible region as estimated in section 4.3.1, indicating that the incompressible region has a similar charge density. Thus the contribution of charge to bulk modulus in the incompressible region is not significantly different from that of the compressible region. Therefore, the simplest interpretation of the incompressible region is that a portion of the TM is incompressible by PEG due to an increase in porosity rather

	wild-type	$Tecta^{Y1870C/+}$
Radial displacement		
d_r, IQR_r	0.24, 0.17	0.43, 0.26
d_l, IQR_l	0.24, 0.11	0.34, 0.26
λ_r, IQR_{λ_r}	28.11, 7.34	33.69, 30.36
λ_l, IQR_{λ_l}	29.70, 6.42	39.55, 10.24
Longitudinal displacement		
d_r, IQR_r	0.26, 0.07 μm	0.15, 0.12 μm
d_l, IQR_l	0.43, 0.09 μm	0.20, 0.12 μm
λ_r, IQR_{λ_r}	26.50, 12.10	18.90, 11.28
λ_l, IQR_{λ_l}	44.42, 16.25	28.90, 8.74

Table 4.1: Median and interquartile range (IQR) for the normalized displacement in the radial (d_r) and longitudinal (d_l) direction between 15-20 μm. Median and IQR for radial (λ_r) and longitudinal (λ_l) space constants for distances greater than 20 μm.

than an increase in mechanical stiffness.

4.4.2 Mutation affects the stress-strain relation

Figure 4-2 shows that at any given stress, TMs from $Tecta^{Y1870C/+}$ mice have less strain than those of wild-types. The fit of the two-component gel model to these measurements suggests counterintuitively that this difference is associated with a *decrease* in the fixed charge concentration, and hence the bulk modulus, of the TM in $Tecta^{Y1870C/+}$ mice. This decrease is also coupled with an increase in the fraction of the TM that is porous, so that 90% of the TM was functionally incompressible by PEG, and this increased porosity leads to the decreased strain at a given osmotic stress. Although the fixed charge concentration in the model fits changed by less than a factor of four, this change decreased the predicted bulk modulus of the TM by a factor of 20, from 0.69 kPa to 0.034 kPa. This increase in compliance suggests that bulk forces, e.g., due to transverse motion of the organ of Corti, will be met with significantly less resistance. However, care must be taken when extrapolating to the *in vivo* scenario since the bulk modulus measured in section 4.3.1 is the *equilibrium*

bulk modulus which may be different from *dynamic* bulk modulus.

4.4.3 Fixed charge concentration may be decreased by mutation

Figure 4-4 shows that a $Y1870C$ missense mutation in *Tecta* caused the fixed charge concentration to decrease by more than a factor of three. One reason for the measured decrease in fixed charge concentration may be due to the increase in the porosity of the TM. The increase in porosity of the TM may provide an electrical shunting pathway for the two bath solutions above and below the TM. However, the fact that the fixed charge concentration for TMs from both wild-type and $Tecta^{Y1870C/+}$ mice measured in section 4.3.2 are consistent with the charge predicted from measurements of bulk modulus in section 4.3.1, suggest that the electrical measurements are not affected significantly by the increase in porosity of the TM.

Another possible explanation for the observed decrease in fixed charge concentration in $Tecta^{Y1870C/+}$ mice is that mutations in α-tectorin may affects the keratan sulfate concentration. The reason to believe this is because *alpha*-tectorin is a keratan sulfate proteoglycan which comprises approximately 15% of the dry weight of the TM (Goodyear and Richardson, 2002). At physiological pH, keratan sulfate is ionized and represents a significant fraction of the fixed charge in the TM (Weiss and Freeman, 1997b). Therefore, a missense mutation in *Tecta* could alter the fixed charge carried by this protein. However, the $Y1870C$ mutation replaces a tyrosine with a cysteine; since both amino acids are polar, the mutation should not have a direct effect on the charge of the protein. Since the mutation affects other non-collagenous proteins such as otogelin and causes a large reduction in the amount of the striated sheet matrix (Legan et al., 2005), it is likely that these indirect effects lead to a reduction in fixed charge concentration.

If the fixed charge concentration is affected by the mutation, it has a mechanical consequence. In other connective tissues, fixed charge is known to resist compression through electrostatic repulsion forces (Buschmann and Grodzinsky, 1995). A sim-

ple model of this process (Weiss and Freeman, 1997b) predicts that the 7.1 mmol/L fixed charge concentration measured for wild-type TMs could contribute 0.34 kPa to the bulk modulus of the TM. Thus the fixed charge in wild-type TMs is responsible for at least 50% of the measured bulk modulus. The reduction of fixed charge concentration to 2.2 mmol/L in TMs from $Tecta^{Y1870C/+}$ mutants reduces the bulk modulus contributed by charge by a factor of thirteen, to 0.027 kPa. This reduction translates directly to a change in TM material properties, indicating that the hearing loss in $Tecta^{Y1870C/+}$ mutants may be mediated by a change in TM fixed charge concentration.

4.4.4 Shear impedance only slightly affected by mutation

In articular cartilage, it was shown that electrostatic interactions between proteoglycans (i.e. fixed charge) do not play an important role in determining shear modulus (Khalsa and Einsenberg, 1997). Similarly, we see only a mild decrease in the shear impedance of TMs from *Tecta* mutants. Since shearing forces do not alter TM volume, fixed charge is not expected to contribute significantly to TM shear impedance. The small reduction seen in this study may be due to a disturbance of the striated sheet matrix of the TM related to the increased porosity of TMs from *Tecta* mice. This finding is consistent with the idea that the shear impedance of the TM is dominated by collagen fibrils.

The 5–7 dB decrease in shear impedance is comparable to the roughly 8 dB decrease in BM sensitivity measured in $Tecta^{Y1870C/+}$ mice (Legan et al., 2005). These small changes are surprising when considered in the context of models of cochlear function. Most models place outer hair cell motility in a positive feedback loop, so that the gain of OHC motility is multiplied severalfold. Consequently, a small change in OHC sensitivity (such as might be produced by a reduction in TM shear modulus) would lead to a large decrease in basilar membrane sensitivity. Models that incorporate negative feedback have the opposite effect: the system is less than linearly sensitive to changes in OHC sensitivity. If the change in TM shear impedance causes a proportionate reduction in the deflection of OHC hair bundles, then neither class

of model can account for the observed reduction in BM sensitivity.

Moreover, the comparable changes in TM shear impedance and BM sensitivity have implications for models of TM mechanics. If the TM behaves as a stiff lever (Davis, 1958) or a mass (Mammano and Nobili, 1993b), the small reduction in shear impedance should have no effect on OHC bundle deflection and therefore no effect on BM sensitivity. If a mechanical resonance of the TM contributes to cochlear tuning (Zwislocki, 1979; Allen, 1980), the reduced shear impedance should lower the resonant frequency of the TM–hair bundle complex, causing a significant decrease in BM sensitivity. Neither of these responses is seen, implying that these models do not fully capture the mechanical role of the TM.

The measured change in TM shear impedance is small compared to the 50–80 dB increase in CAP threshold for $Tecta^{Y1870C/+}$ mice. Although it is generally assumed that the TM exerts shearing forces that deflect hair bundles, the small reduction in TM shear impedance is not sufficient to account for the increased CAP thresholds in these mice. Moreover, such a mechanism would not explain the difference in sensitivity of inner and outer hair cells. This finding demonstrates that properties of the TM other than shear impedance play a critical role in cochlear mechanics.

4.4.5 Implications for the mechanical roles of the TM

Since the hair bundles of OHCs insert into the tectorial membrane, it is reasonable to assume that shearing forces exerted by the TM deflect the bundles. Similarly, shearing forces exerted by the fluid but driven by TM shearing motion are believed to deflect inner hair cell bundles (Billone and Raynor, 1973b). It has been suggested that the effect of the $Tecta^{Y1870C}$ mutation was to reduce the coupling of forces from outer to inner hair cells (Legan et al., 2005). The results of this study show that this reduction is not mediated by a decreased ability of the TM to exert shear forces on hair bundles. Similarly, the reduction is not mediated by increased viscous shear losses internal to the TM, nor by a reduction in the space constant of TM motion. However, the losses could be mediated by a reduction of the bulk modulus of the TM, coupled with an increase in porosity. Such changes could alter IHC sensitivity

by reducing the ability of the TM to pump fluid, a property of the TM suggested by a recent study (Nowotny and Gummer, 2006). Because this mechanism depends on the coupling of the TM to IHC bundles through fluid, it can also explain how the $Tecta^{Y1870C/+}$ mutation affects the sensitivity of IHCs without significantly altering that of OHCs, which are mechanically coupled to the TM.

The measurements reported here suggest that the bulk and shear material properties of the TM are at best loosely coupled. The bulk compressibility of the TM is dominated by charge repulsion, so that a reduction in the fixed charge concentration of TMs from $Tecta^{Y1870C}$ mutant mice causes an even larger decrease in bulk modulus. In contrast, the shear impedance of the TM is nearly independent of fixed charge concentration, and is likely dominated by the prominent collagen fibrillar network of the TM. These two molecular components appear to control two different material properties that in turn affect two distinct mechanical roles of the TM.

Chapter 5

Material Properties of TMs from *Col*11*a*2 −/− Mice

5.1 Introduction

Type XI collagen is a minor fibrillar component of the the TM. However, mutations in *Col*11*a*2, one of the genes that encodes type XI collagen, have been shown to cause hearing disorders which are generally severe and sensorineural. In particular, *Col*11*a*2 has been identified as the gene responsible for deafness in DFNA13 in two large families with isolated hearing loss (McGuirt et al., 1999). These families have mid-frequency hearing loss with no other known phenotypical abnormalities.

To determine the exact cause of the hearing disorder, a mouse model of this mutation was developed. Preliminary measurements have shown that the TM's collagen fibrils appear to have a loss of organization (McGuirt et al., 1999). Moreover, hearing thresholds as measured by auditory brainstem response (ABR) click-responses in a mouse mutant homozygous for a targeted deletion of this gene have a threshold increase of 40–50 dB (McGuirt et al., 1999). To determine if this hearing loss affected both outer hair cell (OHC) and inner hair cell (IHC) functions, the distortion product otoacoustic emission (DPOAE) which probes OHC function and auditory brainstem response (ABR) which probes both OHC and IHC fuction were measured in *Col*11*a*2 −/− mice and compared to that of wild-types.

It was previously suggested that there are two roles attributed to the TM — shearing OHC hair bundles and coupling OHC forces to IHCs — are mediated by different mechanisms, and only the former is affected by collagen fibrils (Masaki, Ghaffari, Gu, Aranyosi, Richardson and Freeman, 2006). This explanation suggests that shear impedance of the TM is mediated by the collagen fibrils while other material properties such as bulk modulus are dependent on fixed charge. In this paper we test this hypothesis by measuring both shear and bulk material properties of TMs from wild-type and $Col11a2$ $-/-$ mice (hereafter referred to as wild-type and $Col11a2$ $-/-$ TMs).

5.2 Methods

5.2.1 Methods for measuring DPOAEs and ABRs

All physiological experiments including measurements of DPOAEs and ABRs were conducted at the Massachusetts Eye and Ear Infirmary (MEEI). Methods used to measure DPOAEs and ABRs have been described in detail previously (Maison et al., 2002). For both of these measurements, mice were anesthetized with xylazine (20 mg/kg) and ketamine (100 mg/kg). All electrophysiological experiments were conducted in a soundproof anechoic chamber maintained at approximately 90°F.

Distortion product otoacoustic emissions (DPOAE)

Otoacoustic emissions (OAEs) can occur spontaneously or be evoked by playing sound into the ear (Kemp, 1986). DPOAEs are produced by playing two continuous tones (at frequencies f_1 and f_2) with appropriate frequency and level separation in the ear. DPOAEs can be measured at a few sum and difference frequecies of f_1 and f_2 but the largest is at $2f_1$-f_2. DPOAEs at $2f_1$-f_2 were recorded using a custom acoustic assembly consisting of two 0.25 inch condenser microphones used to generate the two primary tones and a Knowles miniature microphone (EK3103; Knowles Electronics, Franklin Park, IL) used to record sound pressure in the ear canal. Stimuli were gen-

erated digitally (A0-6; National Instruments, Austin, TX). The tone pip frequencies for the second primary frequency, f_2, were chosen to be 5.65, 8.0, 11.3, 16.0, 22.65, 32.0, and 45.25 kHz. The first primary frequency, f_1, was always chosen so that $f_2 = 1.2f_1$. The amplitude of the tone was initially small enough that it produced no detectable response, it was then increase by 5 dB sound pressure level (SPL) increments up to 80 dB SPL. The f_2 sound level was always 10 dB less than the f_1 sound level. The sound pressure recorded from the ear canal was amplified and digitally sampled at 20 μsec intervals (A-2000; National Instruments). Fast Fourier transforms were computed and averaged over five consecutive waveform traces. DPOAE amplitude of $2f_1$-f_2 and the surrounding noise floor were extracted. DPOAE threshold was defined as the lowest f_2 level above which the DPOAE amplitude was always greater than the surrounding noise floor.

Auditory Brainstem Responses (ABR)

ABRs are evoked potentials recorded from electrodes on the scalp and calculated by averaging the electrical response to many identical acoustic stimuli. The ABR was recorded by inserting electrodes into the vertex, pinnae, and tail. The electrode at the tail served as the grounding electrode. ABR potentials were evoked with 5 msec tone pips at the same frequencies used for the DPOAE second primary f_2. The tone volume was increased with 5 dB steps from 10 dB below threshold up to 80 dB SPL. At each SPL, 1024 responses were amplified (80 dB), filtered (0.1-2 kHz), and averaged (with stimulus polarity alternated) using a LabVIEW data-acquisition system (National Instruments, Austin, TX). Waveforms were discarded when peak-to-peak amplitude exceeded 15 μV. ABR threshold was defined as the lowest SPL where a repeatable waveform could be seen.

5.2.2 Preparation of the isolated TM

Col11a2 transgenic and wild-type mice 6-10 weeks old were asphyxiated with CO_2 and then decapitated. The pinnae and surrounding tissues were removed and the

temporal bone was isolated. While observing through a dissecting microscope the temporal bone was chipped away with a scalpel to isolate the cochlea. The cochlea was placed in an artificial endolymph (AE) solution, containing (in mmol/L): 174 KCl, 2 NaCl, 0.02 $CaCl_2$, and 5 HEPES, with pH adjusted to 7.3. The cochlea was widely opened to allow access to the organ of Corti. The TM was isolated from the rest of the organ by probing the organ with an eyelash. Individual pieces of TM were located and transferred via pipette to a glass slide. This slide had been prepared with 0.3 μL of Cell-Tak adhesive (BD Biosciences, Bedford, MA) to immobilize the TM on the slide surface. This immobilization served three purposes: (1) it kept the TM from being carried out with the effluent as various fluids were perfused; (2) it reduced bulk motion of the TM to allow microfabricated probes to exert shearing forces on the TM; (3) it allowed TM volume to be calculated by tracking the positions of beads on the TM and the surrounding glass slide.

5.2.3 Measuring shear impedance

Shearing forces were applied in both the radial and longitudinal direction by means of a microfabricated probe. The probe consisted of a base which was driven by a piezoactuator, a 30 $\times$ 30 μm shearing plate which contacted the TM, and a flexible arm which connected the base to the plate. A micromanipulator was used to position the microfabricated probe on the TM surface. To ensure contact, the probe was lowered until the TM fibrillar structures were visibly deformed by the plate. The radial fibers of the TM were used to orient the radial and longitudinal axes.

Physiological displacements of approximately 0.5$-$1 μm were applied by means of the piezoactuator at audio frequencies of 10-9000 Hz. Stroboscopic illumination was used so that images of the TM and the probe could be collected at eight evenly spaced phases of the stimulus. Optical flow algorithms were used to measure displacements of both the probe and the TM relative to the base from the images (Horn, 1986; Horn and Weldon Jr., 1988). The noise due to ambient vibrations was estimated by measuring the motion of the probe with the drive to the piezoactuator disconnected. The resulting motion was about 3 nm which constitutes the effective noise floor of

the measurement system.

The shear impedance of the TM was calculated from the displacement data by assuming that the plate and the TM underneath it moved together. The balance of forces was determined by

$$F_p(\omega) = k_p(A_b - A_p e^{j\theta}) = j\omega Z_{TM} A_p e^{j\theta} \tag{5.1}$$

where $F_p(\omega)$ is the force exerted by the probe on the TM, A_b and A_p are the magnitudes of motion of the base and plate of the probe, respectively, θ is the phase of motion of the plate relative to the base, j is $\sqrt{-1}$, ω is angular frequency, $Z_{TM} = b_{TM} - \mathrm{j}\frac{k_{TM}}{\omega}$ is the impedance of the TM, b_{TM} is the damping constant of the TM, and k_{TM} is the point stiffness of the TM. Solving for Z_{TM} gives

$$Z_{TM} = -\frac{k_p}{\omega}\frac{A_b}{A_p}\sin\theta + j\frac{k_p}{\omega}(1 - \frac{A_b}{A_p}\cos\theta). \tag{5.2}$$

The imaginary part of the Z_{TM} is the elastic component of TM impedance, while the real part is the viscous component. This formulation assumes that the mass of the TM does not contribute significantly to the shear impedance, since the base of the TM was attached to the slide. The measurements show that over the frequency range measured, TM mass did not contribute significantly to the impedance (section 5.3.2).

5.2.4 Measuring stress-strain relation

The methods used to measure the stress-strain relation of the TM are as published previously (Masaki, Weiss and Freeman, 2006). Briefly, the TMs from *Col11a2* $-/-$ mice were placed on a glass slide. The surface of the TM was decorated with TransFluoSphere carboxylate modified fluorescent microspheres (i.e. beads) to improve visualization of the TM surface. The TM was immersed in AE containing various concentrations of polyethylene glycol (PEG) with a molecular weight (MW) of 511 kDa. The applied osmotic pressure for each solution ranged from 0–10 kPa, and was computed from the concentration and molecular weight of PEG as described previously (Masaki, Weiss and Freeman, 2006). Images of sections of the specimen were

recorded after the specimen was immersed in a given solution for at least one hour. One hour was found to be sufficient time for the TM position to stabilize (Freeman, Masaki, McAllister, Wei and Weiss, 2003). Position of the beads on the surface were tracked to estimate changes in TM height in solutions of different compositions. The positional accuracy of these measurement is about 0.1 μm. The $z-$component of the strain, ϵ_z, is given by

$$\epsilon_z = 1 - v_z, \tag{5.3}$$

where v_z is the ratio of bead height in the presence of PEG to that in its absence.

5.2.5 Measuring fixed charge concentration

The fixed charge within the TM attracts mobile counterions, and thus established an electrical potential between the TM and the bath according to the Donnan relation (Weiss and Freeman, 1997b). This potential is given by

$$V = \frac{RT}{F} \ln(\sqrt{(\frac{c_f}{C_\Sigma})^2 + 1} - \frac{c_f}{C_\Sigma}), \tag{5.4}$$

where V is the potential of the TM relative to the bath, R is the molar gas constant, T is the absolute temperature, F is Faraday's costant, c_f is the fixed charge concentration in the TM, $C_\Sigma = \Sigma_i c_i$ is the sum of the concentrations c_i of each ion in the bath. Since the TM lacks an insulating membrane, the electrical impedance between the inside and outside of the TM is small. Consequently, stable measurements of the Donnan potential is hard to obtain using microelectrodes, which have a relatively high impedance. If the TM is placed between two baths, however, a Donnan potential will be established between the TM and each bath. When the two baths have differing C_Σ, these two Donnan potentials will not cancel, and a potential difference will be established between baths. This potential difference can be measured with low-impedance electrodes, and the fixed charge concentration c_f of the TM can be determined from the difference of two equations of the form of equation 5.4.

To measure this potential we developed a planar clamp technique (Ghaffari et al., 2005). Briefly, the TM was placed directly over a 15 μm radius microaperture which separated two bath solutions of different ionic strengths. The small size of the aperture guaranteed that the TM formed part of the sole electrical pathway connecting the baths. One bath contained AE, while the other contained variants of AE with a range of KCl concentrations: 21, 32, 43, 87, and 174 mM. The electrical potential between the baths was measured with Ag/AgCl microelectrodes (A-M Systems, WA) immersed in micropipets containing 3 M KCl and agarose. These electrodes were coupled to an amplifier (DAM60-G Differential Amplifier, World Precision Instruments, FL) that drove a multimeter (TX3 True RMS Multimeter, Tektronix). One-second recordings were taken every 2–3 seconds and used to compute both DC and AC potentials. Each test bath was perfused for 10–30 minutes at a time, and each bath was perfused at least twice over the course of an experiment.

In addition to the Donnan potential, a liquid junction potential (LJP) can be established due to the differing ionic strength of the two baths. This LJP occurs because the ions diffusing across the boundary may have differing mobilities; the ion that diffuses more easily establishes a potential that creates an electrodiffusive equilibrium. In the current set of experiments this LJP is expected to be small, since K^+ and Cl^- have similar mobilities. To determine the contribution of the LJP to the measured potential between baths, the TM was periodically lifted from the hole separating the two baths and the resulting LJP measured directly.

5.2.6 Genotyping of *Col11a2* mutants

Genotyping was done by MIT's Department of Comparative Medicine as previously described (Brown et al., 1997).

5.2.7 Animal care

The care and use of animals reported in this study were approved by the Massachusetts Institute of Technology Committee on Animal Care.

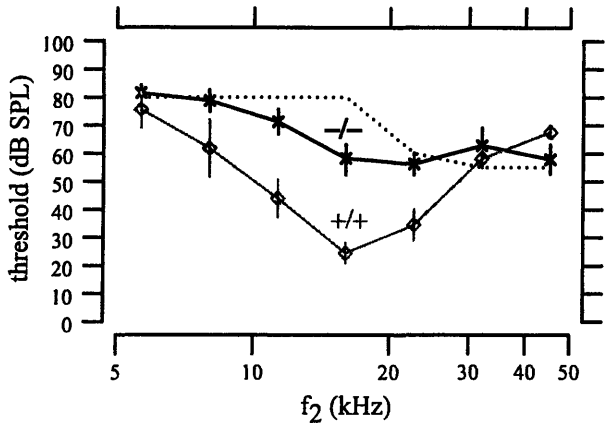

Figure 5-1: DPOAE threshold of *Col*11*a*2 $-/-$ mouse mutants ($N = 36$) compared to wild-types ($N = 36$). Plot symbols represent the median threshold and the lengths of the vertical lines show the interquartile range. The dotted line is the noise floor of the measurement system.

5.3 Results

5.3.1 ABR and DPOAE measurements

To determine the frequency specific hearing loss of *Col*11*a*2 mouse mutants, ABRs and DPOAEs were measured and compared to that of wild-types. ABR measurements represent the synchronized activity of several groups of neurons in the ascending auditory pathway. DPOAE, on the other hand, reflect nonlinear mechanics which are presumably due to outer hair cell electromotility (Kemp, 1986; Liberman et al., 2004).

Figure 5-1 shows the DPOAE threshold as a function of frequency for *Col*11*a*2 $-/-$ mice and wild-types. For the wild-types, the best frequency, i.e. the frequency with the lowest DPOAE threshold, is 16 kHz. The thresholds increase above and below the best frequency value. The DPOAE thresholds of *Col*11*a*2 $-/-$ mice are on average 30-40 dB higher than that of wild-types for $5<f_2<20$ kHz.

The comparison of ABR thresholds as a function of frequency are shown in Figure 5-2. As for the DPOAE measurements, the ABR thresholds increased about 30-40 dB SPL at all frequencies for *Col*11*a*2 $-/-$ mice compared to wild-types.

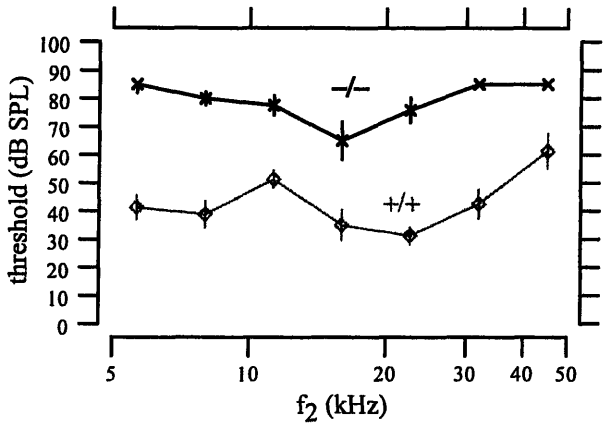

Figure 5-2: ABR threshold of *Col*11*a*2 $-/-$ mouse mutants ($N = 36$) compared to wild-types ($N = 5$). Plot symbols represent the median threshold and the lengths of the vertical lines show the interquartile range.

5.3.2 Shear impedance in the radial and longitudinal direction

To determine the shear impedance, shearing forces were exerted in both the radial and longitudinal direction at different stimulation frequencies using a microfabricated probe. Figure 5-3 summarizes the magnitude and phase of shear impedance of 6 and 3 TM segments from wild-type and *Col*11*a*2 $-/-$ mice, respectively. The magnitudes of the shear impedance for the TMs from *Col*11*a*2 $-/-$ mice were on average 7.2 dB lower than wild-types in the radial direction. However, in the longitudinal direction, there is only a 2.8 dB difference between TMs from wild-types and *Col*11*a*2 $-/-$ mice. Moreover, the slope of the magnitude versus frequency was similar for wild-types (radial: -15.9 ± 0.4 dB/decade, longitudinal: -18.9 ± 0.6 dB/decade) and *Col*11*a*2 $-/-$ (radial: -16.1 ± 0.8 dB/decade, longitudinal: -18.5 ± 0.6 dB/decade) in both the radial and longitudinal direction suggesting that the mutation altered the viscous and elastic components of the shear impedance in the same proportion. The phase for the TMs from wild-types and *Col*11*a*2 $-/-$ mice in both the radial and longitudinal direction were also similiar.

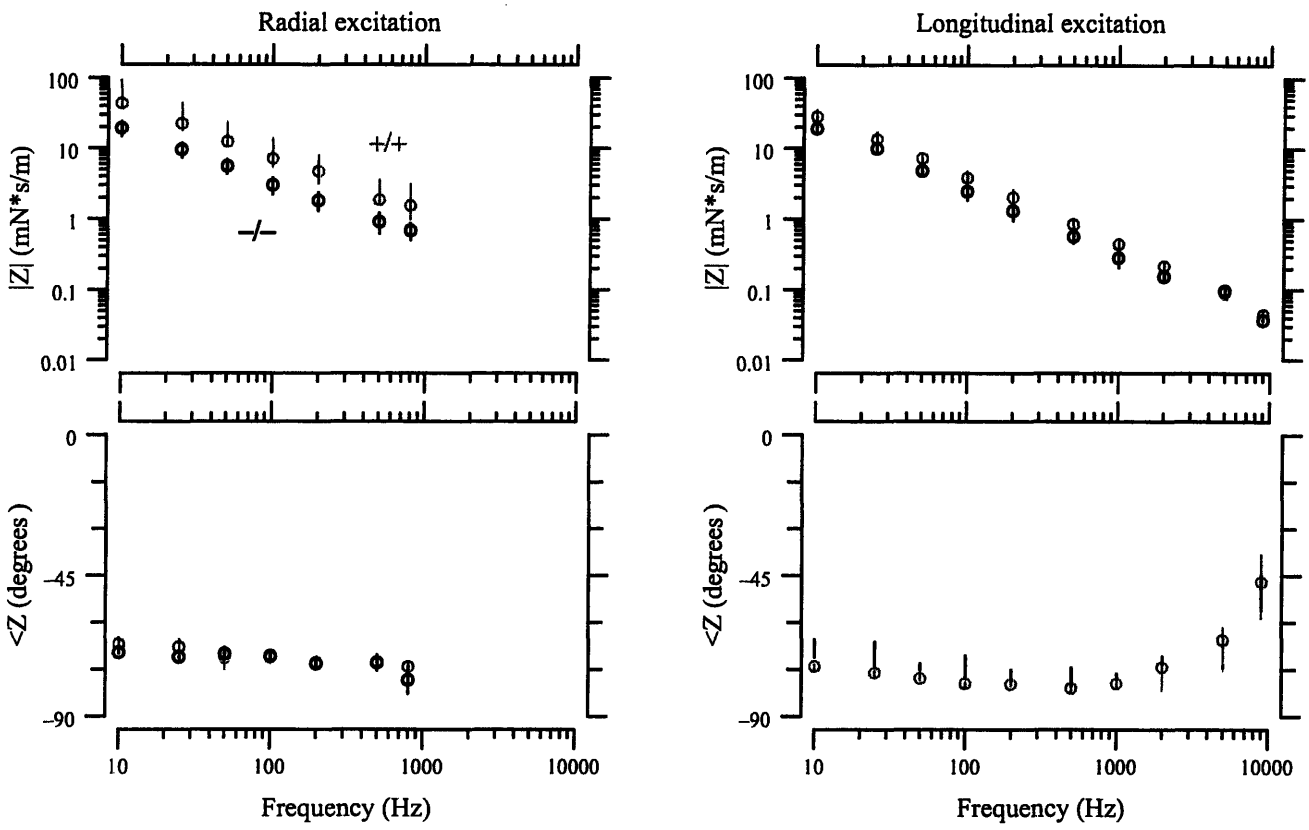

Figure 5-3: Magnitude (top) and phase (bottom) of shear impedance as a function of frequency for both radial (left) and longitudinal (right) excitation. The plot symbols are the median values and the lengths of the vertical lines show the interquartile ranges of the measurements. Normals are grey xs, mutants are black circles.

5.3.3 Stress-strain relation

To determine if mutation in *Col*11*a*2 affects the bulk properties of the TM, the stress-strain relation of the TM was measured in *Col*11*a*2 $-/-$ mouse mutants and wild-types. Stress was applied by subjecting the TM to osmotic pressure in the range 0–10 kPa with solutions that contained PEG with a MW of 511 kDa. We measured the change in thickness of the TM relative to its thickness in AE solutions that contained no PEG and computed strain as described previously (Masaki, Richardson, Smith and Freeman, 2006). Figure 5-4 shows the stress-strain relation of apical and middle segments of the TM from *Col*11*a*2 $-/-$ mice and wild-types. The strain was about 30% smaller for TMs from *Col*11*a*2 $-/-$ mice compared to wild-types at higher stresses ($>$ 250 Pa). However, the stress-strain relation from the TMs from *Col*11*a*2

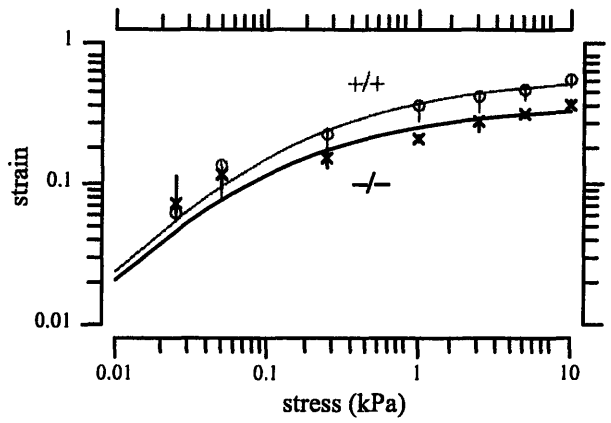

Figure 5-4: TM stress-strain relation for apical-middle *Col*11*a*2 $-/-$ ($n = 5$) and wild-type ($n = 11$) TM segments. The plot symbols are the median strains and the lengths of the vertical lines show the interquartile ranges of the measurements. The curves are least squares fits of a gel model of the TM with one compressible and one incompressible region. For TM segments from wild-types, the compressible region had a fixed charge of -7.9 mmol/L and made up 59% of the TM volume. For TM segments from *Col*11*a*2 $-/-$ mice, the compressible region had a fixed charge of -6.6 mmol/L and made up 37% of the TM volume.

$-/-$ mice and wild-types at lower stress levels are similar.

These measurements were fit with a polyelectrolyte gel model of the TM (Masaki, Weiss and Freeman, 2006). In this model, the TM is effectively split into two functionally distinct material phases. The first phase has an infinite mechanical compliance, so that osmotic pressures are resisted entirely by the presence of fixed charges in the TM matrix. The second phase is functionally incompressible in response to osmotic pressure applied by PEG; i.e., thise phase imposes an upper bound on the strain. The curves in figure 5-4 show the best fit of this model to both sets of measurements. For TMs from wild-type mice, the first region contains a fixed charge concentration of -7.9 mmol/L and makes up 59% of the total volume of the TM. For TMs from *Col*11*a*2 $-/-$ mice, the first region contains a fixed charge concentration of -6.6 mmol/L and makes up 37% of the total volume.

Figure 5-5 shows the stress-strain relation of basal segments from *Col*11*a*2 $-/-$ and wildptypes. The curves show the best fit of the two-component model to both sets of measurements. The best fit parameters for both TMs from wild-type and *Col*11*a*2 $-/-$ mice were the same within measurement error. The first region contains a fixed

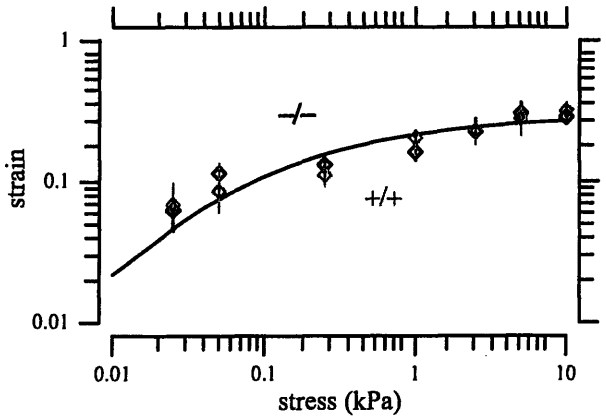

Figure 5-5: TM stress-strain relation for basal $Col11a2$ $-/-$ ($n = 4$) and wild-type ($n = 5$) TM segments. The circles are the median strains and the lengths of the vertical lines show the interquartile ranges of the measurements. The curves are least squares fits of a gel model of the TM with one compressible and one incompressible region. For TM segments from both $Col11a2$ $-/-$ and wild-types, the compressible region had a fixed charge of -5.7 mmol/L and made up 30% of the TM volume.

charge concentration of -5.7 mmol/L and makes up 30% of the total volume of the TM.

5.3.4 Dependence of electrical potential on KCl concentration

A variety of measurements support the idea that the TM contains significant fixed charge, and that this charge plays a mechanical role (reviewed in Freeman et al, 2003a). To determine the concentration of fixed charge in TMs from $Col11a2$ $-/-$ mutants, the electrical potential across the TM was measured as the TM was exposed to various baths. This potential is established according to the Donnan relation (see methods), and is a direct function of fixed charge concentration. Figure 5-6 compares the electrical potentials measured for a TM taken from a wild-type mouse (left panel) to those measured for a TM from a $Col11a2$ $-/-$ mouse (right panel). For a given bath KCl concentration, the potential across the TM was similar for the wild-type and the $Col11a2$ $-/-$ TM. For both TMs, removing the TM from the hole separating the baths shorted the potential to zero, indicating that these potentials resulted from the presence of the TM. When test baths were perfused multiple times for a single

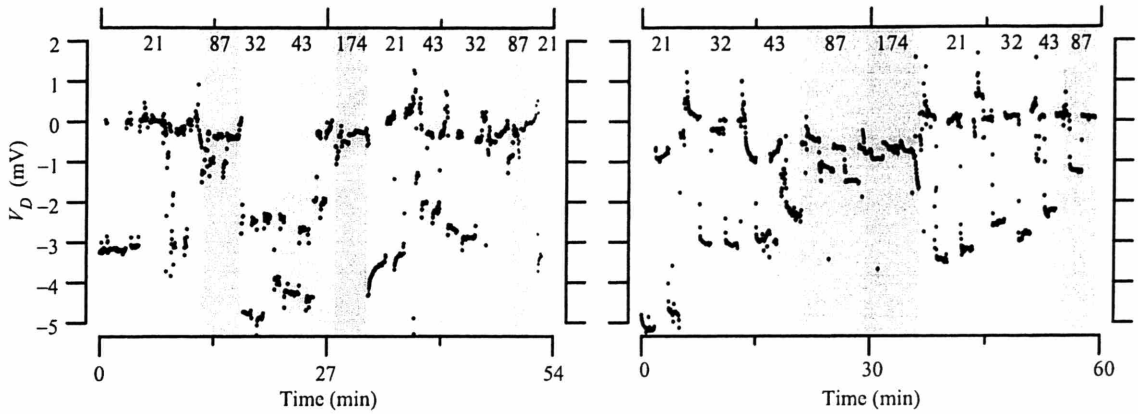

Figure 5-6: Potential difference V_D between two baths as a function of time for TMs from a wild-type (left) and $Col11a2$ $-/-$ (right) mouse. The shaded gray boxes indicate times over which various test baths were perfused. The numbers at the top of each shaded region indicate the KCl concentration of the test bath during that period of time. During each test bath perfusion, the TM was periodically removed from the hole to separate the TM-dependent from the TM-independent contribution to the net potential difference. The rapid transitions between V_D values within one perfusion period indicate times for which the TM was removed or replaced. In each case, the more negative V_D values corresponds to times when the TM covered the aperture.

TM, the potentials were similar for both perfusion periods.

Figure 5-7 summarizes voltage measurements from 5 TM segments from wild-types and 3 TM segments from $Col11a2$ $-/-$ mice. For both wild-type and $Col11a2$ $-/-$ TM segments, the measured potential difference became more negative for smaller KCl concentrations. The measured potential differences for TMs from $Col11a2$ $-/-$ mice and wild-types were within measurement error at each bath concentration.

The fixed charge concentrations c_f of TMs from $Col11a2$ $-/-$ and wild-type mice were determined by fitting the measured voltages with the difference of two equations of the form 5.4. The C_Σ values were taken to be those of the two baths, and a value of c_f was found that best fit the data in a least-squares sense. These fits fell within the interquartile range of the measurements for nearly all bath concentrations. The best fit c_f values for wild-type and $Col11a2$ $-/-$ TMs were 7.1 and 2.0 mmol/L, respectively. These values are comparable to those estimated from measurements of bulk modulus (section 5.3.3).

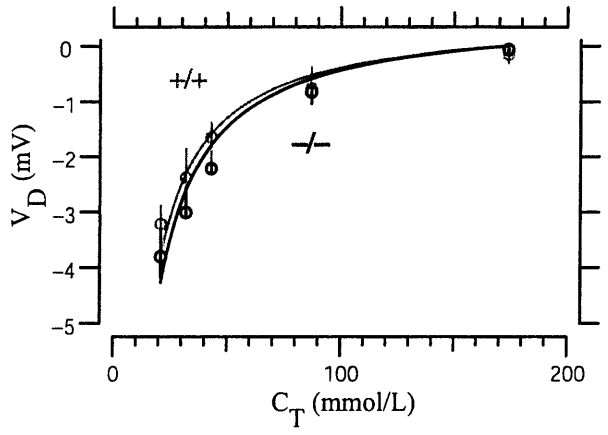

Figure 5-7: Potential difference V_D between two baths as a function of KCl bath concentration C_T for 5 TM segments from wild-type (gray) and 3 TM segments from *Col*11*a*2 $-/-$ mice (black). Circles are the median V_D and vertical lines show the interquartile ranges of the measurements. The solid line is the least squares fit of the medians to equation 5.4. The median and interquartile range for the least squares fit c_f value was 7.1 mM and 2.0 mM for the TM segments from wild-types and 7.9 mM and 2.0 mM for the TM segments from *Col*11*a*2 $-/-$ mice.

5.4 Discussion

5.4.1 ABR and DPOAE similarly affected by mutation

Mutations in *Col*11*a*2 have previously been shown in humans to cause congenital, non-progressive, non-syndromic sensorineural hearing loss which is greatest in the mid-frequency range (McGuirt et al., 1999). Figure 5-2 shows that the mouse mutants had about 30–50 dB threshold increase in ABR threshold compared to wild-types. Figure 5-1 also shows similar threshold increase in DPOAE within the limits of the measurement system. Figure 5-1 However, unlike humans, the mouse models had similar threshold increase across all frequencies measured.

The fact that both ABR and DPOAE thresholds were similarly affected suggests that the mutation affects either OHC functions or some other structures such as the basilar membrane or both. If the mutation changed the material property of the TM, OHC bundle deflection would be reduced, thereby, causing hearing loss. However, mutations in *Col*11*a*2 could also affect other structures other than the TM since *Col*11*a*2 have also been shown to be in cartilaginous otic capsule, spiral limbus, and

lateral wall of the cochlea. Therefore, changes in other structures could also cause hearing loss.

5.4.2 Radial shear impedance reduced by mutation

Figure 5-3 shows that the mutation causes a 7.2 dB decrease in the radial shear impedance but only a 2.8 dB decrease in the longitudinal shear impedance of the TM. This finding is consistent with the idea that the shear impedance of the TM especially in the radial direction is dominated by collagen fibrils including type XI collagen.

In cartilage, type XI collagen is thought to be important for maintaining the interfibrillar spacing and fibril diameter of type II collagen (Mendler et al., 1989; Eikenberry et al., 1991; Li et al., 1995). In the TM, type II collagen is one of the main components of the radial fibers seen under light microscope (Slepecky, Savage, Cefaratti and Yoo, 1992). Therefore, if type XI collagen works in the same manner in the TM as in cartilage, we would expect mutations in type XI collagen to affect the organization and strength of the radial fibers in the TM. This is further supported by the electron microscope images which showed loss of organization of the collagen fibrils in the mutants (McGuirt et al., 1999).

5.4.3 Slight change in the stress-strain relation due to mutation

The model fits to the TM response to applied osmotic pressure suggest that the TM contains two functionally distinct material phases: one in which osmotic pressures are resisted entirely by charge, and one which is functionally incompressible. Measurements of the charge and shear properties of the TMs from $Tecta^{Y1870C/+}$ published elsewhere support the interpretation that the functionally incompressible region is due to the high porosity of the TM.

Figure 5-4 shows that the equilibrium stress-strain relation of apical-middle segments of TMs from $Col11a2$ $-/-$ and wild-type mice are similar. However, at higher

osmotic pressures, TMs from $Col11a2$ $-/-$ have slightly smaller strain than that of wild-types. The fit of the two-component gel model to these measurements suggests that this difference is associated with a slight *decrease* in the fixed charge concentration, and hence the bulk modulus, of the TM in $Col11a2$ $-/-$ mice. This decrease is also coupled with an increase in the fraction of the TM that is porous, so that 63% of the TM was functionally incompressible by PEG, and this increased porosity leads to the decreased strain at a given osmotic stress. This decrease in fixed charge concentration in the model has a mechanical consequence of decreasing the predicted bulk modulus of the TM from 0.44 kPa to 0.31 kPa at 25 Pa.

Figure 5-5 shows that there are no detectable difference in the equilibrium stress-strain relation for basal TM segments from $Col11a2$ $-/-$ and wild-type mice.

5.4.4 Fixed charge concentration not affected significantly by mutation

Figure 4-4 shows that a $Col11a2$ mutation did not affect the fixed charge concentration very much. These values for TMs from both wild-type and $Col11a2$ $-/-$ mice are consistent with the charge predicted from measurements of bulk modulus. These results suggest that mutations in collagen does not significantly affect the fixed charge concentration.

5.4.5 Implications for the mechanical roles of the TM

Since the hair bundles of OHCs insert into the tectorial membrane, the shearing forces exerted by the TM probably deflect the bundles. Similarly, shearing forces exerted by the fluid but driven by TM shearing motion are believed to deflect inner hair cell bundles (Billone and Raynor, 1973b). This study suggests that the shear impedance of the TM is nearly independent of fixed charge concentration but is dominated by the prominent collagen fibrillar network of the TM whose organization is guided by type XI collagen.

Chapter 6

Comparing the Equilibrium Stress-Strain Relations of Tectorial Membranes from TectaY1870C/+ and Col11a2 −/− Mouse Mutants

This paper has been accepted in Auditory Mechanisms: Processes and Models (Masaki, Richardson, Smith and Freeman, 2006).

6.1 Introduction

From mouse models of genetic disorders of hearing we have learned that genetic manipulations of TM proteins can decrease hearing sensitivity (Legan et al., 2000; McGuirt et al., 1999). However, the effect of these mutations at the mechanical level has not been thoroughly investigated. Presently, we are investigating *Col*11*a*2 and *Tecta* mouse mutants. *Col*11*a*2 is one of the genes which encodes type XI collagen, a quantitatively minor fibrillar component of the TM. *Tecta* encodes alpha-tectorin, one of the major glycoproteins of the non-collagenous, striated sheet matrix. Mutations in either of these genes have been shown to cause hearing loss. *Col*11*a*2 −/− mouse mutants have a 40-50 dB increase in auditory brainstem response threshold

compared to wild-types (McGuirt et al., 1999). *Tecta*Y1870C/+ mice have a 50-80 dB hearing loss (Legan et al., 2005). To determine whether these mutations led to changes in the material properties of the TM, we measured TM volume changes in response to osmotic pressure applied with polyethylene glycol (PEG). Interpreting these measurements in terms of a simple model provides insight into the molecular mechanisms that underlie these changes.

6.2 Methods

Many of the methods used to measure the stress-strain relation of the TM are similar to those used in previous studies of the TM (Freeman, Masaki, McAllister, Wei and Weiss, 2003; Shah et al., 1995). Briefly, the TM was placed on a glass slide, decorated with beads, and immersed in a bathing solution. Images of sections of the TM were recorded after the specimen was immersed in a given solution for at least one hour. Since bright-field images show that beads end up resting on the surface of the TM, bead position was used as a marker for the TM surface. Bead positions were tracked to estimate changes in the TM volume in solutions of different composition.

6.2.1 Solutions

All the solutions were variations of an artificial endolymph (AE) solution which contained in mmol/L: 2 NaCl, 3 dextrose, 0.02 $CaCl_2$, 5 HEPES, and 174 KCl. This composition closely matches the measured ionic composition of endolymph in the mammalian cochlea (Sterkers et al., 1988). The pH of the solution was adjusted to 7.3. PEG solutions were made by adding PEG to the same stock solution of AE to ensure that the only differences in solutions were due to PEG. PEGs of molecular weights (MW) of 20, 108, 205, 438, and 511 kDa were used to apply osmotic pressures over the range 0-10 kPa.

6.2.2 Osmotic pressure of PEG solutions

Experimental measurements have shown that the relation between PEG concentration and osmotic pressure is a non-linear function of both concentration and MW (Hasse et al., 1995; Parsegian et al., 1988; Schiller et al., 1988). This relation has been modeled by the virial equation of state (Hasse et al., 1995). Calibration tests show that this model fits measurements well for PEG with $20 \leq \text{MW} \leq 511$ kDa.

6.3 Measurements and Model

6.3.1 Normal Mice

Equilibrium changes in TM volume were measured in response to osmotic stresses exerted using 511 kDa PEG. The left panel of Figure 6-1 shows results for an osmotic stress of 2.5 kPa. The TM shrank at all measured positions. Moreover, the fraction by which the TM shrank was approximately independent of the original thickness, which was 0.62 when the osmotic stress was 2.5 kPa. Similar measurements were made for PEG concentrations exerting osmotic stresses of 0.025, 0.050, 0.250, 1.0, 2.5, 5, and 10 kPa (right panel of Figure 6-1). The bulk modulus of the TM is equal to the negative reciprocal of the slope of the relation between normalized thickness and stress. Thus the large negative slope at low osmotic stress corresponds to a low bulk modulus (0.5 kPa), and the smaller negative slope at high osmotic stress corresponds to a higher value of bulk modulus (60 kPa). At the lowest osmotic stresses, the change in thickness can be predicted by Hooke's law. For higher osmotic stresses, the change in thickness is significantly smaller than that predicted by Hooke's law.

We modeled the stress-strain relation using a homogeneous isotropic gel model (Weiss and Freeman, 1997b) in which the free parameters were the stiffness of the matrix and the fixed charge concentration. The dashed line in Figure 6-2 shows the least squares fit of the model parameters to the measured thicknesses. The best-fitting value of fixed charge was -28 mmol/L and the best-fitting stiffness was negligibly small. The fit overestimates the bulk modulus at low osmotic stresses and under-

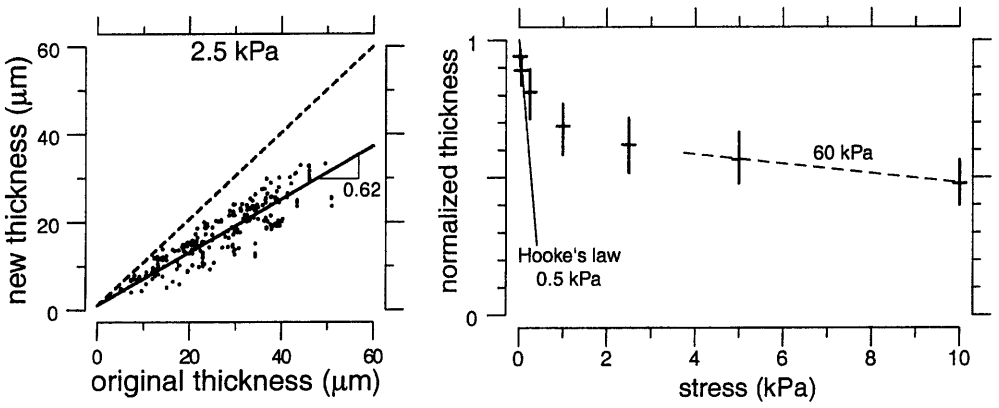

Figure 6-1: Left: Effect of osmotic pressure (2.5 kPa) on bead height. Each dot represents one bead on one of 10 TM's, and relates the bead height in AE with PEG (ordinate) to that in AE alone (abscissa). The ratio of these heights defines a normalized thickness, which for this osmotic pressure had a median value of 0.62. Right: Change in normalized thickness vs. osmotic stress. At each osmotic stress, the horizontal line represents the median normalized thickness as shown in the left panel, and the vertical line represents the interquartile range. The solid line is a least-squares fit of Hooke's law to the measurements at the lowest applied stress. The dashed line indicates the slope at high osmotic stresses.

estimates it at high osmotic stresses. Changing the fixed charge concentration to -10 mmol/L (lower dotted line) improved the fit at low osmotic stresses but made the fit worse at high osmotic stresses. Changing the fixed charge concentration to -34 mmol/L (upper dotted line) had the reverse effect. In all cases, increasing the stiffness of the matrix made the fit worse. Thus, we conclude that the homogeneous isotropic gel model fits the data best when the applied osmotic stress is resisted by electrostatic charge repulsion alone. However, no single value of fixed charge fit the measured thicknesses across the range of applied osmotic stresses. To better match the experimental measurements, we developed a two component model of the TM, in which one component was modeled as a homogeneous isotropic gel and the other was incompressible. This model has two free parameters: the fixed charge concentration of the first component, and the fraction of the TM volume that is compressible. The best-fitting parameters of this model provide a close match to the measured thicknesses at all osmotic stresses (solid line in Figure 6-2).

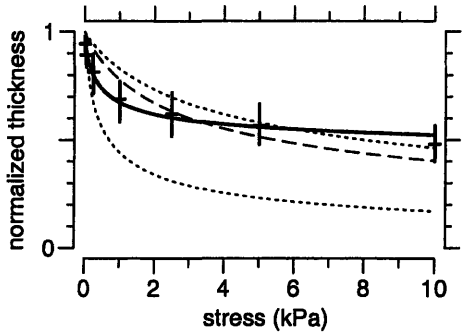

Figure 6-2: Fits of a gel model to the measured thickness change. The dashed line represents the best fit of a model in which TM charge (−28 mmol/L) resists compression. The lower dotted line, fit to the measurements at the two lowest stresses, has −10 mmol/L charge. The upper dotted line, fit to measurements at the highest two stresses, has −34 mmol/L charge. The solid line represents a variation of this model in which the TM also contains an incompressible region. In this model 42% of the TM is incompressible, and the rest has −10 mmol/L charge.

6.3.2 *Col*11*a*2 − /− and *Tecta*Y1870C/+ mice

Mice with mutations in either *Col*11*a*2 or *Tecta*, genes which encode proteins found in the TM, show significant hearing loss. Measuring the stress-strain relation of TMs from these mice serves two purposes: to provide a test of the two component model of TM compressibility, and to determine changes in TM material properties that may underlie the hearing loss in these mutants. The thickness change in response to osmotic pressure was measured as for normal mice. Figure 6-3 shows the normalized thickness as a function of osmotic pressure for the normal and mutant mice. The slope of this relation decreases with increasing stress for both normal and mutant mice. At low stresses, the bulk modulus was about 0.5 kPa for both normal and *Col*11*a*2 − /− mice, and was about 1.1 kPa for *Tecta*Y1870C/+ mice. At higher stresses, TMs from *Col*11*a*2 − /− mice shrank slightly less than those from normals. TMs from *Tecta*Y1870C/+ mice shrank significantly less than those of either normal or *Col*11*a*2 − /− mice at all osmotic stresses.

Figure 6-3 also shows the least squares fit of the two component model to each set of measurements. The model fits were near the median value of measurements at all stresses for both mutants. Beneath each plot, the figure shows the model parameters that best fit the measurements. The predominant effect of either mutation was to

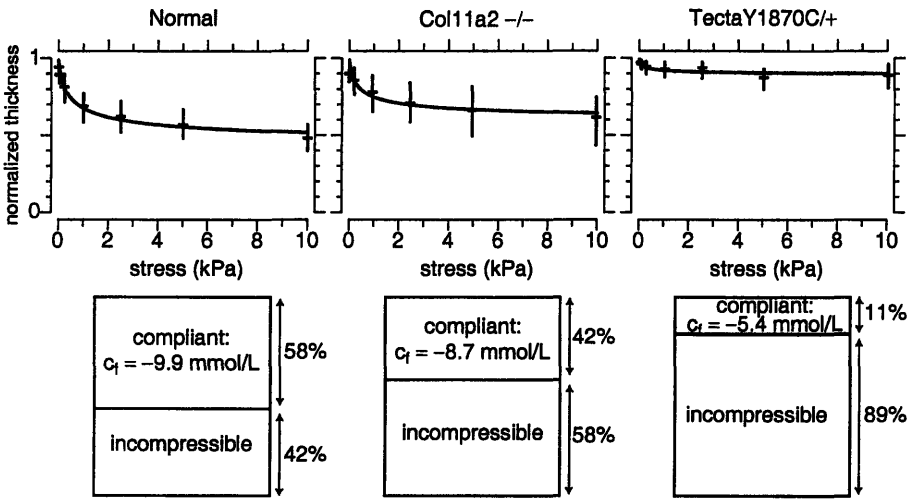

Figure 6-3: TM strain versus applied stress for normal TMs (left) $Col11a2-/-$ mutants (center), and $Tecta$Y1870C/+ mutants (right). In the plots, the symbols represent the median and interquartile ranges of measurements, and the solid lines represent least squares fits of the two component model to the measurements. The resulting parameters are shown beneath each plot, where c_f represents fixed charge concentration and the percentages represent the fractional thicknesses of the compliant and incompressible components.

increase the fraction of TM in the incompressible component; for the $Tecta$Y1870C/+ mutants, the model also predicted a slight decrease in fixed charge concentration in the other component.

6.4 Discussion

TMs from both types of mouse mutants, $Col11a2-/-$ and $Tecta$Y1870C/+, shrank less at a given osmotic pressure than did TMs of normals. The two component model suggests that the origin of this difference is not so much a change in fixed charge concentration but rather a decrease in volume of the compressible region. However, the physical basis for this incompressible region is not clear. The most straightforward interpretation of incompressibility is for the elastic matrix of the TM to be extremely stiff. Other collagen-containing tissues, such as cartilage, have bulk moduli in the MegaPascal range, of which roughly half is due to fixed charge (Grodzinksy, 1983). In this interpretation, the effect of the $Col11a2-/-$ and $Tecta$Y1870C/+ mutations might be to increase the fraction of TM that contains either a stiff elastic matrix or

high fixed charge concentration.

An alternative interpretation of incompressibility is for the TM to be extremely porous. If PEG can penetrate the pores of one component of the TM, it will not be able to exert an osmotic pressure on that component, so its volume will be unchanged. As a result, that component will appear incompressible. In this interpretation, the effect of the $Col11a2-/-$ and $Tecta$Y1870C/+ mutations might be to increase the porosity of the TM. The measurements presented here do not distinguish between these two interpretations. However, the two proposed mechanisms have dramatically different mechanical implications. The first mechanism predicts that the TMs of mutant mice will be extremely stiff mechanically, while the second predicts that these TMs will be more viscous and maybe extremely compliant. Either change could alter the interaction of the TM with hair bundles, and thereby contribute to the hearing loss seen in these mutants.

Chapter 7

Additional Experiments

This chapter discusses additional experiments and analysis done to further clarify the implications of the previous chapters.

7.1 Contribution of fixed charge concentration on bulk modulus

In other connective tissues such as cartilage, fixed charge is thought to play a significant role in resisting compression by electrostatic repulsion forces (Buschmann and Grodzinsky, 1995). To experimentally determine the fraction of the bulk modulus due to fixed charge, the TM was equilibrated in a high ionic strength bath (3 M KCl) and osmotic pressure was applied using PEG. At high KCl concentrations, the fixed charge groups are heavily shielded so that electrostatic forces from the fixed charge are minimized (Buschmann and Grodzinsky, 1995). Therefore, from these experiments, it is possible to differentiate the fraction of bulk modulus due to fixed charge versus that due to stiffness of matrix.

7.1.1 Methods

The equilibrium stress-strain relation was obtained by applying osmotic pressure using 511 kDa PEG and measuring the resulting strain. The method is explained in

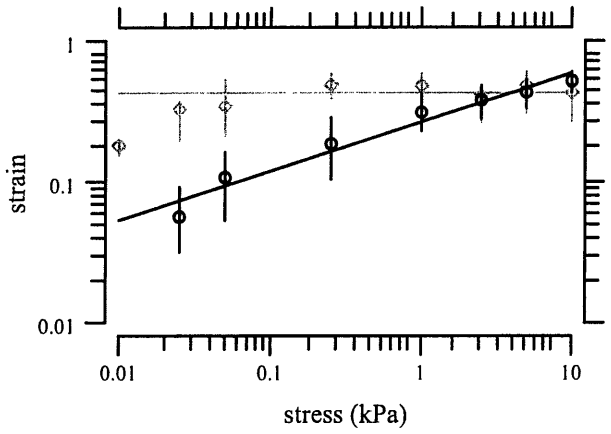

Figure 7-1: The stress-strain function of 11 apical-middle segments of TM in 174 mM KCl (in black) and 3 apical-middle segments of TM in 3 M KCl (in gray). Plot symbols represent the median strains and the lengths of vertical lines show the interquartile range. The strain for both of these experiments are relative to thickness in AE (174 mM KCl). The strain shown at 0.01 kPa is the strain due only to immersing the TM in 3 M KCl solution with no osmotic pressure exerted. The gray horizontal line is the median of all the data points in 3 M KCl with applied osmotic pressure which is equal to 0.43. The black solid line is a power function fit to the data according to 3.10 with a=0.31 and b=0.31.

greater detail in Chapter 3. All the solutions were variations of AE. In one set of solutions, different concentrations of 511 kDa PEG were added to AE which has 174 mM KCl to exert 0−10 kPa of osmotic pressure. In the other set of solutions, different concentrations of 511 kDa PEG were added to a modified AE solution which had 3 M instead of 174 mM of KCl to exert 0−10 kPa of osmotic pressure. To simplify terminology, the modified AE solution with 3 M KCl will be just be called a 3 M KCl solution in the text below.

7.1.2 Results

Figure 7-1 compares the stress-strain relation in 174 mM and 3 M KCl solution. When the TM is placed in a high ionic strength solution of 3 M KCl, the TM shrinks about 18%. When 25 Pa is then exerted on the TM, the TM shrinks 33% from its original thickness. However, when more osmotic pressure is exerted, the thickness does not change significantly. Therefore, in 3 M KCl solution, strain seems to be independent of osmotic pressure. In contrast, in the AE solution, the stress-strain relation follows a power relation as discussed in Chapter 3.

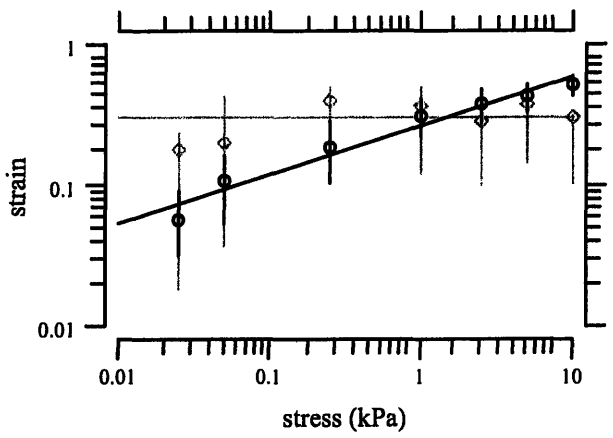

Figure 7-2: The stress-strain function of the same data shown in Figure 7-1. However, the strain for the 3M KCl experiment (in gray) is calculated relative to the thickness in 3 M KCl instead of relative to that in AE. The strain in AE are the same as in Figure 7-1. The gray horizontal line is the median of all the data points in 3 M KCl which is 0.30.

Since placing the TM in 3 M KCl solutions shrinks the TM, the strain measured in 3 M KCl plus PEG solution includes strain not only due to the osmotic pressure but also due to the high ionic bath concentration. Therefore, to determine the strain due only to the osmotic pressure, Figure 7-2 plots the same data as in Figure 7-1 but calculates strain in 3 M KCl solution relative to the TM thickness in 3 M KCl using Equation 3.5. Therefore, strain due to the high ionic bath was cancelled out and the strain plotted is due only to the osmotic pressure.

7.1.3 Discussion

To determine the contribution of fixed charge to the bulk modulus, the chord bulk modulus in AE was compared to that in 3 M KCl solution at 25 Pa. From Figure 7-2, the bulk modulus at 25 Pa in AE was 442 Pa while in 3 M KCl solution it was 139 Pa. If we assume that in 3 M KCl solution the fixed charge is completely shielded, then the bulk modulus measured in the high ionic bath solution is due only to the stiffness of the fibers and not due to electrostatic repulsion forces. Therefore, the upper bound on the compressive stiffness due to the fibers is about 139 Pa. Moreover, this suggests that the rest of the bulk modulus measured in AE (442−139=303 Pa) is due to fixed charge. In other words, about 69% of the bulk modulus is due to electrostatic

repulsion of the fixed charge.

The fact that the strain is mostly independent of stress in 3 M KCl solution suggests that the fraction of the TM that was not resisted by fixed charge has either infinite stiffness or is too porous for PEG to compress as suggested by the two-component gel model introduced in Chapter 6. Since we just determined that the bulk modulus not due to fixed charge has a stiffness less than 139 Pa, this suggests that the second component does not have infinite stiffness but instead is too porous for PEG to compress. Therefore, the fraction of the TM not resisted by fixed charge is a very porous material with bulk modulus less than or equal to 139 Pa.

7.2 Radial profile of strain

Section 3.3.4 showed radial dependence of the stress-strain relation using 511 kDa PEG. This section discusses whether similar radial dependence was seen in the dependence of TM on PEG MW and in the equilibrium stress-strain relations on mouse models.

7.2.1 Dependence of TM on PEG MW for isosmotic solutions

Section 3.3.2 discussed the dependence of TM strain on PEG MW for isosmotic solutions. Figure 3-7 shows the strain as a function of MW. However, in this figure, data was averaged across radial position. To determine whether there is radial dependence to strain, we examined strain as a fuction of radial position for all the data. Figure 7-3 shows a sample data from one TM that shows a small but systematic decrease in strain in the radial direction. In all 3 TMs, the strain was somewhat larger in the outer region of the TM between the outer edge and the limbal attachement than in the inner region between the limbal zone attachment and the inner edge. These two regions have been called the middle and marginal zone and the limbal zone, respectively. To summarize our results we pooled all the data from 3 TMs using 438 kDa

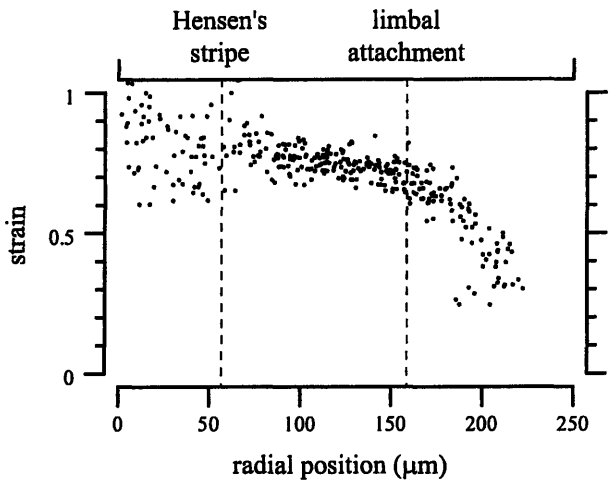

Figure 7-3: Strain as a function of radial position. Strain as a function of radial position measured from outer to the inner edge of the TM at a stress of 250 Pa using 438 kDa PEG. The locations of anatomical landmarks are indicated by dotted vertical lines.

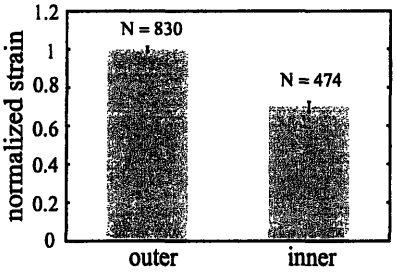

Figure 7-4: Strain as a function of radial positon from 3 TMs at an osmotic pressure of 250 Pa with 438 kDa PEG. For each TM segment, we computed the strain of all points located on the outer segment of the TM from the limbal attachement. We computed the mean of these values and normalized the strain to this mean value. The height of each bar equals the mean strain and the vertical line segments have lengths that equal twice the standard error of the mean. N is the number od data points.

PEG in Figure 7-4. The histogram shows that there is a small difference in strain between the outer and inner regions of the TM which is statically significant. Similar results were obtained at all PEG MW tested.

7.2.2 Mutant experiments

The radial dependence of strain was investigated for both $Tecta^{Y1870C/+}$ and $Col11a2$ $-/-$ mouse mutants. Since the strains for the $Tecta^{Y1870C/+}$ TMs were small, we were not able to see any significant radial dependence of strain at all osmotic pressures

tested. On the other hand, the $Col11a2$ $-/-$ had a radial dependence which was similar to that of wild-types.

Chapter 8

Discussion

This chapter discusses the implications of all the experiments and results discussed in previous chapters.

8.1 Poroelastic properties of TMs from normal mice

The fact that the TM is 97% water and contains macromolecular polyelectrolytes suggests that the TM is a gel. In other biological gels composed of a fluid and solid phase, the theory of poroelasticity has been successfully applied to describe deformational behavior. Poroelastic models explicitly account for the viscous flow of fluid through pores when the specimen undergoes stress. The two important material property of any poroelastic material are the bulk modulus and the pore radius. The bulk modulus characterizes the relation between stress and strain of a material and is a key parameter in models of polyelectrolyte gels (Weiss and Freeman, 1997b). However, conventional methods of measuring the bulk modulus by means of applying an uniform mechanical stress to the tissue are hard to adapt to the TM because the TM is irregularly shaped and small. Therefore, osmotic pressure (i.e. stress) was applied by using different concentration of 511 kDa polyethylene glycol (PEG) and the resulting TM volume change (i.e., strain) was measured. Although the osmotic

pressure exerted by PEG is a nonlinear function of concentration and molecular weight (MW) (Hasse et al., 1995), our calibration experiments confirm that solutions with known osmotic pressures can be prepared using PEGs with MWs as high as 511 kDa.

Volume changes that were measured due to varying concentration of PEG were primarily in the transverse direction. At each location on the TM, the thickness change of the TM was proportional to the original thickness (Figure 3-9). The inverse slope of this proportionality as a function of applied osmotic pressure describes the bulk modulus. This bulk modulus was a nonlinear function of osmotic pressure. For example, for apical segments of the TM, the bulk modulus was about 0.45 kPa at the lowest osmotic pressure measured and increased to more than 20 kPa at higher pressures. The bulk modulus was consistently 2-3 time larger for pieces of TM from the basal region of the cochlea (Figure 3-12), indicating that the bulk modulus varies with longitudinal position. However, this variation is small compared to the change in best frequency, consistent with the idea that bulk modulus is only one of many material properties of the cochlea that vary with longitudinal position. These bulk moduli are among the smallest measured for any connective tissue (Figure 3-18). For example, the TM bulk modulus is two orders of magnitude smaller than that of cornea and nearly four orders of magnitude smaller than cartilage. Thus, the TM is an extremely compliant tissue.

Another important property of a poroelastic material is the effective pore radius, which characterizes the spacing of the macromolecular matrix. PEG molecules that are sufficiently large are excluded from the TM and create an osmotic pressure gradient across the TM boundary, while PEG molecules that are smaller than the pore size can pass into the TM and thus exert no osmotic pressure. By measuring TM volume changes in response to solutions of PEG with different molecular weights but the same osmotic pressure, we have determined the pore radius of the TM to be approximately 16 nm. This radius is large enough to allow small solutes to diffuse freely, but small enough to exclude many proteins. By affecting how readily fluid can flow through the matrix of TM macromolecules, the pore radius also determines the relative importance of viscous and elastic components of TM impedance.

8.2 Two-component gel model

An isotropic polyelectrolyte gel model of the TM (Weiss and Freeman, 1997b) predicts that the bulk modulus should increase with applied stress. The best fit of this model to the measurements predicts that applied stress is resisted entirely by the presence of 28 mmol/L of negative fixed charge. However, this model underestimates the strain at small stresses (Figure 3-19). A more accurate fit is obtained by a two-component gel model. In this model, the TM is effectively split into two functionally distinct material phases. In the first phase, osmotic pressures are resisted entirely by the presence of fixed charges in the TM matrix. The second phase is functionally incompressible in response to osmotic pressure applied by PEG; i.e., this phase imposes an upper bound on the strain. Figure 6-2 shows that PEG exerts osmotic pressure on 58% of the TM volume, and this pressure is resisted by fixed charge with a concentration of $-$ 10 mmol/L.

To test the accuracy of this model, different components of the model were tested separately. The fixed charge concentration was determined by using a planar patch technique developed by Roozbeh Ghaffari in the Freeman lab. Figure 4-4 shows that the fixed charge concentration of TMs from normal mice was estimated to be 7.1$\pm$2.0 mM. These values are consistent with the charge predicted from the fits to the two-component gel model.

The fraction of the TM whose compression is resisted by fixed charge was determined in another study where osmotic pressure was exerted in a high ionic bath solution. Figure 7-2 shows that 65% of the bulk modulus was due to fixed charge. Moreover, the data supported the notion that the second phase of the model was made up of a very porous material with a bulk modulus of 139 Pa.

8.3 Material effect of $Y1870C$ missense mutation of α-tectorin

Measurements of the material properties of TMs from $Tecta^{Y1870C/+}$ mice also provided additional insights into the role of the TM in cochlear mechanics. From previous physiological measurements, the $Tecta^{Y1870C/+}$ mice were known to have a 50-80 dB increase in compound action potential (CAP) threshold. However, the cochlear microphonic response, disportion product otacoustic emissions and basilar membrane displacement tunings were found to be relatively unchanged (Legan et al., 2005). These results suggested that outer hair cells (OHCs) of these mice respond to sound normally but that the inner hair cells (IHCs) were not driven effectively. In other words, the TM exerts shearing forces on the OHC hair bundles, but does not drive the IHCs. These findings suggest that two roles attributed to the TM — shearing OHC hair bundles and coupling OHC forces to IHCs — are mediated by different mechanisms, and only the latter is affected by the *Tecta* mutation. To test this hypothesis, both shear and bulk material properties of TMs from wild-type and $Tecta^{Y1870C/+}$ mice were measured.

Figure 4-2 shows that at any given stress, TMs from $Tecta^{Y1870C/+}$ mice have less strain than those of wild-types. The fit of the two-component gel model to these measurements suggests that the mutation has two effects. One effect was to decrease in the fixed charge concentration, and hence the bulk modulus, of the TM in $Tecta^{Y1870C/+}$ mice. A decrease in fixed charge concentration by a factor of four, decreases the predicted bulk modulus of the TM by a factor of 20, from 0.69 kPa to 0.034 kPa. Another effect of the mutation was to increase the fraction of the TM that is porous, so that 90% of the TM was functionally incompressible by PEG, and this increased porosity leads to the decreased strain at a given osmotic stress. This increase in compliance means that bulk forces, e.g. due to transverse motion of the organ of Corti, will be met with significantly less resistance. Since the motion of inner hair cell bundles is predominantly transverse (Fridberger et al., 2006), this change in bulk modulus can significantly reduce the deflection of IHC bundles.

As in the normals, the predicted fixed charge concentration was confirmed by an independent measure of fixed charge using the planar patch clamp technique. These values for TMs from both wild-type and $Tecta^{Y1870C/+}$ mice are consistent with the charge predicted from measurements of bulk modulus suggesting that the bulk modulus of the TM is determined primarily by the fixed charge. One possible explanation for the observed decrease in fixed charge concentration in $Tecta^{Y1870C/+}$ mice is that α-tectorin is a keratan sulfate proteoglycan which comprises approximately 15% of the dry weight of the TM (Goodyear and Richardson, 2002). At physiological pH, keratan sulfate is ionized and represents a significant fraction of the fixed charge in the TM (Weiss and Freeman, 1997b). Therefore, a missense mutation in *Tecta* could alter the fixed charge carried by this protein. Regardless of the cause, the reduction in fixed charge translates directly to a change in TM material properties, indicating that the hearing loss in $Tecta^{Y1870C/+}$ mutants may be mediated by a change in TM fixed charge concentration.

Unlike the large change in the fixed charge concentration and bulk modulus, Figure 4-5 shows that the shear impedance of the TM was relatively unchanged, consistent with the idea that electrostatic repulsion due to fixed charge does not play an important role in determining shear modulus. The small reduction seen in shear impedance may be due to a disturbance of the striated sheet matrix of the TM related to the increased porosity of TMs from *Tecta* mice. This finding is consistent with the idea that the shear impedance of the TM is dominated by collagen fibrils.

The measured change in TM shear impedance is small compared to the 50–80 dB increase in CAP threshold for $Tecta^{Y1870C/+}$ mice. Although it is generally assumed that the TM exerts shearing forces that deflect hair bundles, the small reduction in TM shear impedance is not sufficient to account for the increased CAP thresholds in these mice. Moreover, such a mechanism would not explain the difference in sensitivity of inner and outer hair cells. This finding demonstrates that properties of the TM other than shear impedance play a critical role in cochlear mechanics.

8.4 Mutation of *Col11a2* for type XI collagen

Mutations in *Col11a2* have previously been shown in humans to cause congenital, non-progressive, non-syndromic sensorineural hearing loss (McGuirt et al., 1999). The fact that Figure 5-1 and Figure 5-2 show a threshold increase of 30–50 dB for both ABR and DPOAE measurements suggests that the hearing loss is primarily due to changes in the material properties of the TM that affect OHC hair bundle deflection. To test this hypothesis, both shear and bulk properties of *Col11a2* $-/-$ and wild-type TMs were measured.

Figure 5-3 shows that the mutation causes a 7.2 dB decrease in the radial shear impedance but only a 2.8 dB decrease in the longitudinal shear impedance of the TM. This finding suggests that the radial fibers that are prominently seen in light microscope images of the TM play an important role in radial shear impedance of the TM. This is further supported by the fact that in cartilage, type XI collagen is thought to be important for maintaining the interfibrillar spacing and fibril diameter of type II collagen (Mendler et al., 1989; Eikenberry et al., 1991; Li et al., 1995). In the TM, type II collagen is one of the main components of the radial fibers (Slepecky, Savage, Cefaratti and Yoo, 1992). Therefore, if type XI collagen works in the same manner in the TM as in cartilage, we would expect mutations in type XI collagen to affect the organization and strength of the radial fibers in the TM and, therefore, the shear impedance in the radial direction.

However, the equilibrium stress-strain relation of apical-middle and basal TM segments from *Col11a2* $-/-$ mice (Figure 5-4 and Figure 5-5) show that the *Col11a2* mutation does not affect the fixed charge and, therefore, the bulk modulus significantly. This further supports the notion that collagen is not important for resisting compression but is important for shearing the OHC hair bundles.

8.5 Role of TM in cochlear mechanics

Since the hair bundles of OHCs insert into the tectorial membrane, shearing forces exerted by the TM probably deflect the bundles. Similarly, shearing forces exerted by the fluid but driven by TM shearing motion are believed to deflect inner hair cell bundles (Billone and Raynor, 1973b). It has been suggested that the effect of the $Tecta^{Y1870C/+}$ mutation was to reduce the coupling of forces from outer to inner hair cells (Legan et al., 2005). Measurements of material properties from $Tecta^{Y1870C/+}$ TMs show that this reduction is not mediated by a decreased ability of the TM to exert shear forces on hair bundles or the reduction in the space constant of TM motion. However, the losses could be mediated by a reduction of the bulk modulus of the TM, coupled with an increase in porosity. Such changes could alter IHC sensitivity by reducing the ability of the TM to pump fluid, as suggested by a recent study (Nowotny and Gummer, 2006). Because this mechanism depends on the coupling of the TM to IHC bundles through fluid, it can also explain how the $Tecta^{Y1870C/+}$ mutation affects the sensitivity of IHCs without significantly altering that of OHCs, which are mechanically coupled to the TM.

The measurements from both $Tecta^{Y1870C/+}$ and $Col11a2$ $-/-$ mice reveal that the bulk and shear material properties of the TM are at best loosely coupled. The bulk compressibility of the TM is dominated by charge repulsion, so that a reduction in the fixed charge concentration of TMs causes an even larger decrease in bulk modulus. Moreover, TM bulk properties seem to control the coupling of energy from OHCs to IHCs. In contrast, the shear impedance of the TM is nearly independent of fixed charge concentration, and is likely dominated by the prominent collagen fibrillar network of the TM. Moreover, shear properties seem to control the shearing of the OHC hair bundles. Therefore, proteoglycans which give the TM its fixed charge and the collagen fibers appear to control two different material properties which in turn affect two distinct mechanical roles of the TM.

Bibliography

Abnet, C. and Freeman, D. (2000). Deformations of the isolated mouse tectorial membrane produced by oscillatory forces, *Hearing Research* **144**: 29–46.

Alberts, B., Bray, D., Lewis, J., Raff, M., Roberts, K. and Watson, J. D. (1994). *Molecular Biology of the Cell*, 3rd edn, Garland Publishing.

Allen, J. B. (1980). Cochlear micromechanics — a physical model of transduction, *J Acoust Soc Am* **68**: 1660–1670.

Basser, P., Schneiderman, R., Bank, R., Wachtel, E. and Maroudas, A. (1998). Mechanical properties of the collagen network in human articular cartilage as measured by osmotic stress technique, *Archives of Biochemistry and Biophysics* **351**: 207–219.

Bhat, R. and Timasheff, S. (1992). Steric exclusion is the principal source of the preferential hydration of proteins in the presence of polyethylene glycols, *Protein Science* **1**: 1133–1143.

Billone, M. and Raynor, S. (1973a). Transmission of radial shear forces to cochlear hair cells, *J. Acoust. Soc. Am.* **54**: 1143–1156.

Billone, M. and Raynor, S. (1973b). Transmission of radial shear forces to cochlear hair cells, *J Acoust Soc Am* **54**: 1143–1156.

Bosher, S. and Warren, R. (1978). Very low calcium content of cochlear endolymph, an extracellular fluid, *Nature* **273**: 377–378.

Brown, M. R., Tomek, M. S., Van Laer, L., Smith, S., Kenyon, J. B., Van Camp, G. and Smith, R. J. H. (1997). A novel locus for autosomal dominant nonsyndromic hearing loss, DFNA13, maps to chromosome 6p, *Am. J. Hum. Genet.* **61**: 924–927.

Brownell, W. E., Bader, C. R., Bertrand, D. and de Ribaupierre, Y. (1985). Evoked mechanical responses of isolated cochlear hair cells, *Science* **227**: 194–196.

Buschmann, M. D. and Grodzinsky, A. J. (1995). A molecular model of proteoglycan-associated electrostatic forces in cartilage mechanics, *J. Biomech. Eng.* **117**: 179–192.

Chirila, T. (1998). The intraocular lens, *in* J. Black and G. Hastings (eds), *Handbook of Biomaterial Properties*, Chapman Hall, London, pp. 106–113.

Chirila, T. and Hong, Y. (1998). The vitreous humor, *in* J. Black and G. Hastings (eds), *Handbook of Biomaterial Properties*, Chapman Hall, London, pp. 125–131.

Cohen-Salmon, M., El-Amraoui, A., Leibovici, M. and Petit, C. (1997). Otogelin: A glycoprotein specific to the acellular membranes of the inner ear, *Proceeding of National Academy of Science* **94**: 14450–14455.

Currey, J. (1998). Cortical bone, *in* J. Black and G. Hastings (eds), *Handbook of Biomaterial Properties*, Chapman Hall, London, pp. 3–14.

Currey, J. D. (1980). Mechanical properties of mollusc shell, *The Mechanical Properties of Biological Materials*, number XXXIV in *Symposia of the Society for Experimental Biology*, Cambridge Univ. Press, Cambridge, pp. 75–97.

Dallos, P., Billone, M. C., Durrant, J. D., Wang, C. Y. and Raynor, S. (1972). Cochlear inner and outer hair cells: Functional differences, *Science* **177**: 356–358.

Davis, H. (1958). A mechano-electrical theory of cochlear action, *Ann. Otol., Rhinol. and Laryngol.* **67**: 789–801.

Deng, X. and Guidoin, R. (1998). Cortical bone, *in* J. Black and G. Hastings (eds), *Handbook of Biomaterial Properties*, Chapman Hall, London, pp. 86–105.

Denny, M. and Gosline, J. (1980). The physical properties of the pedal mucus of the terrestrial slug, ariolimax columbianus, *J. Exp. Biol.* **88**: 375–393.

Edge, R., Evans, B., Pearce, M., Richter, C.-P., Hu, X. and Dallos, P. (1998). Morphology of the unfixed cochlea, *Hearing Research* **124**: 1–16.

Eikenberry, E. F., Mendler, M., Burgin, R., Winterhalter, K. H. and Burckner, P. (1991). Fibrillar organization in cartilage, *Articular Cartilage and Osteoarthritis*, Raven Press, New York, pp. 133–149.

Frank, E. H., Grodzinsky, A. J., Phillips, S. L. and Grimshaw, P. E. (1990). Physiochemical and bioelectrical determinants of cartilage material properties, *in* V. C. Mow, A. Ratcliffe and S. L. Y. Woo (eds), *Biomechanics of Diarthrodial Joints: Volume 1*, Springer-Verlag, New York, pp. 261–282.

Freeman, D., Abnet, C., Hemmert, W., Tsai, B. and Weiss, T. (2003). Dynamic material properties of the tectorial membrane: A summary, *Hearing Research* **180**: 1–10.

Freeman, D., Cotanche, D., Ehsani, F. and Weiss, T. (1994). Osmotic responses of the isolated tectorial membrane of the chick to isoosmotic solutions: Effect of Na^+, K^+, and Ca^{+2} concentration, *Hearing Research* **79**: 197–215.

Freeman, D., Hattangadi, S. and Weiss, T. (1997). Osmotic responses of the isolated mouse tectorial membrane to changes in pH, *Auditory Neuroscience* **3(4)**: 363–375.

Freeman, D., Masaki, K., McAllister, A., Wei, J. and Weiss, T. (2003). Static material properties of the tectorial membrane: A summary, *Hearing Research* **180**: 11–27.

Fridberger, A., Tomo, I., Ulfendahl, M. and de Monvel, J. B. (2006). Imaging hair cell transduction at the speed of sound: Dynamic behavior of mammalian stereocilia, *Proc Nat Acad Sci USA* **103**: 1918–1923.

Geisler, C. D. (1986). A model of the effect of outer hair cell motility on cochlear vibrations, *Hearing Res.* **24**: 125–131.

Ghaffari, R., Aranyosi, A. J. and Freeman, D. M. (2005). Measuring the electrical properties of the tectorial membrane, *Abstracts of the Twenty-Eight Annual Midwinter Research Meeting*, Association for Research in Otolaryngology, New Orleans, Louisiana, p. 240.

Gharpuray, V. (1998). Fibrocartilage, *in* J. Black and G. Hastings (eds), *Handbook of Biomaterial Properties*, Chapman Hall, London, pp. 48–58.

Goodyear, R. and Richardson, G. (2002). Extracellular matrices associated with the apical surfaces of sensory epithelia in the inner ear: Molecular and structural diversity, *J. Neurobiol.* **53(2)**: 212–227.

Gosline, J. M. (1971). Connective tissue mechanics of *Metridium senile*, *J. Exp. Biol.* **55**: 775–795.

Grodzinksy, A. (1983). Electromechanical and physicochemical properties of connective tissues, *CRC Crit. Rev. Biomed. Eng.* **9**: 133–199.

Hasako, J. and Richardson, G. (1988a). The ultrastructure organization and properties of the mouse tectorial membrane matrix, *Hearing Research* **35**: 21–38.

Hasako, J. and Richardson, G. (1988b). The ultrastructure organization and properties of the mouse tectorial membrane matrix, *Hearing Research* **35**: 21–38.

Hasse, H., Kany, H., Tintinger, R. and Maurer, G. (1995). Osmotic virial coefficients of aqueous poly(ethylene glycol) from laser-light scattering and isopiestic measurements, *Macromolecules* **28**: 3540–3552.

Healy, K. (1998). Dentin and emanel, *in* J. Black and G. Hastings (eds), *Handbook of Biomaterial Properties*, Chapman Hall, London, pp. 24–39.

Hiyama, S., Abe, K., Mikuni, H., Fukuda, S. and Inuyama, Y. (1998). Type a fibril of the mouse tectorial membrane shows d-periodicity: An atomic force microscopic examination, *Hearing Research* **124**: 118–123.

Hoeltzel, D. A., Altman, P., Buzard, K. and Choe, K. (1992). Strip extensiometry for comparison of the mechanical response of bovine, *J. Biomech. Eng.* **114**: 202–215.

Horn, B. K. P. (1986). *Robot Vision*, MIT Press, Cambridge, MA.

Horn, B. K. P. and Weldon Jr., E. J. (1988). Direct methods for recovering motion, *Internatl J. of Computer Vision* **2**: 51–76.

Ikeda, K., Kusakari, J., Takasaka, T. and Saito, Y. (1987). The Ca^{+2} activity of cochlear endolymph of the guinea pig and the effect of inhibitors, *Hearing Research* **26**: 117–125.

Johnstone, J. R. and Johnstone, B. M. (1966). Origin of summating potential, *J. Acoust. Soc. Am.* **40**: 1405–1413.

Katz, J. (1995). Mechanics of hard tissue, *in* J. Bronzino (ed.), *The Biomedical Engineering Handbook*, CRC Press, Inc., Boca Raton, FL, pp. 273–290.

Keaveny, T. (1998). Cancellous bone, *in* J. Black and G. Hastings (eds), *Handbook of Biomaterial Properties*, Chapman Hall, London, pp. 15–23.

Keiler, S. and Richter, C.-P. (2001). Cochlear dimensions obtained in hemicochleae of four different strains of mice: CBA/CaJ, 129/CD1, 129/SvEv, and C57BL/6J, *Hearing Research* **162**: 91–104.

Kemp, D. T. (1986). Otoacoutic emissions, travelling waves and cochlear mechanisms, *Hearing Research* **22**: 95–104.

Kennedy, H. J., Crawford, A. C. and Fettiplace, R. (2005). Force generation by mammalian hair bundles supports a role in cochlea amplification, *Nature* **433**: 880–883.

Khalkhali-Ellis, Z., Hemming, F. W. and Steel, K. (1987). Glycoconjugates of the tectorial membrane, *Hearing Research* **25**: 185–191.

Khalsa, P. S. and Einsenberg, S. R. (1997). Compressive behavior of articular cartilage is not completely explained by proteoglycan osmotic pressure, *J. Biomechanics* **30**: 589–594.

Killick, R., Legan, P. K., Malenczak, C. and Richardson, G. P. (1995). Molecular cloning of chick β-tectorin, an extracellular matrix molecule of the inner ear, *Journal of Cell Biology* **129**: 535–547.

Koehl, M. (1977). Mechanical diversity of connective tissue of the body wall of sea anemones, *J. Exp. Biol.* **69**: 107–125.

Kolston, P. J. (1988). Sharp mechanical tuning in a cochlear model without negative damping, *J. Acoust. Soc. Am.* **83**: 1481–1487.

Langer, M., Fink, S., Koitschev, A., Rexhausen, U., Horber, J. and Rupperberg, J. (2001). Lateral mechanical coupling of stereocilia in cochlear hair bundles, *Biophysical Journal* **80**: 2608–2621.

Legan, P. K., Rau, A., Keen, J. and Richardson, G. (1997). The mouse tectorins, *Journal of Biological Chemistry* **272**: 8791–8801.

Legan, P., Lukashkina, V., Goodyear, R., Kossl, M., Russell, I. and Richardson, G. (2000). A targeted deletion of α-tectorin reveals that the tectorial membrane is required for the gain and timing of cochlear feedback, *Neuron* **28**: 273–285.

Legan, P., Lukashkina, V., Goodyear, R., Lukashkin, A., Verhoeven, K., Camp, G., Russell, I. and Richardson, G. (2005). A deafness mutation isolates a second role for the tectorial membrane in hearing, *Nature Neuroscience* **8**: 1035–1042.

Li, Y., Lacerda, D. A., Warman, M. L., Beier, D. R., Yoshioka, H., Ninomiya, Y., Oxford, J. T., Morris, N. P., Andrikopoulos, K., Ramirez, F., Wardell, B. B., Lifferth, G. D., Teuscher, C., Woodward, S. R., Taylor, B. A., Seegmiller, R. E.

and Olson, B. R. (1995). A fibrillar collagen gene, col11a1, is essential for skeletal morphogenesis, *Cell* **80(3)**: 435–430.

Liberman, M. C., Zuo, J. and Guinan, J. J. J. (2004). Otoacoustic emissions without somatic motility: can stereocilia mechanics drive the mammalian cochlea, *J. Acoust. Soc. Am.* **116(3)**: 1649–1655.

Lim, D. (1972). Fine morphology of the tectorial membrane: Its relationship to the organ of corti., *Arch. Otolaryng.* **96**: 199–215.

Lim, D. (1986). Functional structure of the organ of corti: A review, *Hearing Research* **22**: 117–146.

Maison, S. F., Luebke, A. E., Liberman, M. C. and Zuo, J. (2002). Efferent protection from acoustic injury is mediated via $\alpha 9$ nicotinic acetylcholine receptors on outer hair cells, *Journal of Neuroscience* **22(24)**: 10838–10846.

Mak, A. F. T. and Zhang, M. (1998). Skin and muscle, *in* J. Black and G. Hastings (eds), *Handbook of Biomaterial Properties*, Chapman & Hall, London, pp. 66–69.

Mammano, F. and Nobili, R. (1993a). Biophysics of the cochlea: Linear appoximation, *J. Acoust. Soc. Am.* **93**: 3320–3332.

Mammano, F. and Nobili, R. (1993b). Biophysics of the cochlea: linear approximation, *J Acoust Soc Am* **93**: 3320–3332.

Maroudas, A. and Bannon, C. (1981). Measurement of swelling pressure in cartilage and comparison with the osmotic pressure of constituent proteoglycans, *Biorheology* **18**: 619–632.

Masaki, K., Copeland, A., Johnson, E., Smith, R. and Freeman, D. (2002). Measuring the equilibrium stress/strain relationship of the isolated tectorial membrane, *Abstracts of the Twenty-Fifth Annual Midwinter Research Meeting*, Association for Research in Otolaryngology, St. Petersburg Beach, Florida, p. 240.

Masaki, K., Ghaffari, R., Gu, J. W., Aranyosi, A. J., Richardson, G. and Freeman, D. (2006). A mutation in α-tectorin decreases the bulk modulus and fixed charge density of the tectorial membrane.

Masaki, K., Richardson, G., Smith, R. J. H. and Freeman, D. M. (2006). Measuring the material properties of normal and mutant Tectorial Membrane, *in* F. Nuttall (ed.), *Auditory Mechanisms: Processes and Models*, World Scientific, Singapore, pp. 48–54.

Masaki, K., Weiss, T. and Freeman, D. (2006). Poroelastic bulk properties of the tectorial membrane measured with osmotic stress, *Biophysical Journal* p. (in press).

Mauro, A. (1957). Nature of solvent transfer in osmosis, *Science* **126**: 252–253.

McCutchen, C. W. (1982). Cartilages is poroelastic, not viscoelastic (including an exact theorem about strain energy and viscous loss, and an order of magnitude relation for equilibrium time), *J. Biomechanics* **15(4)**: 325–327.

McGuirt, W., Prasad, S., Griffith, A., Kunst, H., Green, G., Shpargel, K., Runge, C., Huybrechts, C., Mueller, R., Lynch, E., King, M.-C., Brunner, H., Cremers, C., Takanosu, M., Li, S.-W., Arita, M., Mayne, R., Prockop, D., Van Camp, G. and Smith, R. (1999). Mutations in COL11A2 cause non-syndromic hearing loss (DFNA13), *Nature Genetics* **23**: 413–419.

Mendler, M., Eich-Bender, S. G., Vaughan, L., Winterhalter, K. H. and Bruckner, P. J. (1989). Cartilage contains mixed fibrils of collagen types ii, ix, and xi, *Cell Biol.* **108**: 191–197.

Motokawa, T. (1984). Viscoelasticity of Holothurian body wall, *J. Exp. Biol.* **109**: 63–75.

Munyer, P. D. and Schulte, B. A. (1994). Immunohistochemical localization of keratan sulfate and chondroitin 4- and 6- sulfate proteoglycans in subregions of the tectorial and basilar membranes, *Hearing Research* **79**: 83–93.

Neely, S. T. and Kim, D. O. (1986). A model for active elements in cochlear biomechanics, *J. Acoust. Soc. Am.* **79**: 1472–1480.

Neely, S. T. and Kim, K. O. (1983). An active cochlear model showing sharp tuning and high sensitivity, *Hearing Res.* **9**: 123–130.

Ngola, S., Fintschendor, Y., Choi, W.-Y. and Shepodd, T. (2001). Conduct-as-cast polymer monoliths as separation media for capillary electrochromatography, *Anal. Chem.* **73**: 849–856.

Nowotny, M. and Gummer, A. W. (2006). Nanomechanics of the subtectorial space caused by electromechanics of cochlear outer hair cells, *Proc Nat Acad Sci USA* **103**: 2120–2125.

Özkaya, N. and Nordin, M. (1999). *Fundamentals of Biomechanics: Equilibrium, Motion, and Deformation*, Springer-Verlag, New York, NY.

Parry, D. and Craig, A. (1988). Collagen fibrils during development and maturation and their contribution to the mechanical attributes of connective tissue, *in* M. Nimni (ed.), *Collagen , Volume II, Biochemistry and Biomechanics*, CRC Press, Inc., Boca Raton, FL, pp. 1–23.

Parsegian, V., Rand, R., Fuller, N. and Rau, D. (1988). Osmotic stress for the direct measurement of intermolecular forces, *Meth. Enzymol.* **127**: 400–416.

Parsons, J. (1998). Cartilage, *in* J. Black and G. Hastings (eds), *Handbook of Biomaterial Properties*, Chapman Hall, London, pp. 40–47.

Quinn, T. and Grodzinsky, A. (1993). Longitudinal modulus and hydraulic permeability of poly(methacrylic acid) gels: Effects of charge density and solvent content, *Macromolecules* **26**: 4332–4338.

Rhode, W. S. and Geisler, C. D. (1967). Model of the displacement between opposing points on the tectorial membrane and reticular lamina, *J. Acoust. Soc. Am.* **42**: 185–190.

Richardson, G. P., Russel, I. J., Duance, V. C. and Bailey, A. J. (1987). Polypeptide composition of the mammalian tectorial membrane, *Hearing Research* **25**: 45–60.

Richter, C.-P. and Dallos, P. (2003). Tectorial membrane bulk stiffness measurements in the gerbil hemicochlea, *Abstracts of the Twenty-Sixth Annual Midwinter Research Meeting*, Association for Research in Otolaryngology, Daytona Beach, Florida, p. 30.

Schiller, L., Emmett, M., Santa Ana, C. and Fordtran, J. (1988). Osmotic effects of polyethylene glycol, *Gastroenterol* **94**: 933–941.

Schneiderman, R., Keret, D. and Maroudas, A. (1986). Effect of mechanical and osmotic pressure on the rate of glycosaminoglycan synthesis in the human adult femoral head cartilage: An in vitro study, *Journal of Orthopaedic Research* **4**: 393–408.

Shah, D., Freeman, D. and Weiss, T. (1995). Osmotic response of the isolated, unfixed mouse tectorial membrane to isosmotic solutions: Effect of Na^+, K^+, and Ca^{+2} concentration, *Hearing Research* **87**: 187–207.

Shoelson, B., Dimitriadis, E., Cai, H., Kachar, B. and Chadwick, R. (2004). Evidence and implications of inhomogeneity in tectorial membrane elasticity, *Biophysical Journal* **87**: 2768–2777.

Simmler, M., Cohen-Salmon, M., El-Amraoui, A., Guillaud, L., Benichou, J., Petit, C. and Panthier, J. (2000). Targeted disruption of *otog* results in deafness and severe imbalance, *Nat. Genet.* **24**: 139–143.

Slepecky, N. B., Savage, J. E., Cefaratti, L. K. and Yoo, T. J. (1992). Electron-microscopic localization of type ii, ix, and v collagen in the organ of corti of the gerbil, *Cell Tissue Research* **267**: 413–418.

Slepecky, N. B., Savage, J. E. and Yoo, T. J. (1992). Localization of type ii, ix, and v collagen in the inner ear, *Acta Otolaryngology* **112**: 611–617.

Steel, K. (1980). The proteins of normal and abnormal tectorial membranes, *Acta Otolaryngology* **89**: 27–32.

Sterkers, O., Ferrary, E. and Amiel, C. (1984). Inter- and intracompartmental osmotic gradients within the rat cochlea, *Am. J. Physiol.* **247**: F602–F606.

Sterkers, O., Ferrary, E. and Amiel, C. (1988). Production of inner ear fluids, *Physiol. Rev.* **68**: 1083–1128.

Suzuki, H., Lee, Y. C., Tachibana, M., Hozawa, K., Wataya, H. and Takasaka, T. (1992). Quantitative carbohydrate analyses of the tectorial and otoconial membranes of the guinea pig, *Hearing Research* **60**: 45–52.

Thalmann, I., Machiki, K., Calabro, A., Hascall, V. C. and Thalmann, R. (1993a). Uronic acid-containing glycosaminoglycans and keratan sulfate are present in the tectorial membrane of the inner ear: Functional implications, *Archives of Biochemistry and Biophysics* **307**: 391–396.

Thalmann, I., Machiki, K., Calabro, A., Hascall, V. and Thalmann, R. (1993b). Uronic acid-containing glycosaminoglycans and keratan sulfate are present in the tectorial membrane of the inner ear: Fuctional implications, *Arch. Biochem. Biophys.* **307**: 391–396.

Thalmann, I., Thallinger, G., Comegys, T., Crouch, E. C., Barrett, N. and Thalmann, R. (1987). Composition and supramolecular organization of the tectorial membrane, *Laryngoscope* **97**: 357–367.

Timoshenko, S. and Goodier, J. (1970). *Theory of Elasticity*, 1st edn, McGraw-Hill.

Van't Hoff, J. H. (1886). Une propriété général de la matiére diluée, *Svenska Vet. Akad. Handl.* **21**: 42–49.

von Bekesy, G. (1960). *Experiments in Hearing*, 1st edn, McGraw-Hill.

Weiss, T. F. (1996). *Cellular Biophysics: Volume 1 Transport*, MIT Press, Cambridge, MA.

Weiss, T. and Freeman, D. (1997a). Equilibrium behavior of an isotropic polyelectrolyte gel model of the tectorial membrane: Effect of pH, *Hearing Res.* **111**: 55–64.

Weiss, T. and Freeman, D. (1997b). Equilibrium behavior of an isotropic polyelectrolyte gel model of the tectorial membrane: The role of fixed charge, *Auditory Neuroscience* **3(4)**: 351–361.

Woo, S. L. Y. and Levine, R. E. (1998). Ligaments, tendon and fascia, *in* J. Black and G. Hastings (eds), *Handbook of Biomaterial Properties*, Chapman & Hall, London, pp. 59–63.

Zwislocki, J. and Cefaratti, L. (1989). Tectorial membrane II: Stiffness measurements in vivo, *Hearing Research* **42**: 211–228.

Zwislocki, J. J. (1979). Tectorial membrane: A possible sharpening effect on the frequency analysis in the cochlea, *Acta Otolaryngol.* **87:3-4**: 267–279.

Zwislocki, J. J. and Kletsky, E. J. (1979). Tectorial membrane: A possible effect on frequency analysis in the cochlea, *Science* **204**: 639–641.

Zwislocki, J. J. and Kletsky, E. J. (1980). Micromechanics in the theory of cochlear mechanics, *Hearing Res.* **2**: 505–512.